# Evaluating stratospheric ozone and water vapor changes in CMIP6 models from 1850-2100

James Keeble[1,2], Birgit Hassler[3], Antara Banerjee[4,24], Ramiro Checa-Garcia[5], Gabriel Chiodo[6,7], Sean Davis[4], Veronika Eyring[3,8], Paul T. Griffiths[1,2], Olaf Morgenstern[9], Peer Nowack[10,11], Guang Zeng[9], Jiankai Zhang[12], Greg Bodeker[13,14], David Cugnet[15], Gokhan Danabasoglu[16], Makoto Deushi[17], Larry W. Horowitz[18], Lijuan Li[19], Martine Michou[20], Michael J. Mills[21], Pierre Nabat[20], Sungsu Park[22], Tongwen Wu[23]

[1]Department of Chemistry, University of Cambridge, Cambridge, UK
[2]National Centre for Atmospheric Science (NCAS), University of Cambridge, Cambridge, UK
[3]Deutsches Zentrum für Luft- und Raumfahrt (DLR), Institut für Physik der Atmosphäre, Oberpfaffenhofen, Germany
[4]NOAA Earth System Research Laboratory Chemical Sciences Division, Boulder, CO USA
[5]Laboratoire des sciences du climat et de l'environnement: Gif-sur-Yvette, Île-de-France, FR
[6]Department of Environmental Systems Science, Swiss Federal Institute of Technology, Zurich, Switzerland
[7]Department of Applied Physics and Applied Math, Columbia University, New York, NY, USA
[8]University of Bremen, Institute of Environmental Physics (IUP), Bremen, Germany.
[9]National Institute of Water and Atmospheric Research (NIWA), Wellington, New Zealand
[10]Grantham Institute, Department of Physics and the Data Science Institute, Imperial College London, London, UK.
[11]School of Environmental Sciences, University of East Anglia, Norwich, UK.
[12]Key Laboratory for Semi-Arid Climate Change of the Ministry of Education, College of Atmospheric Sciences, Lanzhou University, Lanzhou, 730000, Gansu, China
[13]Bodeker Scientific, 42 Russell Street, Alexandra, 9320, New Zealand
[14]School of Geography, Environment and Earth Sciences, Victoria University, New Zealand
[15]Laboratoire de Météorologie Dynamique, Institut Pierre-Simon Laplace, Sorbonne Université / CNRS / École Normale Supérieure – PSL Research University / École Polytechnique – IPP, Paris, France
[16]National Center for Atmospheric Research, Boulder, Colorado
[17]Meteorological Research Institute (MRI), Tsukuba, Japan
[18]GFDL/NOAA, Princeton, NJ, USA.
[19]State Key Laboratory of Numerical Modeling for Atmospheric Sciences and Geophysical Fluid Dynamics (LASG), Institute of Atmospheric Physics, Chinese Academy of Sciences, Beijing 100029, China
[20]CNRM, Université de Toulouse, Météo-France, CNRS, Toulouse, France
[21]Atmospheric Chemistry Observations and Modeling Laboratory, National Center for Atmospheric Research, Boulder, CO, USA
[22]Seoul National University, Seoul, South Korea
[23]Beijing Climate Center, China Meteorological Administration, Beijing, China
[24]Cooperative Institute for Research in Environmental Sciences (CIRES), University of Colorado Boulder, Boulder, CO, USA

Correspondence to: James Keeble (james.keeble@atm.ch.cam.ac.uk)

**Abstract.** Stratospheric ozone and water vapor are key components of the Earth system, and past and future changes to both have important impacts on global and regional climate. Here we evaluate long-term changes in these species from the pre-industrial (1850) to the end of the 21st century in CMIP6 models under a range of future emissions scenarios. There is good

40 agreement between the CMIP multi-model mean and observations, although there is substantial variation between the individual CMIP6 models. For the CMIP6 multi-model mean, global total column ozone (TCO) has increased from ~300 DU in 1850 to ~305 DU in 1960, before rapidly declining in the 1970s and 1980s following the use and emission of halogenated ozone depleting substances (ODSs). TCO is projected to return to 1960's values by the middle of the 21st century under the SSP2-4.5, SSP3-7.0, SSP4-3.4, SSP4-6.0 and SSP5-8.5 scenarios, and under the SSP3-7.0 and SSP5-8.5 scenarios TCO values

45 are projected to be ~10 DU higher than the 1960's values by 2100. However, under the SSP1-1.9 and SSP1-1.6 scenarios, TCO is not projected to return to the 1960's values despite reductions in halogenated ODSs due to decreases in tropospheric ozone mixing ratios. This global pattern is similar to regional patterns, except in the tropics where TCO under most scenarios is not projected to return to 1960's values, either through reductions in tropospheric ozone under SSP1-1.9 and SSP1-2.6, or through reductions in lower stratospheric ozone resulting from an acceleration of the Brewer-Dobson Circulation under other

50 SSPs. CMIP6 multi-model mean stratospheric water vapor mixing ratios in the tropical lower stratosphere have increased by ~0.5 ppm from the pre-industrial to the present day and are projected to increase further by the end of the 21st century. The largest increases (~2 ppm) are simulated under the future scenarios with the highest assumed forcing pathway (e.g. SSP5-8.5). Both TCO and tropical lower stratospheric water vapor show large variability following explosive volcanic eruptions.

## 1 Introduction

55 Stratospheric ozone and water vapor are key components of the Earth system, and past changes in both have had important impacts on global and regional climate (e.g. Solomon et al., 2010; Dessler et al., 2013; Eyring et al., 2013; WMO 2018). Depletion of the ozone layer over the last few decades of the 20th century, driven by emissions of ozone depleting substances (ODSs), provides an excellent illustration of a forcing that has caused large dynamical and regional surface impacts, despite an overall small global radiative forcing (-0.05±0.10 $Wm^{-2}$ from 1750 to 2011; Myhre et al. 2013). The Antarctic ozone hole

60 has cooled the springtime Antarctic lower stratosphere and has driven a poleward expansion of the tropospheric circulation and dry zones of the SH during the summer season (e.g. Thompson and Solomon, 2002; Gillett and Thompson, 2003; McLandress et al., 2010; Son et al., 2010; Polvani et al., 2011; Braesicke et al., 2013, Keeble et al., 2014, Morgenstern et al., 2018). Measurements of stratospheric water vapor (SWV) are uncertain and a long-term trend has not been established (Scherer et al., 2008; Hurst et al., 2011; Hegglin et al., 2014). Nonetheless, large decadal variations in SWV have been suggested to

65 affect surface temperatures (e.g. Solomon et al., 2010). Given these climate impacts, it is important to understand the drivers of stratospheric ozone and water vapor and to distinguish long-term trends from interannual and decadal variability.

The Intergovernmental Panel on Climate Change (IPCC) Fifth Assessment Report (AR5) highlights tropospheric ozone as the third most important anthropogenic greenhouse gas (GHG) with a global mean radiative forcing of 0.35±0.2 $Wm^{-2}$, while stratospheric water vapor changes resulting from $CH_4$ oxidation exert a global mean radiative forcing of 0.07±0.05 $Wm^{-2}$

70    (Hansen et al 2005, Myhre et al, 2007; Myhre et al., 2013). The primary contributor to the radiative forcing estimate for ozone is increases in tropospheric ozone ($0.4\pm0.2$ Wm$^{-2}$), while recent depletion of stratospheric ozone due to the use and emission of halogenated ODSs, compounded with impacts on ozone of increasing $CO_2$, $CH_4$, and $N_2O$, has resulted in a weakly negative radiative forcing ($-0.05\pm0.1$ Wm$^{-2}$). Recently, Checa-Garcia at al., (2018) estimated ozone radiative forcing using the ozone forcing dataset that was developed for the Coupled Model Intercomparison Project Phase 6 (CMIP6, Eyring et al., 2016), and

75    calculated values of 0.28 Wm$^{-2}$, which, while consistent with the IPCC-AR5 estimate, represents an increase of ~80% compared to the CMIP5 ozone forcing dataset (Cionni et al 2011, Stevenson et al, 2013). The relative uncertainties in radiative forcing estimates for both stratospheric ozone and water vapor are large due to the challenges in constraining the concentrations of both during the pre-satellite era. As a result, the current radiative forcing estimates rely on ozone and water vapor fields derived from simulations performed by global climate models and Earth system models.

80    Stratospheric ozone concentrations are determined by a balance between production and destruction of ozone through gas phase chemical reactions and transport (e.g. Brewer and Wilson, 1968). Gas phase ozone chemistry consists of sets of oxygen only photo-chemical reactions first described by Chapman (1930), alongside ozone destroying catalytic cycles involving chlorine, nitrogen, hydrogen and bromine radical species (e.g. Bates and Nicolet, 1950; Crutzen, 1970; Johnston, 1971; Molina and Rowland, 1974; Stolarski and Cicerone, 1974). Heterogeneous processes play a major role in determining ozone

85    abundances in the polar lower stratosphere (e.g. Solomon, 1999) and following large volcanic eruptions (e.g. Solomon et al., 1996; Telford et al., 2009).

Changes in anthropogenic emissions of halogenated ODSs, $N_2O$, $CH_4$, $CO_2$ and other GHGs during the 21$^{st}$ century are expected to perturb these chemical cycles either directly through their role as source gases or by changing stratospheric temperatures and dynamics (Eyring et al., 2010; Keeble et al., 2017). Following the implementation of the Montreal Protocol

90    and its subsequent Amendments, stratospheric concentrations of inorganic chlorine and bromine levelled off in the mid-1990s and are now in decline (Mäder et al., 2010; WMO, 2018), which has led to early signs of recovery of stratospheric ozone (Keeble et al., 2018; Weber et al., 2018; WMO 2018) and the detection of statistically robust positive trends in September Antarctic ozone (Solomon et al., 2016). Total column ozone in the mid- and high latitudes is projected to return to pre-1980 values during the coming decades (Eyring et al., 2013; Dhomse et al., 2018; WMO, 2018). Future emissions of $CH_4$ and $N_2O$,

95    which are not regulated in the same way as halogenated ODSs, are associated with greater uncertainty and future concentrations of $HO_x$ (H, OH, $HO_2$) and $NO_x$ (NO, $NO_2$) radicals are highly sensitive to assumptions made about their future emissions. Additionally, increases in GHG concentrations are expected to lead to an acceleration of the Brewer–Dobson circulation (BDC; Butchart et al., 2006, 2010; Shepherd and McLandress, 2011; Hardiman et al., 2014; Palmeiro et al., 2014), which may affect ozone concentrations directly through transport (e.g. Plumb, 1996; Avallone and Prather, 1996) and by controlling the

100    oxidation of $Cl_y$, $NO_y$ and $HO_x$, reservoir species (e.g. Revell et al., 2012; Meul et al., 2014). However, recent research (Polvani et al., 2018, 2019) has shown that stratospheric ozone depletion caused by increasing ODSs has accounted for around half of

the acceleration of the BDC in recent decades. As concentrations of ODSs decline, stratospheric ozone recovery may offset, at least in part, future changes to the speed of the BDC resulting from GHG changes.

Stratospheric water vapor concentrations are determined predominantly through a combination of the dehydration air masses experience as they pass through the cold point tropical tropopause (Brewer, 1949; Fueglistaler et al., 2005) and *in-situ* production from $CH_4$ oxidation (Brasseur and Solomon, 1984; Jones et al., 1986; LeTexier et al., 1988). Direct injection by convective overshooting (Dessler et al., 2016) or following volcanic eruptions (Murcray et al., 1981; Sioris et al. 2016) are also sources of SWV.

Observations of stratospheric water vapor show a net increase during the late 20th century (e.g. Rosenlof et al., 2001; Scherer et al., 2008; Hurst et al., 2011), followed by a sudden decrease of ~10% after 2000 (e.g. Solomon et al., 2010). Virtually all models project increases in SWV concentrations under increased $CO_2$ (e.g. Gettelman et al., 2010; Banerjee et al., 2019). Projected increases over the course of the 21st century occur due to the predominant effect of increases in upper tropospheric temperatures, offset in part by the effects of a strengthening BDC (Dessler et al., 2013; Smalley et al., 2017), with additional impacts from future $CH_4$ emissions (Eyring et al., 2010; Gettelman et al., 2010). Eyring et al. (2010) calculate a mean increase of 0.5-1 ppm per century in SWV concentrations for models contributing to the Chemistry-Climate Model Validation (CCMVal) inter-comparison project, although agreement between models on the absolute increase is poor.

To advance our understanding of long-term changes to a number of components of the Earth system, including stratospheric ozone and water vapor, the CMIP Panel, operating under the auspices of the Working Group on Coupled Modelling (WGCM) of the World Climate Research Programme (WCRP), has defined a suite of climate model experiments, which together form CMIP6 (Eyring et al., 2016). Between the previous phase (CMIP5; Taylor et al., 2012) and CMIP6 there has been further development of existing models; new models have joined and a new set of future scenarios, the shared socioeconomic pathways (SSPs; Riahi et al., 2017) that are used in climate projections by CMIP6 models as part of the Scenario Model Intercomparison Project (ScenarioMIP; O'Neill et al., 2015), have been established. Earth system models have been further developed with improved physical parametrizations and some have added additional Earth system components (e.g., atmospheric chemistry, nitrogen cycle, ice sheets). As a result of this advancement in model complexity, the CMIP6 multi-model ensemble provides an opportunity to re-assess past and projected future stratospheric ozone and water vapor changes. In this study, we evaluate these changes against observations over the last three decades and examine long-term changes in these quantities from 1850 to 2100 under the SSP scenarios. Section 2 describes the simulations and models used in this study, with a focus on the treatment of stratospheric ozone and water vapor. Long-term changes in ozone and water vapor are evaluated in Sections 3 and 4, respectively, and implications are discussed in Section 5. Our results inform future studies that use CMIP6 simulations to investigate stratospheric composition changes and associated impacts.

## 2 Models and Simulations

This study evaluates long-term ozone and water vapor changes in 14 models which have performed the CMIP historical simulations and a subset of which have performed ScenarioMIP simulations. The treatment of stratospheric chemistry varies

135 significantly across the 14 models evaluated in this study. We evaluate all models which have produced ozone and water vapor output, regardless of the complexity of the stratospheric chemistry used, as these models may be used in other studies to diagnose the impacts of stratospheric composition changes on radiative forcing and/or regional climate change. In this section, the models and simulations used in the subsequent analysis sections are described, along with the observational datasets used for evaluation. Several of the figures were created with the Earth System Model Evaluation Tool (ESMValTool) version 2.0

140 (Eyring et al., 2019; Righi et al., 2019), a diagnostic and performance metric tool for enhanced and more comprehensive Earth system model evaluation in CMIP.

### 2.1 Models

At the time of the preparation of this manuscript, 14 models (BCC-CSM2-MR, BCC-ESM1, CESM2, CESM2-WACCM, CNRM-CM6-1, CNRM-ESM2-1, E3SM-1-0, FGOALS-g3, GFDL-CM4, GFDL-ESM4, IPSL-CM6A-LR, MRI-ESM2-0,

145 SAM0-UNICON, and UKESM1-0-LL) have provided ozone mixing ratios and 10 models (BCC-CSM2-MR, BCC-ESM1, CESM2, CESM2-WACCM, CNRM-CM6-1, CNRM-ESM2-1, GFDL-CM4, IPSL-CM6A-LR, MRI-ESM2-0, and UKESM1-0-LL) have provided water vapor as diagnostics. Of the 14 models analysed in this study, five (CESM2-WACCM, CNRM-ESM2-1, GFDL-ESM4, MRI-ESM2-0, and UKESM1-0-LL) use fully coupled, online stratospheric chemistry, while two (CNRM-CM6-1 and E3SM-1-0) use a simple chemistry scheme. The remaining seven (BCC-CSM2-MR, BCC-ESM1,

150 CESM2, FGOALS-g3, GFDL-CM4, IPSL-CM6A-LR and SAM0-UNICON) do not include an interactive chemistry scheme, and instead prescribe stratospheric ozone according to the CMIP6 ozone database (except in the case of CESM2, which prescribes ozone values from the CESM2-WACCM model). Relevant details of each model are provided in the appendix, and a summary is provided in Table 1.

The CMIP6 ozone dataset is designed to be used by those models without interactive chemistry, and was created using a

155 different approach from the previous CMIP5 ozone database (Cionni et al., 2011). The Cionni et al. (2011) dataset was based on stratospheric ozone values from a combination of model and observational datasets between the 1970s and 2011, and extended into the past and future based on assumptions of changes to EESC and the 11-year solar cycle. Tropospheric ozone values were based on a mean field of two models with interactive chemistry. The CMIP6 ozone dataset was created using simulations from the CMAM and CESM-WACCM models which both performed the REF-C2 simulation as part of the

160 Chemistry-Climate Model Initiative (Eyring, et al., 2013; Morgenstern et al., 2017). As a result, the CMIP6 dataset provides a full three-dimensional field of ozone mixing ratios created using a single, consistent approach for both the stratosphere and

troposphere, extending from preindustrial times to present day, and until the end of the 21ˢᵗ century following the different SSP scenarios (O'Neill et al., 2015).

**BCC-CSM2-MR:** The BCC-CSM2-MR model, developed by the Beijing Climate Center, is a coupled ocean–atmosphere
165 model. Ozone in the stratosphere and troposphere is prescribed using monthly mean time-varying gridded data from the CMIP6 dataset. Other GHG concentrations including $CO_2$, $N_2O$, $CH_4$, CFC11, CFC12 are monthly zonal-mean values using the CMIP6 datasets (Meinshausen et al., 2017, 2019). Stratospheric water vapor concentrations are prognostic values calculated in a similar way to those in the troposphere. A full description and evaluation of the BCC-CSM2-MR model is provided by Wu et al. (2019a).

170 **BCC-ESM1:** The BCC-ESM1 model, developed by the Beijing Climate Center, is a fully coupled global climate-chemistry-aerosol model. Tropospheric ozone is modelled interactively using the MOZRT2 chemistry scheme, while stratospheric ozone is prescribed to the zonally averaged, monthly mean values from 1850 to 2014 derived from the CMIP6 data package in the top two model layers, and relaxed towards the CMIP6 dataset between these layers and the tropopause. GHG concentrations including $CH_4$, $N_2O$, $CO_2$, CFC-11, and CFC-12 are prescribed using CMIP6 historical forcing data as suggested in the
175 AerChemMIP protocol (Collins et al., 2017). Stratospheric water vapor is a prognostic variable without any special treatment of $CH_4$ oxidation. A full description and evaluation of the BCC-ESM1 model is provided by Wu et al. (2019b).

**CESM2:** The Community Earth System Model version 2 (CESM2) is the latest generation of the coupled climate/Earth system models developed as a collaborative effort between scientists, software engineers, and students from the National Center for Atmospheric Research (NCAR), universities, and other research institutions. CESM2(CAM6) uses the Community
180 Atmosphere Model version 6 as its atmosphere component, which has 32 vertical levels from the surface to 3.6 hPa (about 40 km) and a horizontal resolution of 1.25° longitude by 0.95° latitude, and limited interactive chemistry for tropospheric aerosols. GHG concentrations including $CH_4$, $N_2O$, $CO_2$, CFC11eq, and CFC12 are prescribed using CMIP6 historical forcing data. CESM2 uses datasets derived from previous runs of CESM2-WACCM6, which includes complete interactive chemistry, for tropospheric oxidants ($O_3$, OH, $NO_3$, and $HO_2$; 3D monthly means), stratospheric water vapor production from $CH4$ oxidation
185 (3D monthly means), stratospheric aerosol (zonal 5-day means), and $O_3$ for use in radiative transfer calculations (zonal 5-day means). A full description and evaluation of the CESM2 model is provided by Danabasoglu et al. (2019).

**CESM2-WACCM:** The CESM2-WACCM model uses the Whole Atmosphere Community Climate Model version 6 (WACCM6) as its atmosphere component. WACCM6 has 70 vertical levels from the surface to $6 \times 10^{-6}$ hPa (about 140 km), a horizontal resolution of 1.25° longitude by 0.95° latitude. WACCM6 features a comprehensive chemistry mechanism with a
190 description of the troposphere, stratosphere, mesosphere, and lower thermosphere (TSMLT), including 231 species, 150 photolysis reactions, 403 gas-phase reactions, 13 tropospheric heterogeneous reactions, and 17 stratospheric heterogeneous reactions. The photolytic calculations are based on both inline chemical modules and a lookup table approach. The chemical

species within the TSMLT mechanism include the extended $O_x$, $NO_x$, $HO_x$, $ClO_x$, and $BrO_x$ chemical families, $CH_4$ and its degradation products, $N_2O$ (major source of $NO_x$), $H_2O$ (major source of $HO_x$), plus various natural and anthropogenic precursors of the $ClO_x$ and $BrO_x$ families. The TSMLT mechanism also includes primary nonmethane hydrocarbons and related oxygenated organic compounds, and two very short-lived halogens ($CHBr_3$ and $CH_2Br_2$) which add an additional ~5 ppt of inorganic bromine to the stratosphere. WACCM6 features a new prognostic representation of stratospheric aerosols based on sulfur emissions from volcanoes and other sources, and a new detailed representation of secondary organic aerosols (SOAs) based on the volatility basis set approach from major anthropogenic and biogenic volatile organic compound precursors. A full description of WACCM6 is provided by Gettelman et al. (2019).

**CNRM-CM6-1:** The CNRM-CM6-1 model, developed by the Centre National de Recherches Météorologiques, is a global climate model which uses a linearised scheme to model stratospheric ozone, in which ozone mixing ratios are treated as a prognostic variable with photochemical production and loss rates computed from its associated Earth System Model CNRM-ESM2-1. Details of the linearization of the net photochemical production in the ozone continuity equation are provided by Michou et al. (2019). Tropospheric ozone mixing ratios are not calculated interactively, and are instead prescribed form the CMIP6 dataset. Methane oxidation is parameterized throughout the model domain by the introduction of a simple relaxation of the upper-stratospheric moisture source due to methane oxidation Untch (2011). A sink representing photolysis in the mesosphere is also included. A full description and evaluation of the CNRM-CM6-1 model is provided by Voldoire et al. (2019).

**CNRM-ESM2-1:** The CNRM-ESM2-1 model, developed by the Centre National de Recherches Météorologiques, is a coupled Earth System model. The chemistry scheme of CNRM-ESM2-1 is an on-line scheme in which the chemistry routines are part of the physics of the atmospheric climate model and are called at each time-step (Michou et al., 2011). The scheme considers 168 chemical reactions, among which 39 are photolysis reactions and 9 represent the heterogeneous chemistry. The scheme does not include tropospheric ozone non-methane hydrocarbon chemistry. The 3D concentrations of several trace gases interact with the atmospheric radiative code at each call of the radiation scheme. In addition to the non-orographic gravity wave drag parameterization, a sponge layer is also used in the upper levels to reduce spurious reflections of vertically propagating waves from the model top. This parameterization consists simply of a linear relaxation of the wind towards zero. The linear relaxation is active above 3 Pa. A full description and evaluation of the CNRM-ESM2-1 model is provided by Seferian et al. (2019), while an evaluation of the ozone radiative forcing is detailed in Michou et al. (2019).

**E3SM-1-0:** The E3SM-1-0 model, developed by the U.S. Department of Energy, is a coupled Earth System Model. It uses a simplified, linearized ozone photochemistry scheme to predict stratospheric ozone changes (Linoz v2; Hsu & Prather, 2009). Stratospheric water vapor does not include a source from methane oxidation. A full description of the E3SM-1-0 model is provided by Golaz et al. (2019).

**FGOALS-g3:** The FGOALS-g3 model, developed by the Chinese Academy of Sciences, is a coupled ocean–atmosphere
225    model. FGOALS-g3 does not include an interactive chemistry module, and ozone is prescribed in the stratosphere and
troposphere following the recommendations by CMIP6. Stratospheric water vapor concentrations are prognostic values
calculated in a similar way to those in the troposphere. A full description and evaluation of the FGOALS-g3 model is provided
by Li et al. (2019).

**GFDL-CM4:** The GFDL-CM4 model, developed by the National Oceanic and Atmospheric Administration's Geophysical
230    Fluid Dynamics Laboratory, is a coupled ocean–atmosphere model. Ozone is prescribed using the recommended CMIP6
dataset throughout the troposphere and stratosphere, while stratospheric water vapor is interactive, but does not include a
source from methane oxidation. A full description and evaluation of the GFDL-CM4 model is provided by Held et al. (2019).

**GFDL-ESM4:** The GFDL-ESM4 model, developed by the National Oceanic and Atmospheric Administration's Geophysical
Fluid Dynamics Laboratory, is a fully coupled chemistry-climate model. Stratospheric ozone is calculated using an interactive
235    tropospheric and stratospheric gas-phase and aerosol chemistry scheme. The atmospheric component (AM4.1) includes 56
prognostic (transported) tracers and 36 diagnostic (non-transported) chemical tracers, with 43 photolysis reactions, 190 gas-
phase kinetic reactions, and 15 heterogeneous reactions. The tropospheric chemistry includes reactions for the $NO_x$-$HO_x$-$O_x$-
CO-$CH_4$ system and oxidation schemes for other non-methane volatile organic compounds. The stratospheric chemistry
accounts for the major ozone loss cycles ($O_x$, $HO_x$, $NO_x$, $ClO_x$, and $BrO_x$) and heterogeneous reactions on liquid and solid
240    stratospheric aerosols (Austin et al., 2013). Photolysis rates are calculated interactively using the FAST-JX version 7.1 code,
accounting for the radiative effects of simulated aerosols and clouds. Details on the chemical mechanism will be included in
Horowitz et al. (in prep). A full description and evaluation of the GFDL-ESM4 model is provided by Dunne et al. (2019).

**IPSL-CM6A-LR:** The IPSL-CM6A-LR model, developed by the Institut Pierre-Simon Laplace, is a coupled atmosphere-
land-ocean-sea ice model. Stratospheric and tropospheric ozone is prescribed using the CMIP6 dataset but implemented so
245    that profiles are stretched in a thin region (few kilometres only) around the tropopause, ensuring that the tropopause of the
ozone climatology and that of the model match. Differences in tropopauses heights would lead to spurious ozone transport
between the upper troposphere and lower stratosphere, a region where the corresponding non-physical radiative impact would
be particularly high (see e.g., Hardiman et al., 2019). Stratospheric methane oxidation is not included in the version of the
model evaluated here. A full description and evaluation of the IPSL-CM6A-LR model is provided by Servonnat et al., (2020).

250    **MRI-ESM2-0:** The MRI-ESM2-0 model, developed by the Meteorological Research Institute, Japan Meteorological Agency,
is a fully coupled global climate model which includes interactive chemistry. MRI-ESM2-0's chemistry component is the
MRI-CCM2.1 module, which simulates the distribution and evolution of ozone and other trace gases in the troposphere and
middle atmosphere. MRI-CCM2.1 is an updated version of MRI-CCM2 (Deushi and Shibata, 2011), which calculates a total
of 90 chemical species and 259 chemical reactions. MRI-ESM2-0 simulates the stratospheric water vapor interactively with

255 consideration for production of water vapor from CH₄ oxidation. A full description and evaluation of the MRI-ESM2-0 model is provided by Yukimoto et al. (2019).

**SAM0-UNICON:** The SAM0-UNICON, developed by the Seoul National University, is a general circulation model based on the CESM1 model with a Unified Convection Scheme (Park 2014a, b) that replaces shallow and deep convection schemes in CESM1. Stratospheric and tropospheric ozone is prescribed as a monthly mean 3D field with a specified annual cycle.

260 Stratospheric water vapor does not include a source from methane oxidation. A full description of the SAM0-UNICON model is provided by Park et al. (2019).

**UKESM1-0-LL:** The UKESM1-0-LL model, developed jointly by the United Kingdom's Met Office and Natural Environment Research Council, is a fully coupled Earth System Model. UKESM1-0-LL uses a combined troposphere-stratosphere chemistry scheme (Archibald et al., 2019), which includes 84 tracers, 199 bimolecular reactions, 25 uni- and

265 termolecular reactions, 59 photolytic reactions, 5 heterogeneous reactions and 3 aqueous phase reactions for the sulfur cycle. As a result, stratospheric ozone and water vapor are fully interactive. A full description and evaluation of the UKESM1-0-LL model is provided by Sellar et al. (2019).

## 2.2 Simulations

To evaluate changes in stratospheric ozone and water vapor from 1850-2100, this study makes use of two types of simulations

270 performed as part of the wider CMIP6 activity (Eyring et al., 2016): the CMIP6 historical simulation and the ScenarioMIP future simulations (O'Neill et al., 2015).

The CMIP6 historical simulation runs from 1850-2014, in which the models are forced by common datasets based on observations which include historical changes in short-lived species and long-lived GHGs, global land use, solar forcing, stratospheric aerosols from volcanic eruptions and, for models without ozone chemistry, prescribed time varying ozone

275 concentrations. These simulations are initialised from the pre-industrial control (piControl) simulation, a time-slice simulation run with 1850 perpetual pre-industrial conditions performed by each model.

The ScenarioMIP future simulations run from 2015-2100 and follow the newly developed SSPs, which provide future emissions and land use changes based on scenarios directly relevant to societal concerns regarding climate change impacts, adaptation and mitigation (Riahi et al., 2017). Broadly, the shared socioeconomic pathways follow 5 categories: sustainability

280 (SSP1), middle of the road (SSP2), regional rivalry (SSP3) inequality (SSP4) and fossil-fueled development (SSP5). Further, each scenario has an associated forcing pathway (i.e. the forcing reached by 2100 relative to the pre-industrial), and each specific scenario is referred to as SSPx-y, where x is the SSP and y is the radiative forcing pathway (the radiative forcing at the end of the century, in W/m$^2$). For example, SSP3-7.0 follows SSP3 (regional rivalry), and has a 2100 global mean forcing of 7.0 W/m$^2$ relative to the pre-industrial.

285 The SSP scenarios span a broad range of future emissions and land use changes, both of which have the potential to change total column ozone through changes in both the troposphere and/or stratosphere, and stratospheric water vapor through changes in tropical tropopause layer (TTL) temperatures or $CH_4$. In general, low SSPs assume lower abundances of long-lived GHGs ($CO_2$, $CH_4$, $N_2O$; Meinshausen et al., 2019) and lower emissions of ozone precursors (Hoesly et al., 2018). All SSPs follow the same emissions scenario for ozone depleting substances, based on continued compliance with the Montreal Protocol

290 (Velders and Daniel, 2014), but the concentrations of ODSs vary slightly between scenarios due to changes in the lifetimes of each species associated with climate change (Meinshausen et al., 2019). It should be noted that recent studies have identified unreported emissions of CFC-11 (e.g. Montzka et al., 2018), and that the trajectory of ozone recovery is sensitive to the magnitude and duration of these emissions (e.g. Dhomse et al., 2019; Keeble et al., 2019), which are not included in the emissions assumptions of Velders and Daniel (2014).

295 In this study, we use ozone and water vapor output for the SSP1-1.9, SSP1-2.6, SSP2-4.5, SSP3-7.0, SSP4-3.4, SSP4-6.0 and SSP5-8.5 scenarios. Details of which simulations were performed by each model are provided in Table 1.

**2.3 Observation datasets**

The evaluation of stratospheric ozone and water vapor makes use of two datasets: the NIWA-BS combined total column ozone database and SWOOSH zonal mean ozone and water vapor datasets.

300 The NIWA-BS combined total column ozone (TCO) database takes daily gridded TCO fields from 17 different satellite-based instruments, bias corrects them against the global Dobson and Brewer spectrophotometer network, and merges them into a seamless homogeneous daily gridded (1.25° longitude x 1.0° latitude) TCO data record. First, overpass data from the TOMS instruments flown onboard Nimbus-7, Meteor-3, Earth Probe, and Adeos, and from the OMI instrument on Aura, are bias corrected against the ground-based TCO measurements. Those five bias-corrected datasets then provide the basis for correcting

305 the remaining datasets i.e. those from the GOME, GOME-2 and SCIAMACHY instruments, the SBUV instrument flown on Nimbus-7, and the SBUV-2 instruments flown on NOAA-9, 11, 14. 16, 17, 18 and 19. The bias corrected measurements are then combined in a way that traces uncertainties from the source data through to the final merged data product.

A filled version 3.3 dataset was created by first filling missing data that could easily be interpolated between neighbouring values and then fitting a regression model, comprising an offset and trend basis function, expanded in spherical harmonics to

310 account for latitudinal and longitudinal structure, to available TCO measurements from fields on day N-1, N, and N+1. The expansion indices for the spherical harmonics are adapted to the data to avoid over-fitting of the regression model. Once fitted, the regression model was then used to estimate TCO values in regions where data were missing. Such regression model derived fields were spliced into the unfilled fields to ensure a smooth transition from the measurements into the regression model

derived values. Monthly mean fields were calculated from the filled daily fields to provide the validation datasets used for the
315 CMIP6 models evaluated here.

The Stratospheric Water and OzOne Satellite Homogenized (SWOOSH) dataset is a merged record of stratospheric ozone and
water vapor measurements collected by a subset of limb sounding and solar occultation satellites spanning 1984 to the present
(see Davis et al., 2016, for details). Specifically, SWOOSH comprises data from the Stratospheric Aerosol and Gas Experiment
instruments (SAGE-II and SAGE-III/Meteor-3M), the Upper Atmosphere Research Satellite HAlogen Occultation Experiment
320 (UARS HALOE), the UARS Microwave Limb Sounder (MLS), and Aura MLS.

The source satellite measurements are homogenized by applying corrections that are calculated from data taken during time
periods of instrument overlap. The primary SWOOSH product is a merged multi-instrument monthly-mean zonal-mean (10°)
dataset on the pressure grid of the Aura MLS satellite (12 levels per decade). Because the merged product contains missing
data, a merged and filled product is also provided for studies requiring a continuous dataset. These merged and filled products
325 for ozone and water vapor (combinedanomfillo3q and combineanomfillh2oq respectively) from SWOOSH version 2.6 are
used in this study for comparison with CMIP6 model fields.

## 3 Ozone

### 3.1 Evaluation over recent decades

Before investigating long-term changes in stratospheric ozone, we evaluate each model's performance, and the performance
330 of the CMIP6 multi-model mean (MMM), against observations. In the following sections we evaluate the 2000-2014
climatological zonal mean distribution of ozone and the seasonal evolution of zonal mean total column ozone against
observations, in the form of the combined zonal mean ozone dataset from SWOOSH and the TCO dataset from NIWA-BS.

### 3.1.1 2000-2014 climatological zonal mean and total column ozone

Latitude-height cross sections of zonal mean ozone volume mixing ratios for each CMIP6 model, the CMIP6 MMM and the
335 SWOOSH dataset, averaged over the years 2000-2014, are shown in Figure 1. There is generally good agreement between the
individual CMIP6 models and the SWOOSH dataset. All models broadly capture tropospheric and stratospheric ozone
gradients, with a clear peak in ozone mixing ratios in the tropical stratosphere at around 10 hPa, the downwards bending of the
contour lines towards high latitudes in the lower stratosphere (e.g. Plumb, 2002) and flat contour lines in the tropical upper
stratosphere in the quasi-equilibrated photochemical regime (e.g. Haigh and Pyle, 1982; Meul et al., 2014; Chiodo et al., 2018;
340 Nowack et al., 2018).

Notable differences between the models occur in the uppermost stratosphere, and around the tropopause (Figure A1). The BCC-ESM1, CESM2, FGOALS-g3 and SAM0-UNICON models all simulate much higher ozone mixing ratios in the upper stratosphere. The BCC-ESM1 and SAM0-UNICON models in particular significantly overestimate ozone mixing ratios with respect to the CMIP6 MMM and observations in the upper stratosphere, and also have a different structure in the distribution

345    of ozone at these levels, with peaks in the mid-latitudes at 1 hPa. In the tropical tropopause region, the MRI-ESM2-0 and UKESM1-0-LL models significantly overestimate ozone mixing ratios, while the SAM0-UNICON model has much lower mixing ratios in this region with respect to the CMIP6 MMM.

The tropical tropopause is a region in which chemistry-climate models have typically performed poorly, due to the fact that ozone mixing ratios in this region are controlled by a combination of chemical production, vertical transport of ozone poor air

350    from the troposphere and mixing of ozone rich stratospheric air. Gettelman et al. (2010) documented the seasonal cycle of ozone at 100 hPa from 18 models involved in the CCMVal-2 inter-comparison project, and showed that while there is good agreement between the MMM and the observations, there is a large spread in ozone mixing ratios between individual models, and many models do not accurately capture the observed seasonal cycle. For the CMIP6 models investigated here, there is also good agreement between the tropical (15°S-15°N) MMM ozone mixing ratios at 70 hPa and the SWOOSH dataset (Figure 2).

355    Further, many models accurately capture the seasonal cycle of ozone, with lower ozone mixing ratios simulated between February and April, and higher values in August and September. However, as for CCMVal-2 models, there is still a large spread in modelled ozone mixing ratios in the tropical tropopause region. Both MRI-ESM2-0 and UKESM1-0-LL are high biased (both use interactive chemistry), while BCC-ESM1 is low biased compared to the observations and the CMIP6 MMM.

Despite the differences between the individual CMIP6 models, there is generally good agreement between the zonal mean

360    distribution of ozone in the CMIP6 MMM and the SWOOSH dataset throughout much of the stratosphere (Figure 4), with differences between 70 hPa and 3 hPa typically less than ±10%. Maximum ozone mixing ratios at ~10 hPa are slightly underestimated by the CMIP6 MMM, while ozone mixing ratios in the lower tropical stratosphere, and at ~1 hPa in the mid-latitudes, are overestimated. The CMIP6 MMM also overestimates ozone mixing ratios at all latitudes in the upper troposphere between 200-100 hPa by ~20-40 %. Since upper tropospheric ozone is a particularly important climate forcing agent (Lacis et

365    al., 1990; Stevenson et al., 2013; Young et al., 2013; Nowack et al., 2015), this has important implications for the ozone radiative forcing estimated from climate model simulations. However, it should be noted that the uncertainties in the SWOOSH dataset are likely to be relatively large in the upper troposphere.

TCO climatologies (latitude vs month) for all 14 discussed CMIP6 models are shown in Figure 3. Overall the observed climatology patterns and annual cycle amplitudes, compared here against the NIWA-BS dataset, are well represented in the

370    CMIP6 MMM and the individual models: lower values and smallest amplitude in the tropics that increase to the poles, with the highest TCO values around 60°S between August and November, and in the NH polar regions between January and May, and the smallest TCO values in the SH polar regions during the ozone hole period. Some models slightly underestimate TCO

in the NH polar regions (CNRM-CM6-1, CNRM-ESM2-1), and some models slightly overestimate TCO globally (MRI-ESM2-0, UKESM1-0-LL). Note that the NIWA-BS dataset statistically models high latitude values during the polar night to provide a global, gap-free data field (see Section 2.3), and therefore uncertainties on the observations in these regions are higher than elsewhere.

The lower row of Figure 4 shows the detailed differences between the TCO CMIP6 MMM and the observations. In the tropics and the NH mid-latitudes the differences are smaller than ±10 DU (<5% of the climatological value in these regions). The differences get slightly larger in the NH polar regions, and are largest in the SH mid-latitudes where the MMM overestimates the observed TCO by up to 40 DU, and the SH polar regions where the MMM underestimates the observed TCO in polar winter (May to July) by 20-30 DU, and then overestimates the observed TCO during September by ~30 DU. Compared to CMIP5, the differences in the NH mid-latitudes and polar regions seem reduced in the MMM (Eyring et al., 2013; Lauer et al., 2017), whereas the differences between MMM and observations are similar in the SH mid-latitudes between CMIP5 and CMIP6. Especially noticeable is the shift of the strongest underestimation of the MMM from SH late spring/early summer in CMIP5 to the SH winter in CMIP6, which may result from a better representation of the polar vortex duration in CMIP6 models.

Figure 5 shows Taylor diagrams of 14 CMIP6 models performance for annual and seasonal mean TCO between 60°S–60°N against the NIWA-BS TCO dataset for the period 2000–2014. On the annual scale, the 14 CMIP6 models can accurately reproduce the spatial pattern of NIWA-BS TCO, with all correlation coefficients being greater than 0.9 and the standard deviations of all the models falling between 0.75 and 1.75. On the seasonal scale, the models perform better during DJF and MAM than during JJA and SON. Overall, the GFDL-ESM4 model scores highest, not only because it is closest to the reference line, but also because its relative bias compared with the NIWA-BS dataset is smallest. Although the UKESM1-0-LL model is also close to the reference line during JJA and SON, it has a high relative bias from the NIWA-BS dataset. The SAM0-UNICON and MRI-ESM2-0 models show a larger standard deviation than other models, indicating they have a much higher interannual variability.

### 3.1.2 Regional Total Column Ozone changes 1960-2014

The temporal evolution of observed global TCO, observed TCO for specific regions, TCO from individual CMIP6 models, and the CMIP6 MMM is shown in Figure 6. In general, the MMM overestimates the observed TCO values by up to 6% (10-20 DU) globally (Figure 6 a), in the NH and SH mid-latitudes, and in the tropics (Figure 6 c-e), but the trend in these regions is well captured. The spread within the analysed CMIP6 models is large, though, with MRI-ESM2-0 and UKESM1-0-LL overestimating TCO by up to 40 DU in, for example, the SH mid-latitudes. Both of these models used an interactive chemistry scheme to calculate ozone abundances in the troposphere and stratosphere. Although these two models overestimate ozone, the other models that calculate ozone fields interactively (CESM2-WACCM, CNRM-ESM2-1, GFDL-ESM4) slightly

underestimate the observed TCO values, indicating that there is no clear distinction of models with and without interactive
405  chemistry as there was in the CMIP5 models (Eyring et al., 2013). While most of the analysed CMIP6 models show distinct
interannual variability, it is noteworthy that there is no interannual variability detectable for two models (CESM2 and SAM0-
UNICON) that used prescribed ozone fields for their historical simulations (see Section 2.1).

The CMIP6 MMM underestimates the observed decline in TCO for March in the NH polar regions during the ozone depletion
period (1980-2000) but tracks the observations well after 2000 (Figure 6f). This is also mirrored in the trends calculated for
410  these periods for observations and the individual CMIP6 models and MMM (Table 2). While the TCO October values in the
SH polar regions are overestimated in the MMM compared to observations, the overall TCO decline from 1980 to 2000 is
stronger in the models than in the observations (see Table 2). These characteristics are very similar to the trends reported in
Eyring et al. (2013) for the CMIP5 model simulations.

Table 2 follows Eyring et al. (2013, their table 2) in showing the observed and modelled trends in TCO over the period 1980-
415  2000. Additionally, we also show trends over the period of 2000-2014. They are calculated for 14 models, of which five models
have interactive stratospheric chemistry (CESM2-WACCM, CNRM-ESM2-1, GFDL-ESM4, MRI-ESM2-0, and UKESM1-
0-LL). For these five models, over the period 1980-2000, annual mean global trends range from -0.19 (MRI-ESM2-0) to -1.04
(UKESM1-0-LL) DU/year. The average trend from these models (hereafter referred to as "INTERACTIVE") is -0.57 DU/year
which is within the uncertainty range of observed trends (from -0.56 to -0.74 DU/year). In the tropics, all models show weak
420  negative trends, and the mean of the 5-member INTERACTIVE models in the tropics (-0.18 DU/year) compares well with the
observed trends. In the northern mid-latitudes, models considerably underestimate the observed negative trends with the
exception of CNRM-ESM2-1 (-0.95 DU/year – within the range of observed trends) and UKEMS1-0-LL (-1.2 DU/year –
slightly stronger than the observed negative trends). Over southern mid-latitudes, modelled trends are generally closer to the
observed trends, with the exceptions of MRI-ESM2-0 and SAM0-UNICON which have substantially weaker negative trends.
425  Again, UKEMS1-0-LL overestimates the observed negative trends. At high latitudes of the NH, most of the models
substantially underestimate the observed negative trends there, with the exception of CNRM-ESM2-0 and UKEMS1-0-LL
with the latter having a higher negative bias. At SH high latitudes, all models calculate large (in absolute terms) negative
trends, indicating that Antarctic ozone depletion is having a pronounced impact on ozone in the CMIP6 models. Overall, the
INTERACTIVE models have larger trends than those models without.

430  Over the period 2000-2014, most models show non-significant (at the 95% confidence level) positive trends in TCO. The
INTERACTIVE models show stronger positive trends in all regions, compared to the all-model mean. Significant and
substantial positive ozone trends occur in MRI-ESM2-0 and UKESM1-0-LL. Significant but weaker positive trends also occur
in SAM0-UNICON and CESM2 at SH high latitudes. Here, the significance is the consequence of small variability in those
models without interactive chemistry.

### 3.2 Long-term evolution of Total Column Ozone from 1850-2014

The regional evolution of zonal mean, annual mean TCO for the CMIP6 MMM from 1850-2100 is shown in Figure 7. For the near global mean (60°S-60°N), TCO increases slowly from ~300 DU in 1850 to ~305 DU in 1960, before rapidly declining through the 1980s and 1990s due to emissions of halogenated ODSs, reaching a minimum in the late 1990s. The increases in TCO are more prominent in the NH and tropics, while the decreases at the end of the 20th century are stronger in the SH. In the NH, TCO values increase by 20-30 DU between 1850 and 1960, and this increase is large enough that despite the emission of halogenated ODSs minimum NH mid-latitude TCO values in the late 1990s are larger than pre-industrial values. In contrast, SH TCO values remain relatively constant from 1850 to 1960, before rapidly declining throughout the 1970s and 1980s. The distinctive 11-year solar cycle in TCO is superimposed on these long-term. In addition, the eruption of Mt. Krakatoa in 1883 can be clearly seen as an increase in TCO of around 3-5 DU, resulting in the highest TCO values for ~100 years between 1850 and 1950.

There is poor agreement in the ability of the individual CMIP6 models to simulation pre-industrial TCO, which vary between 275 and 340 DU (Figure A2). The UKESM1-0-LL and MRI-ESM2-0 models are particularly high, while the GFDL-CM4 values are lowest. Surprisingly, there is a ~20 DU range in pre-industrial TCO values between those models prescribing the CMIP6 ozone dataset. When TCO values from each CMIP6 model are normalised to the 1960 annual mean value (Figure A3), there is a smaller difference between the modelled pre-industrial TCO values, which cover ±5 DU around the MMM. When the models are normalised to the 1960 annual mean, it is also clear that, compared to the CMIP6 MMM, the CNRM-CM6-1, CNRM-ESM2-1 and UKESM1-0-LL models have much stronger ozone declines during the period of halogenated ODS emissions (globally for the UKESM1-0-LL model and in the NH for the CNRM-CM6-1 and CNRM-ESM2-1 models), while the MRI-ESM2-0 model has much weaker TCO declines during this time.

Zonal mean, annual mean partial ozone columns for the full stratosphere, upper stratosphere and lower stratosphere, averaged from 90°S-90°N, for a subset of the models are shown in Figure 8. These partial column values indicate that stratospheric ozone, in both the lower and upper stratosphere, did not change significantly between 1850 and 1960, suggesting that the increases in TCO seen in Figure 8 arise from changes in tropospheric ozone. It is also clear from Figure 8 that much of the high TCO bias for the UKESM1-0-LL model (Figure A2) comes from elevated stratospheric ozone mixing ratios, rather than a large tropospheric ozone bias.

Climatological differences between the present day (2000-2014 average) and the preindustrial (1850-1864) zonal mean ozone mixing ratios and TCO values are shown in Figure 9. The expected general decrease in stratospheric ozone due to ODS-induced stratospheric ozone depletion (e.g. Keeble et al., 2014; Iglesias-Suarez et al., 2016) as well as a general increase in ozone in the troposphere due to the emission of ozone precursors (e.g. Stevenson et al., 2013; Young et al., 2013, 2018) are clearly captured by the CMIP6 MMM. The historical decrease in stratospheric ozone is most pronounced in the SH polar

vortex, with the maximum TCO decrease during SH spring due to the role of heterogeneous activation of chlorine reservoir species on polar stratospheric clouds (e.g. Solomon et al., 1999). In absolute values, the decreases in stratospheric ozone mixing ratios dominate over the larger fractional tropospheric ozone changes in terms of the integrated number of ozone molecules in a vertical column, leading to historically globally reduced TCO. However, there is a pronounced seasonal cycle in these

470 changes and a clear difference between the hemispheres, with widespread ozone decreases throughout the year in the SH but small TCO increases at high latitudes in the NH during the summer and autumn.

### 3.3 Long-term evolution from 2015-2100

From 2015 onwards, models follow the assumptions made in the various SSP scenarios. Most models which performed the historical simulations also provided ozone data from SSP1-2.6, SSP2-4.5, SSP3-7.0 and SSP5-8.5, while a much smaller

475 number provided data from SSP1-1.9, SSP4-3.4 and SSP4-6.0 (see Table 1 for an overview of which models performed which SSP scenarios). Due to the different numbers of models performing each scenario, the MMM for each SSP is normalised to the 2014 value to produce one smooth dataset and allow for comparison between the trajectories of TCO under each SSP scenario.

Zonal mean, annual mean CMIP6 MMM TCO, averaged over 60°S-60°N, is projected in the simulations evaluated here to

480 follow three main trajectories from 2015 to 2100 (Figure 7). Under SSP2-4.5, SSP4-3.4 and SSP4-6.0 TCO values are projected to return to their 1960's values by the middle of the 21$^{st}$ century, while under the SSP3-7.0 and SSP5-8.5 scenarios TCO values are projected to significantly exceed the 1960's values throughout the latter half of the 21$^{st}$ century. Despite the assumption that halogenated ODSs will continue to decline due to the Montreal Protocol, TCO values are not projected to return to the 1960's values under the SSP1-1.9 and SSP1-2.6 scenarios.

485 As for 60°S-60°N, SSP pathways which assume higher radiative forcing result in higher TCO at the end of the century for most latitude ranges (Figure 7), although the timing of the return of TCO to 1960's values varies. Annual mean TCO values at high southern latitudes are only projected to return to the 1960's values in the SSP3-7.0 and SSP5-8.5 scenarios. Conversely, TCO is projected to return to, and in most cases exceed, the 1960 annual mean value in all SSPs in the high northern latitudes. In the mid-latitudes, projected TCO values follow a pattern similar to those seen in the near global mean, although in the NH

490 TCO is projected to return to the 1960s value in the SSP1-2.6 scenario and exceed the 1960 value under most other scenarios. Interestingly, in the NH mid- and high-latitudes the 1980 annual mean TCO is larger than that of the 1960 annual mean, and as a result NH TCO values are projected to return to the 1980 values after returning to 1960 values. However, TCO projections in the tropics are quite different to those at other latitudes, with return to 1960's values only projected to occur in SSP3-7.0 and SSP5-8.5, and under the SSP5-8.5 scenario TCO values are projected to decline again in the latter half of century

495 (consistent with an acceleration of the BDC, e.g. Meul et al., 2016; Keeble et al., 2017).

Climatological differences between the end of the century (2086-2100 average) and the present day (2000-2014 average) zonal mean ozone mixing ratios and TCO values are shown in Figure 10 for SSP1-2.6, SSP2-4.5, SSP3-7.0 and SSP5-8.5. Under each of these SSP scenarios, ozone mixing ratios in the upper stratosphere and SH polar lower stratosphere are projected to increase consistent with the decline in halogenated ODSs assumed in all scenarios. The magnitude of the upper stratospheric

500   increases in ozone is larger for scenarios which project large increases in GHG loading of the atmosphere due to the resulting $CO_2$-induced cooling of the stratosphere. However, significant differences between the scenarios are seen in the troposphere and tropical lower stratosphere. Under the SSP1-2.6 and SSP2-4.5 scenarios, tropospheric ozone mixing ratios are projected to decrease, consistent with the large reduction in the emission of ozone precursors assumed in these scenarios (Gidden et al., 2019). Under SSP1-2.6 the decreases in tropospheric ozone are particularly strong in the NH, while the increases in

505   stratospheric ozone outside of the Antarctic polar lower stratosphere are smaller than in other scenarios (consistent with less $CO_2$ induced cooling), and together these factors explain why TCO does not return to 1960 values in SSP1 scenarios. Strong emissions mitigation scenarios which decrease tropospheric ozone mixing ratios and thereby help to mitigate climate change and air quality impacts, slow or prevent ozone recovery, as measured by the return of TCO return to historic values. This calls into question whether using TCO return dates as a metric for ozone recovery and the success of the Montreal Protocol is

510   entirely appropriate to evaluate the success of the Montreal Protocol, and if other metrics might not better reflect the recovery of stratospheric ozone driven by changes in stratospheric chlorine loading (as discussed by Eyring et al., 2013; WMO 2018).

In contrast, ozone mixing ratios are projected to increase throughout much of the troposphere and upper stratosphere in the SSP3-7.0 and SSP5-8.5 scenarios, explaining the projected super-recovery of TCO values in the mid- and high-latitudes under these scenarios by the end of the century. However, ozone mixing ratios are projected to be lower in the tropical lower

515   stratosphere by the end of the century (Figure 10) due in part to the acceleration of the BDC and reduced production of ozone at these altitudes due to the thicker overhead column (Eyring et al., 2013; Meul et al., 2016; Keeble et al., 2017). These lower stratospheric decreases offset the increases at higher altitudes, resulting in TCO values being lower at the end of the 21$^{st}$ century compared to the present day under most emissions scenarios, despite reductions in stratospheric halogens.

## 4 Stratospheric Water Vapor

520   As with ozone, before investigating long-term changes in stratospheric water vapor we evaluate each model's performance, and the performance of the CMIP6 MMM, against observations. In the following sections we evaluate the 2000-2014 climatological zonal mean distribution of water vapor against the SWOOSH combined dataset and evaluate the source of stratospheric water vapor from CH4 oxidation.

## 4.1 Evaluation of recent changes

525 Ten of the models used in this study provide stratospheric water vapor output from the historical simulations, with a smaller subset providing water vapor from the SSP scenarios (see Table 1). Zonal mean water vapor volume mixing ratios for each CMIP6 model, the CMIP6 MMM and the SWOOSH dataset, average over the years 2000-2014, are shown in Figure 11. There is relatively poor agreement between the individual CMIP6 models and the observations. The CESM2, CESM2-WACCM and MRI-ESM2-0 models all capture the distribution of stratospheric water vapor mixing ratios reasonably well, with the largest

530 percentage differences in the polar regions, most likely related to the formation and sedimentation of polar stratospheric cloud particles. Several models (BCC-CSM2-MR, BCC-ESM1, GFDL-CM4 and IPSL-CM6-LR) do not accurately capture the increase in water vapor with altitude throughout the stratosphere, as these models do not include a representation of water vapor produced from $CH_4$ oxidation. In contrast, CNRM-CM6-1 and CNRM-ESM2-1 simulate very large changes in stratospheric water vapor between the tropical lower stratosphere and upper stratosphere, consistent with an overestimate in

535 the water vapor production from $CH_4$ oxidation in the CNRM-ESM2-1 model (discussed below). Water vapor mixing ratios in the UKESM1-0-LL model are biased high throughout the stratosphere compared to the SWOOSH dataset. Differences between the individual models and the CMIP6 MMM are shown in Figure A4.

As for ozone mixing ratios, models have typically performed poorly in simulating water vapor mixing ratios in the tropical tropopause region. Gettelman et al. (2010), show the seasonal cycle of water vapor at 80 hPa from 16 models involved in the

540 CCMVal-2 inter-comparison project, and while there is good agreement between the CMIP6 MMM and the observations, there is a large spread in model mixing ratios, and many models do not accurately capture the seasonal cycle. Climatological (2000-2014) tropical stratospheric water vapor mixing ratios (average over 15°S to 15°N) at 70hPa, which lies just above the cold point entry into the stratosphere, are shown for the CMIP6 models in Figure 13. There is reasonable agreement between the seasonality of the CMIP6 MMM and that calculated for the SWOOSH combined dataset, although the CMIP6 MMM is

545 between 0.5-1.0 ppm lower than the observations throughout the annual cycle and the minima and maxima in the seasonal cycle both occur a few months earlier in the MMM than in the observations. However, individual models display a wide range of water vapor concentrations (between 1.5-6 ppm). As seen in Figure 11, the UKESM1-0-LL model has high stratospheric water vapor mixing ratios compared to the SWOOSH dataset but captures the seasonal cycle well, while the IPSL-CM6A-LR, CNRM-CM6-1 and CNRM-ESM2-1 models all have much lower stratospheric water vapor mixing ratios and muted seasonal

550 cycles.

The correlation between water vapor and $CH_4$ mixing ratios can be used to infer the stratospheric water vapor source from $CH_4$ oxidation in each model. Based on observations and chemical understanding, 2 molecules of stratospheric water vapor will be produced for every molecule of $CH_4$ oxidised (LeTexier et al., 1988). Given this oxidation, typical water vapor mixing ratios of ~3.5 ppm at the tropical tropopause and mean tropospheric mixing ratios of $CH_4$ ~1.75 ppm, it is expected that

555    throughout the tropical stratosphere $H_2O$ will equal $7.0-2.0*CH_4$ (SPARC, 2010). Observations made by ACE and MIPAS
satellites support this expected gradient (e.g. Archibald et al., 2019).

Of the models evaluated here, output of both water vapor and $CH_4$ mixing ratios are available from six: BCC-CSM2-MR,
BCC-ESM1, CESM2-WACCM, CNRM-ESM2-1, MRI-ESM2-0 and UKESM1-0-LL. Even from this small sample, it is clear
that there is a wide range in the complexity and accuracy of modelling $H_2O$ formed from the oxidation of $CH_4$. Neither BCC-
560    CSM2-MR nor BCC-ESM1 includes stratospheric water vapor production from $CH_4$ oxidation, and so $H_2O$ does not increase
as $CH_4$ decreases. Other models capture the relationship, $H2O = 7.0-2.0*CH_4$, to greater or lesser extents. UKESM1-0-LL and
MRI-ESM2-0 slightly under produce $H_2O$ from CH4, while stratospheric water vapor increases too rapidly for every molecule
of $CH_4$ oxidised in the CNRM-ESM2-1 model. These differences in the treatment of CH4 oxidation has important
consequences for estimates of methane's impact on the climate system and for future radiative forcing calculations, particularly
565    under high $CH_4$ emissions scenarios (e.g. SSP3-7.0).

**4.2 Long-term evolution from 1850-2014**

The evolution of annual mean water vapor mixing ratios at 70 hPa, averaged from 15°S-15°N, in the CMIP6 MMM and
individual CMIP6 models is shown in Figure 15. Water vapor mixing ratios are simulated to have remained relatively constant
at just below 3 ppm from 1850 to ~1950, before slowly increasing throughout the latter half of the 20th century and first decades
570    of the 21st century. However, there is broad disagreement between the individual CMIP6 models throughout the historical
period, with simulated stratospheric water vapour mixing ratios varying between 1.5-5.5 ppm in the pre-industrial period.

During this time, the largest variations in water vapor mixing ratios are associated with large magnitude volcanic eruptions,
which by increasing TTL temperatures result in increased annual mean water vapor mixing ratios by up to 0.5 ppm. However,
the individual models show very different sensitivities to volcanic eruptions, with very large increases in water vapor mixing
575    ratios following eruptions in the MRI-ESM2-0 and BCC-CSM2-MR models, more muted responses in the BCC-ESM1,
UKESM-0-LL, CESM2, CESM2-WACCM, CNRM-CM6-1 and CNRM-ESM2-1 models, and almost no response in the
GFDL-CM4 and IPSL-ESM2-0 models.

To understand the long-term trends in stratospheric water vapor, it is instructive to analyse changes in temperature in the
tropics at 100 hPa, which is close to the cold point and so controls the entry values of water vapor into the stratosphere. Long-
580    term changes in CMIP6 MMM 100 hPa temperatures, averaged from 15°S-15°N, are shown in Figure 16. The rise in 70 hPa
water vapor mixing ratios in the latter part of the 20th century, and following volcanic eruptions, can be attributed to the increase
in temperature at the 100 hPa level. In the CMIP6 MMM, TTL temperatures have increased by ~1 K between 1850 and 2014,
and can rise by 1-2 K following explosive volcanic eruptions.

Climatological annual mean, zonal mean $H_2O$ mixing ratio differences between the present day (2000-2014 averaged) and pre-
585  industrial (1850-1864 averaged) periods are shown in Figure 17. Simulated stratospheric water vapor mixing ratios have
increased between the pre-industrial and present-day periods throughout the stratosphere. In the lower stratosphere, this
increase is ~0.2-0.4 ppm, consistent with the increase in water vapour mixing ratios seen at 70 hPa in the tropics, and reflects
the warming of the cold point between pre-industrial and present-day. However, the increase in stratospheric water vapor
mixing ratios increases with altitude and is largest in the upper stratosphere (~0.8 ppm), reflecting increased $CH_4$ mixing ratios
590  and resulting increases in $H_2O$ mixing ratios formed from $CH_4$ oxidation.

**4.3 Long-term evolution from 2015-2100**

An increase in stratospheric water vapor concentrations under climate change is projected by virtually all climate models
(Gettelman et al. 2010; Smalley et al. 2017; Banerjee et al. 2019). Eyring et al. (2010) calculate a mean increase of 0.5-1 ppm
per century in stratospheric water vapor concentrations for models involved in the CCMVal-2 inter-comparison project,
595  although agreement between models on the absolute increase is poor. The increase is likely due to the prevailing effect of a
warming troposphere over other driving factors (Dessler et al. 2013; Smalley et al. 2017), and represents a climate feedback,
as the associated radiative effect of the increases are correlated with increasing surface temperatures (Banerjee et al. 2019).
Here we find consistent results, with increasing stratospheric water vapor concentrations under each SSP scenario of climate
change (Figure 15). The magnitude of the increases generally follows the radiative forcing across the scenarios (and thus the
600  degree of tropospheric warming). Low forcing scenarios (SSP1-1.9 and SSP1-2.6) project increasing stratospheric water vapor
until the middle of the century and then a stabilization to around 3.5 ppm. Middle of the road scenarios (SSP2-4.5, SSP4-6.0
and SSP4-3.4) reach around 4 ppm by 2100. High forcing scenarios (SSP3-7.0 and SSP5-8.5) show rapid increases in
stratospheric water vapor throughout the century, reaching around 5 ppm by 2100.

As for the historical changes explored in section 4.2, projected changes in water vapor mixing ratios at 70 hPa are strongly
605  correlated with simulated changes to 100 hPa temperatures (compare Figures 15 and 16). In general, the higher the assumed
GHG emissions in the SSP scenario, the larger the projected 100 hPa temperatures by the end of the century. Under SSP1-1.9
and SSP1-2.6, 100 hPa temperatures are projected to remain relatively close to present day values but are projected to increase
by ~4.5 K under the SSP5-8.5 scenario.

Climatological annual mean, zonal mean $H_2O$ mixing ratio differences between the end of the century (2086-2100 averaged)
610  and present day (2000-2014 averaged) periods for SSP1-2.6, SSP2-4.5, SSP3-7.0 and SSP5-8.5 are shown in Figure 18. Under
the SSP1-2.6 scenario, stratospheric water vapor mixing ratios are projected to remain close to present day values throughout
the stratosphere. However, in all other scenarios shown in Figure 18, stratospheric water vapor is projected to increase due to
the increases in projected 100 hPa temperatures and due to increased $CH_4$ mixing ratios (particularly under SSP3-7.0, the

scenario which assumes the largest increases in $CH_4$ emissions, which shows larger stratospheric water vapor increases in the
615 upper stratosphere due to increased water vapor production from $CH_4$ oxidation).

## 5 Discussion and conclusions

This study presents an evaluation of stratospheric ozone and water vapor changes from the pre-industrial to the end of the 21$^{st}$
century in simulations performed by CMIP6 models under a range of future SSP scenarios. In total, for the historical period
1850-2014 ozone data was available from 14 models, while water vapor data was available from 10, and a subset of these
620 models had also performed simulations under several SSP scenarios.

For zonal mean stratospheric ozone mixing ratios there is good agreement between the CMIP6 MMM and observations from
the SWOOSH combined dataset, with biases within ±10%, while for TCO there is good agreement between the CMIP6 MMM
and the NIWA-BS dataset from 40°S-90°N, with biases within ±20 DU (<±10%). Largest percentage zonal mean ozone mixing
ratios biases occur in the tropical upper stratosphere, while for TCO the largest biases occur between 90°S-40°S. However,
625 despite the agreement between the CMIP6 MMM and the observations, there are significant differences between the individual
CMIP6 models.

From 1850 to 1960, global TCO in the CMIP6 MMM increased from 300 DU to 305 DU, before rapidly declining through the
1970s and 1980s with the onset of halogenated ODS emissions. TCO increases in the early part of the historical period were
driven by increases in tropospheric ozone, particularly in the NH. Superimposed on the long-term trend is the 11-year solar
630 cycle, which causes TCO averaged from 60°S-60°N to vary by around ±1 DU, while the 1883 eruption of Krakatoa caused
TCO values to increase by around 3-5 DU and resulted in the highest TCO values for ~100 years between 1850 and 1950.
However, there is poor agreement between the individual CMIP6 models in the pre-industrial and throughout the historical
period, with model TCO values spread across a range of ~60 DU.

For the future period, from 2015-2100, the higher the forcing pathway assumed by the various SSPs evaluated here, the higher
635 the TCO at the end of the century. Annual mean TCO at most latitudes is projected to return to the 1960s values by the middle
of the 21$^{st}$ century, and under the SSP3-7.0 and SSP5-8.5 scenarios significant increases above the 1960s value is simulated,
driven in part by the decline in ODS concentrations, large increases in ozone mixing ratios in the upper stratosphere associated
with $CO_2$ cooling and increases in the tropospheric ozone mixing ratios. However, TCO values are not projected to return to
the 1960's values at most latitude ranges in the SSP1-1.9 and SSP1-2.6 scenarios, due, in part, to smaller ozone mixing ratio
640 increases in the stratosphere, consistent with reduced $CO_2$ induced cooling, and strong decreases in tropospheric ozone mixing
ratios throughout the troposphere, driven by reductions in the emission of ozone precursors. While decreases in tropospheric
ozone prevent TCO from returning to 1960's values, the decrease is undoubtedly a positive result for air quality, and perhaps

calls into question whether TCO values are an accurate measure of stratospheric ozone recovery, or if other metrics can more accurately reflect the profile changes expected for stratospheric ozone recovery without being influenced by tropospheric changes.

Stratospheric water vapor mixing ratios are poorly represented in many of the CMIP6 models investigated in this study. For the climatological 2000-2014 period, the models are dry biased, particularly in the upper stratosphere. This results from several of the models studied here not including any representation of water vapor formed from the oxidation of $CH_4$ in the stratosphere. The seasonal cycle and water vapor mixing ratios for individual CMIP6 models at 70 hPa in the tropics shows poor agreement with the SWOOSH dataset, and further highlights the difficulties climate models have had over several generations of model intercomparison projects in the tropical tropopause region. Despite this, when averaged together the CMIP6 MMM agrees reasonably well with the observed climatological seasonal cycle.

For the CMIP6 MMM, 70 hPa water vapor mixing ratios remain relatively constant from 1850 to 1950, before slowly increasing to 2014. During this period, the largest variations in water vapor mixing ratios occur at the time of major volcanic eruptions. From 2014, tropical water vapor mixing ratios at 70 hPa are projected to increase under all SSP scenarios, with the magnitude of the increases generally following the radiative forcing across the scenarios. Under SSP1-1.9 and SSP1-2.6 water vapor mixing ratios are projected to increase from 3.2 ppm to 3.5 ppm by the middle of the $21^{st}$ century before stabilising, while under SSP3-7.0 and SSP5-8.5 water vapor mixing ratios show rapid increases throughout the century, reaching around 5 ppm by the 2100.

The data available from the CMIP6 models evaluated here do not allow for thorough investigation into the drivers of the changes identified here. In addition, the models evaluated here span a broad range of complexity, and so it is likely that modelled stratospheric ozone and water vapor mixing ratios have different sensitivity to changes in emissions. It is hoped that new datasets generated by models performing AerChemMIP simulations will provide greater insight into the wider chemical changes occurring throughout the atmosphere, including changes to stratospheric catalytic loss cycles and water vapor produced through $CH_4$ oxidation.

## 6 Acknowledgements

We acknowledge the World Climate Research Programme, which, through its Working Group on Coupled Modelling, coordinated and promoted CMIP6. We thank the climate modeling groups for producing and making available their model output, the Earth System Grid Federation (ESGF) for archiving the data and providing access, and the multiple funding agencies who support CMIP6 and ESGF. JK and PTG thank NERC for financial support through NCAS. BH was supported by the European Union's Horizon 2020 Framework Programme for Research and Innovation "Coordinated Research in Earth Systems and Climate: Experiments, kNowledge, Dissemination and Outreach (CRESCENDO)" project under Grant

Agreement No. 641816. GZ and OM were supported by the NZ Government's Strategic Science Investment Fund (SSIF) through the NIWA programme CACV. We thank the GFDL model development team, who led the development of GFDL-CM4 and GFDL-ESM4, as well as the numerous scientists and technical staff at GFDL who contributed to the development of these models and conducted the CMIP6 simulations used here.

# References

Archibald, A. T., O'Connor, F. M., Abraham, N. L., Archer-Nicholls, S., Chipperfield, M. P., Dalvi, M., Folberth, G. A., Dennison, F., Dhomse, S. S., Griffiths, P. T., Hardacre, C., Hewitt, A. J., Hill, R., Johnson, C. E., Keeble, J., Köhler, M. O., Morgenstern, O., Mulchay, J. P., Ordóñez, C., Pope, R. J., Rumbold, S., Russo, M. R., Savage, N., Sellar, A., Stringer, M., Turnock, S., Wild, O., and Zeng, G.: Description and evaluation of the UKCA stratosphere-troposphere chemistry scheme (StratTrop vn 1.0) implemented in UKESM1, Geosci. Model Dev. Discuss., https://doi.org/10.5194/gmd-2019-246, in review, 2019.

Austin, J., Horowitz, L. W., Schwarzkopf, M. D., Wilson, R. J., and Levy, H.: Stratospheric ozone and temperature simulated from the preindustrial era to the present day, J. Clim., 26, 3528–3543, doi:10.1175/JCLI-D-12-00162.1, 2013.

Avallone, L. M. and Prather, M. J.: Photochemical evolution of ozone in the lower tropical stratosphere, J. Geophys. Res., 101, 1457–1461, https://doi.org/10.1029/95JD03010, 1996.

Bader, David C.; Leung, Ruby; Taylor, Mark; McCoy, Renata B. (2019). E3SM-Project E3SM1.0 model output prepared for CMIP6 CMIP historical. Version 20191101 Earth System Grid Federation. https://doi.org/10.22033/ESGF/CMIP6.4497

Banerjee, A., Chiodo, G., Previdi, M., Ponater, M., Conley, A. J., and Polvani, L. M.: Stratospheric water vapor: An important climate feedback. Climate Dynamics, 53, 1697-1710. https://doi.org/10.1007/s00382-019-04721-4, 2019.

Bates, D. R. and Nicolet, M.: The photochemistry of atmospheric water vapor, J. Geophys. Res., 55, 301–327, https://doi.org/10.1029/JZ055i003p00301, 1950.

Boucher, Olivier; Denvil, Sébastien; Caubel, Arnaud; Foujols, Marie Alice (2018). IPSL IPSL-CM6A-LR model output prepared for CMIP6 CMIP historical. Version 20191101 Earth System Grid Federation. https://doi.org/10.22033/ESGF/CMIP6.5195

Boucher, Olivier; Denvil, Sébastien; Caubel, Arnaud; Foujols, Marie Alice (2019). IPSL IPSL-CM6A-LR model output prepared for CMIP6 ScenarioMIP ssp119. Version 20191101 Earth System Grid Federation. https://doi.org/10.22033/ESGF/CMIP6.5261

700 Boucher, Olivier; Denvil, Sébastien; Caubel, Arnaud; Foujols, Marie Alice (2019). IPSL IPSL-CM6A-LR model output prepared for CMIP6 ScenarioMIP ssp126. Version 20191101 Earth System Grid Federation. https://doi.org/10.22033/ESGF/CMIP6.5262

Boucher, Olivier; Denvil, Sébastien; Caubel, Arnaud; Foujols, Marie Alice (2019). IPSL IPSL-CM6A-LR model output prepared for CMIP6 ScenarioMIP ssp245. Version 20191101 Earth System Grid Federation.
705 https://doi.org/10.22033/ESGF/CMIP6.5264

Boucher, Olivier; Denvil, Sébastien; Caubel, Arnaud; Foujols, Marie Alice (2019). IPSL IPSL-CM6A-LR model output prepared for CMIP6 ScenarioMIP ssp370. Version 20191101 Earth System Grid Federation. https://doi.org/10.22033/ESGF/CMIP6.5265

Boucher, Olivier; Denvil, Sébastien; Caubel, Arnaud; Foujols, Marie Alice (2019). IPSL IPSL-CM6A-LR model output
710 prepared for CMIP6 ScenarioMIP ssp434. Version 20191101 Earth System Grid Federation. https://doi.org/10.22033/ESGF/CMIP6.5267

Boucher, Olivier; Denvil, Sébastien; Caubel, Arnaud; Foujols, Marie Alice (2019). IPSL IPSL-CM6A-LR model output prepared for CMIP6 ScenarioMIP ssp460. Version 20191101 Earth System Grid Federation. https://doi.org/10.22033/ESGF/CMIP6.5268

715 Braesicke, P., Keeble, J., Yang, X., Stiller, G., Kellmann, S., Abraham, N. L., Archibald, A., Telford, P., and Pyle, J. A.: Circulation anomalies in the SH and ozone changes, Atmos. Chem. Phys., 13, 10677–10688, https://doi.org/10.5194/acp-13-10677-2013, 2013.

Brasseur, G. and Solomon, S.: Aeronomy of the Middle Atmosphere, D. Reidel Publishing Company, Dordrecht, 1984.

Brewer, A. W. and Wilson, A. W.: The regions of formation of atmospheric ozone, Q. J. Roy. Meteor. Soc., 94, 249-265,
720 https://doi.org/10.1002/qj.49709440103, 1968.

Brewer, A. W.: Evidence for a world circulation provided by the measurements of helium and water vapor distribution in the stratosphere, Q. J. Roy. Meteor. Soc., 75, 351–363, 1949.

Butchart, N., Cionni, I., Eyring, V., Shepherd, T. G., Waugh, D. W., Akiyoshi, H., Austin, J., Brühl, C., Chipperfield, M. P., Cordero, E., Dameris, M., Deckert, R., Dhomse, S., Frith, S. M., Garcia, R. R., Gettelman, A., Giorgetta, M. A., Kinnison, D.
725 E., Li, F., Mancini, E., Mclandress, C., Pawson, S., Pitari, G., Plummer, D. A., Rozanov, E., Sassi, F., Scinocca, J. F., Shibata, K., Steil, B., and Tian, W.: Chemistry-climate model simulations of twentyfirst century stratospheric climate and circulation changes, J. Climate, 23, 5349–5374, https://doi.org/10.1175/2010JCLI3404.1, 2010.

Butchart, N., Scaife, A. A., Bourqui, M., de Grandpre, J., Hare, S. H. E., Kettleborough, J., Langematz, U., Manzini, E., Sassi, F., Shibata, K., Shindell, D., and Sigmond, M.: Simulations of anthropogenic change in the strength of the Brewer–Dobson circulation, Clim. Dynam., 27, 727–741, 2006.

Chapman, S.: A Theory of Upper-Atmospheric Ozone, Memories of Royal Meteorological Society, 3, 103–125, 1930.

Checa-Garcia, R., Hegglin, M. I., Kinnison, D., Plummer, D. A., and Shine, K. P.: Historical Tropospheric and Stratospheric Ozone Radiative Forcing Using the CMIP6 Database, Geophys. Res. Lett., 45, 3264–3273, https://doi.org/10.1002/2017GL076770, 2018.

Chiodo, G., Polvani, L.M., Marsh, D.R., Ball, W., Muthers, S., Stenke, A., Rozanov, E., and Tsigaridis, K.: The ozone response to quadrupled CO2 concentrations. J. Climate, 31, no. 10, 3893-3907, doi:10.1175/JCLI-D-17-0492.1, 2018.

Cionni, I., Eyring, V., Lamarque, J. F., Randel, W. J., Stevenson, D. S., Wu, F., Bodeker, G. E., Shepherd, T. G., Shindell, D. T., and Waugh, D. W.: Ozone database in support of CMIP5 simulations: results and corresponding radiative forcing, Atmos. Chem. Phys., 11, 11267–11292, https://doi.org/10.5194/acp-11-11267-2011, 2011.

Collins, W. J., Lamarque, J.-F., Schulz, M., Boucher, O., Eyring, V., Hegglin, M. I., Maycock, A., Myhre, G., Prather, M., Shindell, D., and Smith, S. J.: AerChemMIP: quantifying the effects of chemistry and aerosols in CMIP6, Geosci. Model Dev., 10, 585–607, https://doi.org/10.5194/gmd-10-585-2017, 2017.

Crutzen, P. J.: The influence of nitrogen oxides on the atmospheric ozone content, Q. J. Roy. Meteor. Soc., 96, 320–325, https://doi.org/10.1002/qj.49709640815, 1970.

Danabasoglu, G., J.-F. Lamarque, J. Bacmeister, D. A. Bailey, A. K. DuVivier, J. Edwards, L. K. Emmons, J. Fasullo, R. Garcia, A. Gettelman, C. Hannay, M. M. Holland, W. G. Large, D. M. Lawrence, J. T. M. Lenaerts, K. Lindsay, W. H. Lipscomb1, M. J. Mills, R. Neale, K. W. Oleson, B. Otto-Bliesner, A. S. Phillips, W. Sacks, S. Tilmes, L. van Kampenhout, M. Vertenstein, A. Bertini, J. Dennis, C. Deser, C. Fischer, B. Fox-Kemper, J. E. Kay, D. Kinnison, P. J. Kushner, M. C. Long, S. Mickelson, J. K. Moore, E. Nienhouse, L. Polvani, P. J. Rasch, and W. G. Strand, The Community Earth System Model version 2 (CESM2), submitted to Journal of Advances in Modeling Earth Systems.

Danabasoglu, Gokhan (2019). NCAR CESM2 model output prepared for CMIP6 ScenarioMIP ssp126. Version 20191101 Earth System Grid Federation. https://doi.org/10.22033/ESGF/CMIP6.7746

Danabasoglu, Gokhan (2019). NCAR CESM2 model output prepared for CMIP6 ScenarioMIP ssp245. Version 20191101 Earth System Grid Federation. https://doi.org/10.22033/ESGF/CMIP6.7748

Danabasoglu, Gokhan (2019). NCAR CESM2 model output prepared for CMIP6 ScenarioMIP ssp370. Version 20191101 Earth System Grid Federation. https://doi.org/10.22033/ESGF/CMIP6.7753

Danabasoglu, Gokhan (2019). NCAR CESM2 model output prepared for CMIP6 ScenarioMIP ssp585. Version 20191101 Earth System Grid Federation. https://doi.org/10.22033/ESGF/CMIP6.7768

Danabasoglu, Gokhan (2019). NCAR CESM2-WACCM model output prepared for CMIP6 CMIP historical. Version 20191101 Earth System Grid Federation. https://doi.org/10.22033/ESGF/CMIP6.10071

Danabasoglu, Gokhan (2019). NCAR CESM2-WACCM model output prepared for CMIP6 ScenarioMIP ssp126. Version 20191101 Earth System Grid Federation. https://doi.org/10.22033/ESGF/CMIP6.10100

Danabasoglu, Gokhan (2019). NCAR CESM2-WACCM model output prepared for CMIP6 ScenarioMIP ssp245. Version 20191101 Earth System Grid Federation. https://doi.org/10.22033/ESGF/CMIP6.10101

Danabasoglu, Gokhan (2019). NCAR CESM2-WACCM model output prepared for CMIP6 ScenarioMIP ssp370. Version 20191101 Earth System Grid Federation. https://doi.org/10.22033/ESGF/CMIP6.10102

Danabasoglu, Gokhan (2019). NCAR CESM2-WACCM model output prepared for CMIP6 ScenarioMIP ssp585. Version 20191101 Earth System Grid Federation. https://doi.org/10.22033/ESGF/CMIP6.10115

Danabasoglu, Gokhan; Lawrence, David; Lindsay, Keith; Lipscomb, William; Strand, Gary (2019). NCAR CESM2 model output prepared for CMIP6 CMIP historical. Version 20191101 Earth System Grid Federation. https://doi.org/10.22033/ESGF/CMIP6.7627

Davis, S. M., Rosenlof, K. H., Hassler, B., Hurst, D. F., Read, W. G., Vömel, H., Selkirk, H., Fujiwara, M., and Damadeo, R.: The Stratospheric Water and Ozone Satellite Homogenized (SWOOSH) database: a long-term database for climate studies, Earth System Science Data, 8, 461–490, doi:10.5194/essd-8-461-2016, 2016.

Dessler, A. E., Schoeberl, M. R., Wang, T., Davis, S. M., and Rosenlof, K. H.: Stratospheric water vapor feedback, PNAS, 110, 18 087–18 091, https://doi.org/10.1073/pnas.1310344110, 2013.

Dessler, A. E., Ye, H., Wang, T., Schoeberl, M. R., Oman,L. D., Douglass, A. R., Butler, A. H., Rosenlof, K. H., Davis, S. M., and Portmann, R. W.: Transport of ice into the stratosphere and the humidification of the stratosphere over the 21st century, Geophys. Res. Lett., 43, 2323–2329, https://doi.org/10.1002/2016GL067991, 2016.

Deushi, M., and K. Shibata, 2011, Pap. Meteor. Geophys., 62, 1−46, https://doi.org/10.2467/mripapers.62.1

Dhomse, S., Feng, W., Montzka, S. A., Hossaini, R., Keeble, J., Pyle, J. A., Daniel, J. S., Chipperfield, M. P.: How much longer will there be an Antarctic ozone hole? Impact of unexpected chlorine emissions, submitted to Nature Communications, 2019.

Dhomse, S., Kinnison, D., Chipperfield, M. P., Cionni, I., Hegglin, M., Abraham, N. L., Akiyoshi, H., Archibald, A. T., Bednarz, E. M., Bekki, S., Braesicke, P., Butchart, N., Dameris, M., Deushi, M., Frith, S., Hardiman, S. C., Hassler, B.,

Horowitz, L. W., Hu, R.-M., Jöckel, P., Josse, B., Kirner, O., Kremser, S., Langematz, U., Lewis, J., Marchand, M., Lin, V., Mancini, E., Marécal, V., Michou, M., Morgenstern, O., O'Connor, F. M., Oman, L., Pitari, G., Plummer, D. A., Pyle, J. A., Revell, L. E., Rozanov, E., Schofield, R., Stenke, A., Stone, K., Sudo, K., Tilmes, S., Visioni, D., Yamashita, Y., Zeng, G.: Estimates of ozone return dates from Chemistry-Climate Model Initiative simulations, Atmos. Chem. Phys., 18, 8409–8438, https://doi.org/10.5194/acp-18-8409-2018, 2018.

Dunne, J.P., et al.: The GFDL Earth System Model version 4.1 (GFDL-ESM4.1): Model description and simulation characteristics, in prep.

Eyring, V., Arblaster, J. M., Cionni, I., Sedláček, J., Perlwitz, J., Young, P. J., Bekki, S., Bergmann, D., Cameron-Smith, P., Collins, W. J., Faluvegi, G., Gottschaldt, K.-D., Horowitz, L. W., Kinnison, D. E., Lamarque, J.-F., Marsh, D. R., Saint-Martin, D., Shindell, D. T., Sudo, K., Szopa, S., and Watanabe, S.: Long-term ozone changes and associated climate impacts in CMIP5 simulations, J. Geophys. Res.-Atmos., 118, 5029-5060, doi:10.1002/jgrd.50316, 2013.

Eyring, V., Bock, L., Lauer, A., Righi, M., Schlund, M., Andela, B., Arnone, E., Bellprat, O., Brötz, B., Caron, L.-P., Carvalhais, N., Cionni, I., Cortesi, N., Crezee, B., Davin, E., Davini, P., Debeire, K., de Mora, L., Deser, C., Docquier, D., Earnshaw, P., Ehbrecht, C., Gier, B. K., Gonzalez-Reviriego, N., Goodman, P., Hagemann, S., Hardiman, S., Hassler, B., Hunter, A., Kadow, C., Kindermann, S., Koirala, S., Koldunov, N. V., Lejeune, Q., Lembo, V., Lovato, T., Lucarini, V., Massonnet, F., Müller, B., Pandde, A., Pérez-Zanón, N., Phillips, A., Predoi, V., Russell, J., Sellar, A., Serva, F., Stacke, T., Swaminathan, R., Torralba, V., Vegas-Regidor, J., von Hardenberg, J., Weigel, K., and Zimmermann, K.: ESMValTool v2.0 – Extended set of large-scale diagnostics for quasi-operational and comprehensive evaluation of Earth system models in CMIP, Geosci. Model Dev. Discuss., https://doi.org/10.5194/gmd-2019-291, in review, 2019.

Eyring, V., Bony, S., Meehl, G. A., Senior, C. A., Stevens, B., Stouffer, R. J., and Taylor, K. E.: Overview of the Coupled Model Intercomparison Project Phase 6 (CMIP6) experimental design and organization, Geosci. Model Dev., 9, 1937–1958, https://doi.org/10.5194/gmd-9-1937-2016, 2016.

Eyring, V., Cionni, I., Bodeker, G. E., Charlton-Perez, A. J., Kinnison, D. E., Scinocca, J. F., Waugh, D. W., Akiyoshi, H., Bekki, S., Chipperfield, M. P., Dameris, M., Dhomse, S., Frith, S. M., Garny, H., Gettelman, A., Kubin, A., Langematz, U., Mancini, E., Marchand, M., Nakamura, T., Oman, L. D., Pawson, S., Pitari, G., Plummer, D. A., Rozanov, E., Shepherd, T. G., Shibata, K., Tian, W., Braesicke, P., Hardiman, S. C., Lamarque, J. F., Morgenstern, O., Pyle, J. A., Smale, D., and Yamashita, Y.: Multimodel assessment of stratospheric ozone return dates and ozone recovery in CCMVal-2 models, Atmos. Chem. Phys., 10, 9451-9472, https://doi.org/10.5194/acp-10-9451-2010, 2010.

Fueglistaler, S. and Haynes, P. H.: Control of interannual and longer-term variability of stratospheric water vapor, J. Geophys. Res., 110, https://doi.org/10.1029/2005JD006019, 2005.

Gettelman, A. et al.: The Whole Atmosphere Community Climate Model Version 6 (WACCM6), J Geophys Res-Atmos, 121(22), 10,328, doi:10.1029/2019JD030943, 2019.

Gettelman, A., Hegglin, M. I., Son, S.-W., Kim, J., Fujiwara, M., Birner, T., Kremser, S., Rex, M., J. A., Akiyoshi, H., Austin, J., Bekki, S., Braesicke, P., Brühl, C., Butchart, N., Chipperfield, M., Dameris, M., Dhomse, S., Garny, H., Hardiman, S. C., JöCkel, P., Kinnison, D. E., Lamarque, J. F., Mancini, E., Marchand, M., Michou, M., Morgenstern, O., Pawson, S., Pitari, G., Plummer, D., Pyle, J. A., Rozanov, E., Scinocca, J., Shepherd, T. G., Shibata, K., Smale, D., TeyssèDre, H., and Tian, W.: Multimodel assessment of the upper troposphere and lower stratosphere: Tropics and global trends, Journal of Geophysical Research (Atmospheres), 115, D00M08, doi:10.1029/2009JD013638, 2010.

Gidden, M. J., Riahi, K., Smith, S. J., Fujimori, S., Luderer, G., Kriegler, E., van Vuuren, D. P., van den Berg, M., Feng, L., Klein, D., Calvin, K., Doelman, J. C., Frank, S., Fricko, O., Harmsen, M., Hasegawa, T., Havlik, P., Hilaire, J., Hoesly, R., Horing, J., Popp, A., Stehfest, E., and Takahashi, K.: Global emissions pathways under different socioeconomic scenarios for use in CMIP6: a dataset of harmonized emissions trajectories through the end of the century, Geosci. Model Dev., 12, 1443–1475, https://doi.org/10.5194/gmd-12-1443-2019, 2019.

Gillett, N. P. and Thompson, D. W. J.: Simulation of recent SH climate change, Science, 302, 273–275, doi:10.1126/science.1087440, 2003.

Golaz, J., Caldwell, P. M., Roekel, L. P. Van, Petersen, M. R., Tang, Q., Wolfe, J. D., Abeshu, G., Anantharaj, V., Asay-davis, X. S., Bader, D. C., Baldwin, S. A., Bisht, G., Bogenschutz, P. A., Branstetter, M., Brunke, M. A., Brus, S. R., Burrows, S. M., Cameron-smith, P. J., Donahue, A. S., Deakin, M., Easter, R. C., Evans, K. J., Feng, Y., Flanner, M., Foucar, J. G., Fyke, J. G., Hunke, E. C., Jacob, R. L., Jacobsen, D. W., Jeffery, N., Jones, P. W., Keen, N. D., Klein, S. A., Larson, V. E., Leung, L. R., Li, H., Lin, W., Lipscomb, W. H., Ma, P., Mccoy, R. B., Neale, R. B., Price, S. F., Qian, Y., Rasch, P. J., Eyre, J. E. J. R., Riley, W. J., Ringler, T. D., Roberts, A. F., Roesler, E. L., Salinger, A. G., Shaheen, Z., Shi, X., Singh, B., Veneziani, M., Wan, H., Wang, H., Wang, S., Williams, D. N., Wolfram, P. J., Worley, P. H., Xie, S., Yang, Y., Yoon, J.-H., Zelinka, M. D., Zender, C. S., Zeng, X., Zhang, C., Zhang, K., Zhang, Y., Zheng, X., Zhou, T., and Zhu, Q.: The DOE E3SM Coupled Model Version 1?: Overview and Evaluation at Standard Resolution, J. Adv. Model. Earth Sy., 11, 1–41, https://doi.org/10.1029/2018MS001603, 2019.

Good, Peter; Sellar, Alistair; Tang, Yongming; Rumbold, Steve; Ellis, Rich; Kelley, Douglas; Kuhlbrodt, Till (2019). MOHC UKESM1.0-LL model output prepared for CMIP6 ScenarioMIP ssp119. Version 20191101 Earth System Grid Federation. https://doi.org/10.22033/ESGF/CMIP6.6329

Good, Peter; Sellar, Alistair; Tang, Yongming; Rumbold, Steve; Ellis, Rich; Kelley, Douglas; Kuhlbrodt, Till (2019). MOHC UKESM1.0-LL model output prepared for CMIP6 ScenarioMIP ssp119. Version 20191101 Earth System Grid Federation. https://doi.org/10.22033/ESGF/CMIP6.6329

Good, Peter; Sellar, Alistair; Tang, Yongming; Rumbold, Steve; Ellis, Rich; Kelley, Douglas; Kuhlbrodt, Till (2019). MOHC UKESM1.0-LL model output prepared for CMIP6 ScenarioMIP ssp245. Version 20191101 Earth System Grid Federation. https://doi.org/10.22033/ESGF/CMIP6.6339

850    Good, Peter; Sellar, Alistair; Tang, Yongming; Rumbold, Steve; Ellis, Rich; Kelley, Douglas; Kuhlbrodt, Till (2019). MOHC UKESM1.0-LL model output prepared for CMIP6 ScenarioMIP ssp370. Version 20191101 Earth System Grid Federation. https://doi.org/10.22033/ESGF/CMIP6.6347

Good, Peter; Sellar, Alistair; Tang, Yongming; Rumbold, Steve; Ellis, Rich; Kelley, Douglas; Kuhlbrodt, Till (2019). MOHC UKESM1.0-LL model output prepared for CMIP6 ScenarioMIP ssp434. Version 20191101 Earth System Grid Federation.

855    https://doi.org/10.22033/ESGF/CMIP6.6389

Good, Peter; Sellar, Alistair; Tang, Yongming; Rumbold, Steve; Ellis, Rich; Kelley, Douglas; Kuhlbrodt, Till (2019). MOHC UKESM1.0-LL model output prepared for CMIP6 ScenarioMIP ssp585. Version 20191101 Earth System Grid Federation. https://doi.org/10.22033/ESGF/CMIP6.6405

Guo, Huan; John, Jasmin G; Blanton, Chris; McHugh, Colleen; Nikonov, Serguei; Radhakrishnan, Aparna; Zadeh, Niki T.;

860    Balaji, V; Durachta, Jeff; Dupuis, Christopher; Menzel, Raymond; Robinson, Thomas; Underwood, Seth; Vahlenkamp, Hans; Dunne, Krista A.; Gauthier, Paul PG; Ginoux, Paul; Griffies, Stephen M.; Hallberg, Robert; Harrison, Matthew; Hurlin, William; Malyshev, Sergey; Naik, Vaishali; Paulot, Fabien; Paynter, David J; Ploshay, Jeffrey; Schwarzkopf, Daniel M; Seman, Charles J; Shao, Andrew; Silvers, Levi; Wyman, Bruce; Zeng, Yujin; Adcroft, Alistair; Dunne, John P.; Held, Isaac M; Krasting, John P.; Horowitz, Larry W.; Milly, P.C.D; Shevliakova, Elena; Winton, Michael; Zhao, Ming (2018). NOAA-

865    GFDL GFDL-CM4 model output prepared for CMIP6 CMIP historical. Version 20191101 Earth System Grid Federation. https://doi.org/10.22033/ESGF/CMIP6.8594

Guo, Huan; John, Jasmin G; Blanton, Chris; McHugh, Colleen; Nikonov, Serguei; Radhakrishnan, Aparna; Zadeh, Niki T.; Balaji, V; Durachta, Jeff; Dupuis, Christopher; Menzel, Raymond; Robinson, Thomas; Underwood, Seth; Vahlenkamp, Hans; Dunne, Krista A.; Gauthier, Paul PG; Ginoux, Paul; Griffies, Stephen M.; Hallberg, Robert; Harrison, Matthew; Hurlin,

870    William; Malyshev, Sergey; Naik, Vaishali; Paulot, Fabien; Paynter, David J; Ploshay, Jeffrey; Rand, Kristopher; Schwarzkopf, Daniel M; Seman, Charles J; Shao, Andrew; Silvers, Levi; Wyman, Bruce; Zeng, Yujin; Adcroft, Alistair; Dunne, John P.; Held, Isaac M; Krasting, John P.; Horowitz, Larry W.; Milly, Chris; Shevliakova, Elena; Winton, Michael; Zhao, Ming; Yan, Xiaoqin; Zhang, Rong (2018). NOAA-GFDL GFDL-CM4 model output prepared for CMIP6 ScenarioMIP ssp245. Version 20191101 Earth System Grid Federation. https://doi.org/10.22033/ESGF/CMIP6.9263

875    Guo, Huan; John, Jasmin G; Blanton, Chris; McHugh, Colleen; Nikonov, Serguei; Radhakrishnan, Aparna; Zadeh, Niki T.; Balaji, V; Durachta, Jeff; Dupuis, Christopher; Menzel, Raymond; Robinson, Thomas; Underwood, Seth; Vahlenkamp, Hans; Dunne, Krista A.; Gauthier, Paul PG; Ginoux, Paul; Griffies, Stephen M.; Hallberg, Robert; Harrison, Matthew; Hurlin,

William; Malyshev, Sergey; Naik, Vaishali; Paulot, Fabien; Paynter, David J; Ploshay, Jeffrey; Rand, Kristopher; Schwarzkopf, Daniel M; Seman, Charles J; Shao, Andrew; Silvers, Levi; Wyman, Bruce; Zeng, Yujin; Adcroft, Alistair;

880    Dunne, John P.; Held, Isaac M; Krasting, John P.; Horowitz, Larry W.; Milly, Chris; Shevliakova, Elena; Winton, Michael; Zhao, Ming; Yan, Xiaoqin; Zhang, Rong (2018). NOAA-GFDL GFDL-CM4 model output prepared for CMIP6 ScenarioMIP ssp585. Version 20191101 Earth System Grid Federation. https://doi.org/10.22033/ESGF/CMIP6.9268

Haigh, J. D. and Pyle, J. A.: Ozone perturbation experiments in a two-dimensional circulation model, Q. J. Roy. Meteor. Soc., 108, 551–574, https://doi.org/10.1002/qj.49710845705, 1982.

885    Hansen, J., Sato, M., Ruedy, R., Nazarenko, L., Lacis, A., Schmidt, G., Russell, G., Aleinov, I., Bauer, M., and Bauer, S.: Efficacy of climate forcings, J. Geophys. Res.-Atmos., 110, D18104, https://doi.org/10.1029/2005JD005776, 2005.

Hardiman, S. C., Andrews, M. B., Andrews, T., Bushell, A. C., Dunstone, N. J., Dyson, H., et al.: The impact of prescribed ozone in climate projections run with HadGEM3-GC3.1 Journal of Advances in Modeling Earth Systems, 11, https://doi.org/10.1029/2019MS001714, 2019.

890    Hardiman, S. C., Butchart, N., and Calvo, N.: The morphology of the Brewer-Dobson circulation and its response to climate change in CMIP5 simulations, Q. J. Roy. Meteor. Soc., 140, doi:10.1002/qj.2258, 2014.

Hegglin, M. I., Plummer, D. A., Shepherd, T. G., Scinocca, J. F., Anderson, J., Froidevaux, L., Funke, B., Hurst, D., Rozanov, A., Urban, J., von Clarmann, T., Walker, K. A., Wang, H. J., Tegtmeier, S., and Weigel7, K.: Vertical structure of stratospheric water vapor trends derived from merged satellite data, Nat. Geosci., 7, 768–776, https://doi.org/10.1038/ngeo2236, 2014.

895    Held, I.M., et al, 2019: Structure and Performance of GFDL's CM4.0 Climate Model, in prep.

Hoesly, R. M., Smith, S. J., Feng, L., Klimont, Z., Janssens-Maenhout, G., Pitkanen, T., Seibert, J. J., Vu, L., Andres, R. J., Bolt, R. M., Bond, T. C., Dawidowski, L., Kholod, N., Kurokawa, J.-I., Li, M., Liu, L., Lu, Z., Moura, M. C. P., O'Rourke, P. R., and Zhang, Q.: Historical (1750–2014) anthropogenic emissions of reactive gases and aerosols from the Community Emissions Data System (CEDS), Geosci. Model Dev., 11, 369–408, https://doi.org/10.5194/gmd-11-369-2018, 2018.

900    Hurst, D. F., Oltmans, S. J., Vömel, H., Rosenlof, K. H., Davis, S. M., Ray, E. A., Hall, E. G., and Jordan, A. F.: Stratospheric water vapor trends over Boulder, Colorado: Analysis of the 30 year Boulder record, J. Geophys. Res., 116, D02306, doi:10.1029/2010JD015065, 2011.

Iglesias-Suarez, F., Young, P. J., and Wild, O.: Stratospheric ozone change and related climate impacts over 1850–2100 as modelled by the ACCMIP ensemble, Atmos. Chem. Phys., 16, 343–363, https://doi.org/10.5194/acp-16-343-2016, 2016.

905    IPCC: Climate Change 2007: The Physical Science Basis, edited by: Solomon, S., Qin, D., Manning, M., Marquis, M., Averyt, K., Tignor, M. M. B., Miller, H. L., and Chen, Z., Cambridge University Press, Cambridge, UK, 996 pp., 2007.

IPCC: Climate Change 2013: The Physical Science Basis. Contribution of Working Group I to the Fifth Assessment Report of the Intergovernmental Panel on Climate Change, edited by: Stocker, T. F., Qin, D., Plattner, G.-K., Tignor, M., Allen, S. K., Boschung, J., Nauels, A., Xia, Y., Bex, V., and Midgley, P. M., Cambridge University Press, Cambridge, UK and New York, NY, USA, 2013.

John, Jasmin G; Blanton, Chris; McHugh, Colleen; Nikonov, Serguei; Radhakrishnan, Aparna; Rand, Kristopher; Vahlenkamp, Hans; Zadeh, Niki T.; Gauthier, Paul PG; Ginoux, Paul; Harrison, Matthew; Horowitz, Larry W.; Malyshev, Sergey; Naik, Vaishali; Paynter, David J; Ploshay, Jeffrey; Silvers, Levi; Stock, Charles; Winton, Michael; Zeng, Yujin; Dunne, John P. (2018). NOAA-GFDL GFDL-ESM4 model output prepared for CMIP6 ScenarioMIP ssp119. Version 20191101 Earth System Grid Federation. https://doi.org/10.22033/ESGF/CMIP6.8683

John, Jasmin G; Blanton, Chris; McHugh, Colleen; Nikonov, Serguei; Radhakrishnan, Aparna; Rand, Kristopher; Vahlenkamp, Hans; Zadeh, Niki T.; Gauthier, Paul PG; Ginoux, Paul; Harrison, Matthew; Horowitz, Larry W.; Malyshev, Sergey; Naik, Vaishali; Paynter, David J; Ploshay, Jeffrey; Silvers, Levi; Stock, Charles; Winton, Michael; Zeng, Yujin; Dunne, John P. (2018). NOAA-GFDL GFDL-ESM4 model output prepared for CMIP6 ScenarioMIP ssp126. Version 20191101 Earth System Grid Federation. https://doi.org/10.22033/ESGF/CMIP6.8684

John, Jasmin G; Blanton, Chris; McHugh, Colleen; Nikonov, Serguei; Radhakrishnan, Aparna; Rand, Kristopher; Vahlenkamp, Hans; Zadeh, Niki T.; Gauthier, Paul PG; Ginoux, Paul; Harrison, Matthew; Horowitz, Larry W.; Malyshev, Sergey; Naik, Vaishali; Paynter, David J; Ploshay, Jeffrey; Silvers, Levi; Stock, Charles; Winton, Michael; Zeng, Yujin; Dunne, John P. (2018). NOAA-GFDL GFDL-ESM4 model output prepared for CMIP6 ScenarioMIP ssp245. Version 20191101 Earth System Grid Federation. https://doi.org/10.22033/ESGF/CMIP6.8686

John, Jasmin G; Blanton, Chris; McHugh, Colleen; Nikonov, Serguei; Radhakrishnan, Aparna; Rand, Kristopher; Vahlenkamp, Hans; Zadeh, Niki T.; Gauthier, Paul PG; Ginoux, Paul; Harrison, Matthew; Horowitz, Larry W.; Malyshev, Sergey; Naik, Vaishali; Paynter, David J; Ploshay, Jeffrey; Silvers, Levi; Stock, Charles; Winton, Michael; Zeng, Yujin; Dunne, John P. (2018). NOAA-GFDL GFDL-ESM4 model output prepared for CMIP6 ScenarioMIP ssp370. Version 20191101 Earth System Grid Federation. https://doi.org/10.22033/ESGF/CMIP6.8691

John, Jasmin G; Blanton, Chris; McHugh, Colleen; Nikonov, Serguei; Radhakrishnan, Aparna; Rand, Kristopher; Vahlenkamp, Hans; Zadeh, Niki T.; Gauthier, Paul PG; Ginoux, Paul; Harrison, Matthew; Horowitz, Larry W.; Malyshev, Sergey; Naik, Vaishali; Paynter, David J; Ploshay, Jeffrey; Silvers, Levi; Stock, Charles; Winton, Michael; Zeng, Yujin; Dunne, John P. (2018). NOAA-GFDL GFDL-ESM4 model output prepared for CMIP6 ScenarioMIP ssp585. Version 20191101 Earth System Grid Federation. https://doi.org/10.22033/ESGF/CMIP6.8706

Johnston, H. S.: Reduction of stratospheric ozone by nitrogen oxide catalysts from supersonic transport exhaust, Science, 173, 517–522, 1971.

Jones, R.L., Pyle, J.A., Harries, J.E., Zavody, A.M., Russell III, J.M., and Gille, J.C.: The water vapor budget of the stratosphere using LIMS and SAMS satellite data, Quart.J.R.Met.Soc., 112, 1127-1144, 1986.

940  Keeble, J., Abraham, N. L., Archibald, A. T., Chipperfield, M. P., Dhomse, S., Griffiths, P. T., and Pyle, J. A.: Modelling the potential impacts of the recent, unexpected increase in CFC-11 emissions on total column ozone recovery, Atmos. Chem. Phys. Discuss., https://doi.org/10.5194/acp-2019-747, in review, 2019.

Keeble, J., Bednarz, E. M., Banerjee, A., Abraham, N. L., Harris, N. R. P., Maycock, A. C., and Pyle, J. A.: Diagnosing the radiative and chemical contributions to future changes in tropical column ozone with the UM-UKCA chemistry-climate model,
945  Atmos. Chem. Phys., 17, 13801-13818, https://doi.org/10.5194/acp-17-13801-2017, 2017.

Keeble, J., Braesicke, P., Abraham, N. L., Roscoe, H. K., and Pyle, J. A.: The impact of polar stratospheric ozone loss on SH stratospheric circulation and climate, Atmos. Chem. Phys., 14, 13705–13717, https://doi.org/10.5194/acp-14-13705-2014, 2014.

Keeble, J., Brown, H., Abraham, N. L., Harris, N. R. P., and Pyle, J. A.: On ozone trend detection: using coupled chemistry-
950  climate simulations to investigate early signs of total column ozone recovery, Atmos. Chem. Phys., 18, 7625-7637, https://doi.org/10.5194/acp-18-7625-2018, 2018.

Krasting, John P.; John, Jasmin G; Blanton, Chris; McHugh, Colleen; Nikonov, Serguei; Radhakrishnan, Aparna; Rand, Kristopher; Zadeh, Niki T.; Balaji, V; Durachta, Jeff; Dupuis, Christopher; Menzel, Raymond; Robinson, Thomas; Underwood, Seth; Vahlenkamp, Hans; Dunne, Krista A.; Gauthier, Paul PG; Ginoux, Paul; Griffies, Stephen M.; Hallberg,
955  Robert; Harrison, Matthew; Hurlin, William; Malyshev, Sergey; Naik, Vaishali; Paulot, Fabien; Paynter, David J; Ploshay, Jeffrey; Schwarzkopf, Daniel M; Seman, Charles J; Silvers, Levi; Wyman, Bruce; Zeng, Yujin; Adcroft, Alistair; Dunne, John P.; Guo, Huan; Held, Isaac M; Horowitz, Larry W.; Milly, P.C.D; Shevliakova, Elena; Stock, Charles; Winton, Michael; Zhao, Ming (2018). NOAA-GFDL GFDL-ESM4 model output prepared for CMIP6 CMIP historical. Version 20191101 Earth System Grid Federation. https://doi.org/10.22033/ESGF/CMIP6.8597

960  Lacis, A. A., Wuebbles, D. J., and Logan, J. A.: Radiative forcing of climate by changes in the vertical distribution of ozone, J. Geophys. Res., 95, 9971–9981, https://doi.org/10.1029/JD095iD07p09971, 1990.

Lauer, A., Eyring, V., Righi, M., Buchwitz, M., Defourny, P., Evaldsson, M., Friedlingstein, P., de Jeu, R., de Leeuw, G., Loew, A., Merchant, C.J., Müller, B., Popp, T., Reuter, M., Sandven, S., Senftleben, D., Stengel, M., Van Roozendael, M., Wenzel, S., and Willén, U.: Benchmarking CMIP5 models with a subset of ESA CCI Phase 2 data using the ESMValTool,
965  Remote Sensing of Environment, 203, 9-39, https://doi.org/10.1016/j.rse.2017.01.007, 2017.

LeTexier, H., Solomon, S., and Garcia, R. R.: The role of molecular hydrogen and methane oxidation in the water vapor budget of the stratosphere, Q. J. R. Meteorol. Soc., 114, 281–295, 1988.

Li et al., The Flexible Global Ocean–Atmosphere–Land System Model grid-point version3 (FGOALS-g3), in prep.

Li, Lijuan (2019). CAS FGOALS-g3 model output prepared for CMIP6 CMIP historical. Version 20191101 Earth System
970    Grid Federation. https://doi.org/10.22033/ESGF/CMIP6.3356

M. Michou, P. Nabat, D. Saint-Martin, J. Bock, B. Decharme, M. Mallet, R. Roehrig, R. and A. Voldoire: Present-day and
historical aerosol and ozone characteristics in CNRM CMIP6 simulations, Journal of Advances in Modeling Earth Systems,
doi: 10.1029/2019MS001816, 2019.

Mäder, J. A., Staehelin, J., Peter, T., Brunner, D., Rieder, H. E., and Stahel, W. A.: Evidence for the effectiveness of the
975    Montreal Protocol to protect the ozone layer, Atmos. Chem. Phys., 10, 12161-12171, https://doi.org/10.5194/acp-10-12161-
2010, 2010.

McLandress, C., Jonsson, A. I., Plummer, D. A., Reader, M. C., Scinocca, J. F. and Shepherd, T. G.: Separating the dynamical
effects of climate change and ozone depletion. Part I: SH stratosphere, J. Climate, 23, 5002–5020,
doi:10.1175/2010JCLI3586.1, 2010.

980    Meinshausen, M., Smith, S. J., Calvin, K., Daniel, J. S., Kainuma, M. L. T., Lamarque, J., Matsumoto, K., Montzka, S. A.,
Raper, S. C. B., Riahi, K., Thomson, A., Velders, G. J. M., and van Vuuren, D. P. P.: The RCP greenhouse gas concentrations
and their extensions from 1765 to 2300, Climatic Change, 109, 213–241, https://doi.org/10.1007/s10584-011-0156-z, 2011.

Meul, S., Dameris, M., Langematz, U., Abalichin, J., Kerschbaumer, A., Kubin, A., and Oberländer-Hayn, S.: Impact of rising
greenhouse gas concentrations on future tropical ozone and UV exposure, Geophys. Res. Lett., 43, 2919–2927,
985    https://doi.org/10.1002/2016GL067997, 2016.

Meul, S., Langematz, U., Oberländer, S., Garny, H., and Jöckel, P.: Chemical contribution to future tropical ozone change in
the lower stratosphere, Atmos. Chem. Phys., 14, 2959-2971, https://doi.org/10.5194/acp-14-2959-2014, 2014.

Michou, M., Saint-Martin, D., Teyssèdre, H., Alias, A., Karcher, F., Olivié, D., Voldoire, A., Josse, B., Peuch, V.-H., Clark,
H., Lee, J. N., and Chéroux, F.: A new version of the CNRM ChemistryClimate Model, CNRM-CCM: description and
990    improvements from the CCMVal-2 simulations, Geosci. Model Dev., 4, 873–900, https://doi.org/10.5194/gmd-4-873-2011,
2011.

Molina, M. J. and Rowland, F. S.: Stratospheric sink for chlorofluoromethanes: Chlorine atom catalyzed destruction of ozone,
Nature, 249, 810–812, doi:10.1038/249810a0, 1974.

Montzka, S. A., Dutton, R., Yu, P., Ray, E., Portmann, R. W., Daniel, J. S., Kuijpers, L., Hall, B. D., Mondeel, D., Siso, C.,
995    Nance, D. J., Rigby, M., Manning, A. J., Hu, L., Moore, F., Miller, B. R., Elkins, J. W.: A persistent and unexpected increase
in global emissions of ozone-depleting CFC-11, Nature, 557, 413–417, https://doi.org/10.1038/s41586-018-0106-2, 2018.

Morgenstern, O., Hegglin, M. I., Rozanov, E., O'Connor, F. M., Abraham, N. L., Akiyoshi, H., Archibald, A. T., Bekki, S., Butchart, N., Chipperfield, M. P., Deushi, M., Dhomse, S. S., Garcia, R. R., Hardiman, S. C., Horowitz, L. W., Jöckel, P., Josse, B., Kinnison, D., Lin, M., Mancini, E., Manyin, M. E., Marchand, M., Marécal, V., Michou, M., Oman, L. D., Pitari, G., Plummer, D. A., Revell, L. E., Saint-Martin, D., Schofield, R., Stenke, A., Stone, K., Sudo, K., Tanaka, T. Y., Tilmes, S., Yamashita, Y., Yoshida, K., and Zeng, G.: Review of the global models used within phase 1 of the Chemistry–Climate Model Initiative (CCMI), Geosci. Model Dev., 10, 639–671, https://doi.org/10.5194/gmd-10-639-2017, 2017.

Morgenstern, O., Stone, K. A., Schofield, R., Akiyoshi, H., Yamashita, Y., Kinnison, D. E., Garcia, R. R., Sudo, K., Plummer, D. A.,Scinocca, J., Oman, L. D., Manyin, M. E., Zeng, G., Rozanov, E., Stenke, A., Revell, L. E., Pitari, G., Mancini, E., Genova, G. D., Visioni,D., Dhomse, S. S., and Chipperfield, M. P.: Ozone sensitivity to varying greenhouse gases and ozone-depleting substances in CCMI-1simulations, Atmospheric Chemistry and Physics, 18, 1091–1114, https://doi.org/https://doi.org/10.5194/acp-18-1091-2018, https://www.atmos-chem-phys.net/18/1091/2018/, 2018.

Murcray, D. G., Murcray, F. J., and Barker, B. B.: Changes in stratospheric water vapor associated with the Mount St. Helens eruption, Science, 211, 823– 824, doi:10.1126/science.211.4484.823, 1981.

Nowack, P. J., Abraham, N. L., Maycock, A. C., Braesicke, P., Gregory, J. M., Joshi, M. M., Osprey, A., and Pyle, J. A.: A large ozone-circulation feedback and its implications for global warming assessments, Nature Climate Change, 5, 41–45, https://doi.org/10.1038/nclimate2451, 2015.

Nowack, P., Braesicke, P., Haigh, J., Abraham, N. L., Pyle, J., and Voulgarakis, A.: Using machine learning to build temperature-based ozone parameterizations for climate sensitivity simulations, Environ. Res. Lett., 13, 104016, https://doi.org/10.1088/1748-9326/aae2be, 2018.

O'Neill, B. C., Kriegler, E., Ebi, K. L., Kemp-Benedict, E., Riahi, K., Rothman, D. S., van Ruijven, B. J., van Vuuren, D. P., Birkmann, J., Kok, K., Levy, M., and Solecki, W.: The roads ahead: Narratives for shared socioeconomic pathways describing world futures in the 21st century, Global Environ. Chang., doi:10.1016/j.gloenvcha.2015.01.004, online first, 2015.

Palmeiro, F. M., Calvo, N., and Garcia, R. R.: Future changes in the Brewer–Dobson circulation under different greenhouse gas concentrations in WACCM4, J. Atmos. Sci., 71, 2962–2975, doi:10.1175/JAS-D-13-0289.1, 2014.

Park, S., Shin, J., Kim, S., Oh, E., and Kim, Y.: Global Climate Simulated by the Seoul National University Atmosphere Model Version 0 with a Unified Convection Scheme (SAM0-UNICON), J. Climate, 32, 2917–2949, 2019.

Park, S.: A unified convection scheme (UNICON). Part I: Formulation, J. Atmos. Sci., 71, 3902–3930, 2014a.

Park, S.: A unified convection scheme (UNICON). Part II: Simulation, J. Atmos. Sci., 71, 3931–3973, 2014b.

1025 Park, Sungsu; Shin, Jihoon (2019). SNU SAM0-UNICON model output prepared for CMIP6 CMIP historical. Version 20191101 Earth System Grid Federation. https://doi.org/10.22033/ESGF/CMIP6.7789

Plumb, R. A.: A 'tropical pipe' model of stratospheric transport, J. Geophys. Res., 101, 3957–3972, 1996.

Polvani, L. M., Abalos, M., Garcia, R., Kinnison, D., and Randel, W. J.: Significant Weakening of Brewer-Dobson Circulation Trends Over the 21st Century as a Consequence of the Montreal Protocol, Geophys. Res. Lett., 45, 401–409,
1030 https://doi.org/10.1002/2017GL075345, 2018.

Polvani, L. M., Wang, L., Abalos, M., Butchart, N., Chipperfield, M. P., Dameris, M., Deushi, M., Dhomse, S. S., Jöckel, P., Kinnison, D., Michou, M., Morgenstern, O., Oman, L. D., Plummer, D. A., and Stone, K. A.: Large impacts, past and future, of ozone-depleting substances on Brewer-Dobson circulation trends: A multi-model assessment, J. Geophys. Res.-Atmos., 124, 6669–6680, https://doi.org/10.1029/2018JD029516, 2019.

1035 Polvani, L. M., Waugh, D. W., Correa, G. J. P., and Son, S. W.:

Revell, L. E., Bodeker, G. E., Huck, P. E., Williamson, B. E., and Rozanov, E.: The sensitivity of stratospheric ozone changes through the 21st century to N2O and CH4, Atmos. Chem. Phys., 12, 11309–11317, https://doi.org/10.5194/acp-12-11309-2012, 2012.

Riahi, K., van Vuuren, D. P., Kriegler, E., Edmonds, J., O'Neill, B. C., Fujimori, S., Bauer, N., Calvin, K., Dellink, R., Fricko,
1040 O., Lutz, W., Popp, A., Cuaresma, J. C., KC, S., Leimbach, M., Jiang, L., Kram, T., Rao, S., Emmerling, J., Ebi, K., Hasegawa, T., Havlik, P., Humpenöder, F., Silva, L. A. D., Smith, S., Stehfest, E., Bosetti, V., Eom, J., Gernaat, D., Masui, T., Rogelj, J., Strefler, J., Drouet, L., Krey, V., Luderer, G., Harmsen, M., Takahashi, K., Baumstark, L., Doelman, J. C., Kainuma, M., Klimont, Z., Marangoni, G., Lotze-Campen, H., Obersteiner, M., Tabeau, A., and Tavoni, M.: The Shared Socioeconomic Pathways and their energy, land use, and greenhouse gas emissions implications: An overview, Global Environ. Chang., 42,
1045 153–168, https://doi.org/10.1016/j.gloenvcha.2016.05.009, 2017.

Righi, M., Andela, B., Eyring, V., Lauer, A., Predoi, V., Schlund, M., Vegas-Regidor, J., Bock, L., Brötz, B., de Mora, L., Diblen, F., Dreyer, L., Drost, N., Earnshaw, P., Hassler, B., Koldunov, N., Little, B., Loosveldt Tomas, S., & Zimmermann, K.: ESMValTool v2.0 – Technical overview. Geosci. Model Dev. Discuss., 2019, 1-28, 2019.

Rosenlof, K. H., Chiou, E.-W., Chu, W. P., Johnson, D. G., Kelly, K. K., Michelsen, H. A., Nedoluha, G. E., Remsberg, E. E.,
1050 Toon, G. C., and McCormick, M. P.: Stratospheric water vapor increases over the past half-century, Geophys. Res. Lett., 28(7), 1195–1198, 2001.

Scherer, M., Vömel, H., Fueglistaler, S., Oltmans, S. J., and Staehelin, J.: Trends and variability of midlatitude stratospheric water vapor deduced from the re-evaluated Boulder balloon series and HALOE, Atmos. Chem. Phys., 8, 1391–1402, https://doi.org/10.5194/acp-8-1391-2008, 2008.

1055    Seferian, Roland (2018). CNRM-CERFACS CNRM-ESM2-1 model output prepared for CMIP6 CMIP historical. Version 20191101 Earth System Grid Federation. https://doi.org/10.22033/ESGF/CMIP6.4068

Sellar, A. A., C. G. Jones,, J. Mulcahy, Y. Tang, A. Yool, A. Wiltshire, F. M. O'Connor, M. Stringer, R. Hill, J. Palmieri, S. Woodward, L. de Mora, T. Kuhlbrodt, S. Rumbold, D. I. Kelley, R. Ellis, C. E. Johnson, J. Walton, N. L. Abraham, M. B. Andrews, T. Andrews, A. T. Archibald, S. Berthou, E. Burke, E. Blockley, K. Carslaw, M. Dalvi, J. Edwards, G. A. Folberth,
1060    N. Gedney, P. T. Griffiths, A. B. Harper, M. A. Hendry, A. J. Hewitt, B. Johnson, A. Jones, C. D. Jones, J. Keeble, S. Liddicoat, O. Morgenstern, R. J. Parker, V. Predoi, E. Robertson, A. Siahaan, R. S. Smith, R. Swaminathan, M. Woodhouse, G. Zeng, and M. Zerroukat, UKESM1: Description and evaluation of the UK Earth System Model, J. Adv. Modeling Earth Sys., 2019.

Shepherd, T. G. and McLandress, C.: A robust mechanism for the strengthening of the Brewer-Dobson circulation in response to climate change: Critical-layer control of subtropical wave breaking, J. Atmos. Sci., 68, 784–797, 2011.

1065    Sioris, C. E., Malo, A., McLinden, C. A., and D'Amours, R.: Direct injection of water vapor into the stratosphere by volcanic eruptions, Geophys. Res. Lett., 43, 7694– 7700, doi:10.1002/2016GL069918, 2016.

Smalley, K. M., Dessler, A. E., Bekki, S., Deushi, M., Marchand, M., Morgenstern, O., Plummer, D. A., Shibata, K., Yamashita, Y., and Zeng, G.: Contribution of different processes to changes in tropical lower-stratospheric water vapor in chemistry–climate models, Atmos. Chem. Phys., 17, 8031–8044, https://doi.org/10.5194/acp-17-8031-2017, 2017.

1070    Solomon, S., Ivy, D. J., Kinnison, D., Mills, M. J., Neely, R. R., and Schmidt, A.: Emergence of healing in the Antarctic ozone layer, Science, 353, 269-274, https://doi.org/10.1126/science.aae0061, 2016.

Solomon, S., Rosenlof, K. H., Portmann, R. W., Daniel, J. S., Davis, S. M., Sanford, T. J., and Gian-Kasper, P.: Contributions of Stratospheric Water Vapor to Decadal Changes in the Rate of Global Warming, Science, 327, 1219–1223, https://doi.org/10.1126/science.1182488, 2010.

1075    Solomon, S.: Stratospheric ozone depletion: A review of concepts and history, Rev. Geophys., 37, 275–316, doi:10.1029/1999RG900008, 1999

Son, S.-W., Gerber, E. P., Perlwitz, J., Polvani, L. M., Gillett, N. P., Seo, K.-H., Eyring, V., Shepherd, T. G., Waugh, D., Akiyoshi, H., Austin, J., Baumgaertner, A., Bekki, S., Braesicke, P., Bruhl, C., Butchart, N., Chipperfield, M. P., Cugnet, D., Dameris, M., Dhomse, S., Frith, S., Garny, H., Garcia, R., Hardiman, S, C., Jockel, P., Lamarque, J. F., Mancini, E., Marchand,
1080    M., Michou, M., Nakamura, T., Morgenstern, O., Pitari, G., Plummer, D. A., Pyle, J., Rozanov, E., Scinocca, J. F., Shibata, K., Smale, D., Teyssedre, H., Tian, W., and Yamashita, Y.: Impact of stratospheric ozone on SH circulation change: a multimodel assessment, J. Geophys. Res., 115, D00M07, doi:10.1029/2010JD014271, 2010.

SPARC: SPARC Report on the Evaluation of Chemistry-Climate Models, sPARC Report No. 5, WCRP-132, WMO/TD-No. 1526, edited by: Eyring, V., Shepherd, T. G., and Waugh, D. W., 426 pp., available at: http://www.atmosp.physics.utoronto.ca/SPARC, 2010.

Stevenson, D. S., Young, P. J., Naik, V., Lamarque, J.-F., Shindell, D. T., Voulgarakis, A., Skeie, R. B., Dalsoren, S. B., Myhre, G., Berntsen, T. K., Folberth, G. A., Rumbold, S. T., Collins, W. J., MacKenzie, I. A., Doherty, R. M., Zeng, G., van Noije, T. P. C., Strunk, A., Bergmann, D., Cameron-Smith, P., Plummer, D. A., Strode, S. A., Horowitz, L., Lee, Y. H., Szopa, S., Sudo, K., Nagashima, T., Josse, B., Cionni, I., Righi, M., Eyring, V., Conley, A., Bowman, K. W., Wild, O., and Archibald, A.: Tropospheric ozone changes, radiative forcing and attribution to emissions in the Atmospheric Chemistry and Climate Model Intercomparison Project (ACCMIP), Atmos. Chem. Phys., 13, 3063–3085, https://doi.org/10.5194/acp-13-3063-2013, 2013.

Stolarski, R. and Cicerone, R.: Stratospheric chlorine: a possible sink for ozone, Can. J. Chem., 52, 1610–1615, doi:10.1139/v74-233, 1974.

Stratospheric ozone depletion: The main driver of twentiethcentury atmospheric circulation changes in the SH, J. Clim., 24, 795–812, 2011.

Tang, Yongming; Rumbold, Steve; Ellis, Rich; Kelley, Douglas; Mulcahy, Jane; Sellar, Alistair; Walton, Jeremy; Jones, Colin (2019). MOHC UKESM1.0-LL model output prepared for CMIP6 CMIP historical. Version 20191101 Earth System Grid Federation. https://doi.org/10.22033/ESGF/CMIP6.6113

Taylor, K. E., Stouffer, R. J., and Meehl, G. A.: An Overview of CMIP5 and the Experiment Design, B. Am. Meteorol. Soc., 93, 485–498, https://doi.org/10.1175/BAMS-D-11-00094.1, 2012

Telford, P. J., Braesicke, P., Morgenstern, O., and Pyle, J.: Reassessment of causes of ozone column variability following the eruption of Mount Pinatubo using a nudged CCM, Atmos. Chem. Phys., 9, 4251–4260, https://doi.org/10.5194/acp-9-4251-2009, 2009.

Thompson, D. W. J. and Solomon, S.: Interpretation of recent SH climate change, Science, 296, 895–899, 2002.

Velders, G. J. M. and Daniel, J. S.: Uncertainty analysis of projections of ozone-depleting substances: mixing ratios, EESC, ODPs, and GWPs, Atmos. Chem. Phys., 14, 2757–2776, https://doi.org/10.5194/acp-14-2757-2014, 2014.

Voldoire, A., Saint-Martin, D., Sénési, S., Decharme, B., Alias, A., Chevallier, M., Colin, J., Guérémy, J.-F., Michou, M., Moine, M.-P., Nabat, P., Roehrig, R., Salas y Mélia, D., Séférian, R., Valcke, S., Beau, I., Belamari, S., Berthet, S., Cassou, C., Cattiaux, J., Deshayes, J., Douville, H., Franchisteguy, L., Ethé, C., Geoffroy, O., Lévy, C., Madec, G., Meurdesoif, Y., Msadek, R., Ribes, A., Sanchez-Gomez, E., and Terray, L.: Evaluation of CMIP6 DECK Experiments with CNRM-CM6-1, J. Adv. Model. Earth Sy., 11, 2177–2213, https://doi.org/10.1029/2019MS001683, 2019.

Voldoire, Aurore (2018). CMIP6 simulations of the CNRM-CERFACS based on CNRM-CM6-1 model for CMIP experiment historical. Version 20191101 Earth System Grid Federation. https://doi.org/10.22033/ESGF/CMIP6.4066

1115 Voldoire, Aurore (2019). CNRM-CERFACS CNRM-CM6-1 model output prepared for CMIP6 ScenarioMIP ssp126. Version 20191101 Earth System Grid Federation. https://doi.org/10.22033/ESGF/CMIP6.4184

Voldoire, Aurore (2019). CNRM-CERFACS CNRM-CM6-1 model output prepared for CMIP6 ScenarioMIP ssp245. Version 20191101 Earth System Grid Federation. https://doi.org/10.22033/ESGF/CMIP6.4189

Voldoire, Aurore (2019). CNRM-CERFACS CNRM-CM6-1 model output prepared for CMIP6 ScenarioMIP ssp370. Version
1120 20191101 Earth System Grid Federation. https://doi.org/10.22033/ESGF/CMIP6.4197

Voldoire, Aurore (2019). CNRM-CERFACS CNRM-CM6-1 model output prepared for CMIP6 ScenarioMIP ssp585. Version 20191101 Earth System Grid Federation. https://doi.org/10.22033/ESGF/CMIP6.4224

Voldoire, Aurore (2019). CNRM-CERFACS CNRM-ESM2-1 model output prepared for CMIP6 ScenarioMIP ssp119. Version 20191101 Earth System Grid Federation. https://doi.org/10.22033/ESGF/CMIP6.4182

1125 Voldoire, Aurore (2019). CNRM-CERFACS CNRM-ESM2-1 model output prepared for CMIP6 ScenarioMIP ssp126. Version 20191101 Earth System Grid Federation. https://doi.org/10.22033/ESGF/CMIP6.4186

Voldoire, Aurore (2019). CNRM-CERFACS CNRM-ESM2-1 model output prepared for CMIP6 ScenarioMIP ssp245. Version 20191101 Earth System Grid Federation. https://doi.org/10.22033/ESGF/CMIP6.4191

Voldoire, Aurore (2019). CNRM-CERFACS CNRM-ESM2-1 model output prepared for CMIP6 ScenarioMIP ssp370.
1130 Version 20191101 Earth System Grid Federation. https://doi.org/10.22033/ESGF/CMIP6.4199

Voldoire, Aurore (2019). CNRM-CERFACS CNRM-ESM2-1 model output prepared for CMIP6 ScenarioMIP ssp434. Version 20191101 Earth System Grid Federation. https://doi.org/10.22033/ESGF/CMIP6.4213

Voldoire, Aurore (2019). CNRM-CERFACS CNRM-ESM2-1 model output prepared for CMIP6 ScenarioMIP ssp460. Version 20191101 Earth System Grid Federation. https://doi.org/10.22033/ESGF/CMIP6.4217

1135 Voldoire, Aurore (2019). CNRM-CERFACS CNRM-ESM2-1 model output prepared for CMIP6 ScenarioMIP ssp585. Version 20191101 Earth System Grid Federation. https://doi.org/10.22033/ESGF/CMIP6.4226

Weber, M., Coldewey-Egbers, M., Fioletov, V. E., Frith, S. M., Wild, J. D., Burrows, J. P., Long, C. S., and Loyola, D.: Total ozone trends from 1979 to 2016 derived from five merged observational datasets – the emergence into ozone recovery, Atmos. Chem. Phys., 18, 2097–2117, https://doi.org/10.5194/acp18-2097-2018, 2018.

1140   World Meteorological Organization (WMO): Scientific Assessment of Ozone Depletion: 2018, Global Ozone Research and
       Monitoring, Project-Report No. 58, 588 pp., Geneva, Switzerland, 2018.

       Wu, T., Lu, Y., Fang, Y., Xin, X., Li, L., Li, W., Jie, W., Zhang, J., Liu, Y., Zhang, L., Zhang, F., Zhang, Y., Wu, F., Li, J.,
       Chu, M., Wang, Z., Shi, X., Liu, X., Wei, M., Huang, A., Zhang, Y., and Liu, X.: The Beijing Climate Center Climate System
       Model (BCC-CSM): the main progress from CMIP5 to CMIP6 , Geosci. Model Dev., 12, 1573–1600,
1145   https://doi.org/10.5194/gmd-12-1573-2019, 2019a.

       Wu, T., Zhang, F., Zhang, J., Jie, W., Zhang, Y., Wu, F., Li, L., Liu, X., Lu, X., Zhang, L., Wang, J., and Hu, A.: Beijing
       Climate Center Earth System Model version 1 (BCC-ESM1): Model Description and Evaluation, Geosci. Model Dev. Discuss.,
       https://doi.org/10.5194/gmd-2019-172, in review, 2019b.

       Wu, Tongwen; Chu, Min; Dong, Min; Fang, Yongjie; Jie, Weihua; Li, Jianglong; Li, Weiping; Liu, Qianxia; Shi, Xueli; Xin,
1150   Xiaoge; Yan, Jinghui; Zhang, Fang; Zhang, Jie; Zhang, Li; Zhang, Yanwu (2018). BCC BCC-CSM2MR model output
       prepared for CMIP6 CMIP historical. Version 20191101 Earth System Grid Federation.
       https://doi.org/10.22033/ESGF/CMIP6.2948

       Xin, Xiaoge; Wu, Tongwen; Shi, Xueli; Zhang, Fang; Li, Jianglong; Chu, Min; Liu, Qianxia; Yan, Jinghui; Ma, Qiang; Wei,
       Min (2019). BCC BCC-CSM2MR model output prepared for CMIP6 ScenarioMIP ssp126. Version 20191101 Earth System
1155   Grid Federation. https://doi.org/10.22033/ESGF/CMIP6.3028

       Xin, Xiaoge; Wu, Tongwen; Shi, Xueli; Zhang, Fang; Li, Jianglong; Chu, Min; Liu, Qianxia; Yan, Jinghui; Ma, Qiang; Wei,
       Min (2019). BCC BCC-CSM2MR model output prepared for CMIP6 ScenarioMIP ssp245. Version 20191101 Earth System
       Grid Federation. https://doi.org/10.22033/ESGF/CMIP6.3030

       Xin, Xiaoge; Wu, Tongwen; Shi, Xueli; Zhang, Fang; Li, Jianglong; Chu, Min; Liu, Qianxia; Yan, Jinghui; Ma, Qiang; Wei,
1160   Min (2019). BCC BCC-CSM2MR model output prepared for CMIP6 ScenarioMIP ssp370. Version 20191101 Earth System
       Grid Federation. https://doi.org/10.22033/ESGF/CMIP6.3035

       Xin, Xiaoge; Wu, Tongwen; Shi, Xueli; Zhang, Fang; Li, Jianglong; Chu, Min; Liu, Qianxia; Yan, Jinghui; Ma, Qiang; Wei,
       Min (2019). BCC BCC-CSM2MR model output prepared for CMIP6 ScenarioMIP ssp585. Version 20191101 Earth System
       Grid Federation. https://doi.org/10.22033/ESGF/CMIP6.3050

1165   Young, P. J., Archibald, A. T., Bowman, K. W., Lamarque, J.-F., Naik, V., Stevenson, D. S., Tilmes, S., Voulgarakis, A.,
       Wild, O., Bergmann, D., Cameron-Smith, P., Cionni, I., Collins, W. J., Dalsøren, S. B., Doherty, R. M., Eyring, V., Faluvegi,
       G., Horowitz, L. W., Josse, B., Lee, Y. H., MacKenzie, I. A., Nagashima, T., Plummer, D. A., Righi, M., Rumbold, S. T.,
       Skeie, R. B., Shindell, D. T., Strode, S. A., Sudo, K., Szopa, S., and Zeng, G.: Preindustrial to end 21st century projections of

tropospheric ozone from the Atmospheric Chemistry and Climate Model Intercomparison Project (ACCMIP), Atmos. Chem.
Phys., 13, 2063-2090, https://doi.org/10.5194/acp-13-2063-2013, 2013.

Young, P. J., Naik, V., Fiore, A. M., Gaudel, A., Guo, J., Lin, M. Y., Neu, J. L., Parrish, D. D., Rieder, H. E., Schnell, J. L., Tilmes, S., Wild, O., Zhang, L., Ziemke, J. R., Brandt, J., Delcloo, A., Doherty, R. M., Geels, C., Hegglin, M. I., Hu, L., Im, U., Kumar, R., Luhar, A., Murray, L., Plummer, D., Rodriguez, J., Saiz-Lopez, A., Schultz, M. G., Woodhouse, M. T., and Zeng, G.: Tropospheric Ozone Assessment Report: Assessment of global-scale model performance for global and regional ozone distributions, variability, and trends, Elem. Sci. Anth., 6, 10, https://doi.org/10.1525/elementa.265, 2018.

Yukimoto, S., Kawai, H., Koshiro, T., Oshima, N., Yoshida, K., Urakawa, S., Tsujino, H., Deushi, M., Tanaka, T., Hosaka, M., Yabu, S., Yoshimura, H., Shindo, E., Mizuta, R., Obata, A., Adachi, Y. and Ishii, M.: The Meteorological Research Institute Earth System Model version 2.0, MRI-ESM2.0: Description and basic evaluation of the physical component, J. Meteor. Soc. Jpn., 97, https://doi.org/10.2151/jmsj.2019-051, in press, 2019.

Yukimoto, Seiji; Koshiro, Tsuyoshi; Kawai, Hideaki; Oshima, Naga; Yoshida, Kohei; Urakawa, Shogo; Tsujino, Hiroyuki; Deushi, Makoto; Tanaka, Taichu; Hosaka, Masahiro; Yoshimura, Hiromasa; Shindo, Eiki; Mizuta, Ryo; Ishii, Masayoshi; Obata, Atsushi; Adachi, Yukimasa (2019). MRI MRI-ESM2.0 model output prepared for CMIP6 CMIP historical. Version 20191101 Earth System Grid Federation. https://doi.org/10.22033/ESGF/CMIP6.6842

Yukimoto, Seiji; Koshiro, Tsuyoshi; Kawai, Hideaki; Oshima, Naga; Yoshida, Kohei; Urakawa, Shogo; Tsujino, Hiroyuki; Deushi, Makoto; Tanaka, Taichu; Hosaka, Masahiro; Yoshimura, Hiromasa; Shindo, Eiki; Mizuta, Ryo; Ishii, Masayoshi; Obata, Atsushi; Adachi, Yukimasa (2019). MRI MRI-ESM2.0 model output prepared for CMIP6 ScenarioMIP ssp119. Version 20191101 Earth System Grid Federation. https://doi.org/10.22033/ESGF/CMIP6.6908

Yukimoto, Seiji; Koshiro, Tsuyoshi; Kawai, Hideaki; Oshima, Naga; Yoshida, Kohei; Urakawa, Shogo; Tsujino, Hiroyuki; Deushi, Makoto; Tanaka, Taichu; Hosaka, Masahiro; Yoshimura, Hiromasa; Shindo, Eiki; Mizuta, Ryo; Ishii, Masayoshi; Obata, Atsushi; Adachi, Yukimasa (2019). MRI MRI-ESM2.0 model output prepared for CMIP6 ScenarioMIP ssp126. Version 20191101 Earth System Grid Federation. https://doi.org/10.22033/ESGF/CMIP6.6909

Yukimoto, Seiji; Koshiro, Tsuyoshi; Kawai, Hideaki; Oshima, Naga; Yoshida, Kohei; Urakawa, Shogo; Tsujino, Hiroyuki; Deushi, Makoto; Tanaka, Taichu; Hosaka, Masahiro; Yoshimura, Hiromasa; Shindo, Eiki; Mizuta, Ryo; Ishii, Masayoshi; Obata, Atsushi; Adachi, Yukimasa (2019). MRI MRI-ESM2.0 model output prepared for CMIP6 ScenarioMIP ssp245. Version 20191101 Earth System Grid Federation. https://doi.org/10.22033/ESGF/CMIP6.6910

Yukimoto, Seiji; Koshiro, Tsuyoshi; Kawai, Hideaki; Oshima, Naga; Yoshida, Kohei; Urakawa, Shogo; Tsujino, Hiroyuki; Deushi, Makoto; Tanaka, Taichu; Hosaka, Masahiro; Yoshimura, Hiromasa; Shindo, Eiki; Mizuta, Ryo; Ishii, Masayoshi;

Obata, Atsushi; Adachi, Yukimasa (2019). MRI MRI-ESM2.0 model output prepared for CMIP6 ScenarioMIP ssp370. Version 20191101 Earth System Grid Federation. https://doi.org/10.22033/ESGF/CMIP6.6915

1200 Yukimoto, Seiji; Koshiro, Tsuyoshi; Kawai, Hideaki; Oshima, Naga; Yoshida, Kohei; Urakawa, Shogo; Tsujino, Hiroyuki; Deushi, Makoto; Tanaka, Taichu; Hosaka, Masahiro; Yoshimura, Hiromasa; Shindo, Eiki; Mizuta, Ryo; Ishii, Masayoshi; Obata, Atsushi; Adachi, Yukimasa (2019). MRI MRI-ESM2.0 model output prepared for CMIP6 ScenarioMIP ssp434. Version 20191101 Earth System Grid Federation. https://doi.org/10.22033/ESGF/CMIP6.6925

Yukimoto, Seiji; Koshiro, Tsuyoshi; Kawai, Hideaki; Oshima, Naga; Yoshida, Kohei; Urakawa, Shogo; Tsujino, Hiroyuki; 1205 Deushi, Makoto; Tanaka, Taichu; Hosaka, Masahiro; Yoshimura, Hiromasa; Shindo, Eiki; Mizuta, Ryo; Ishii, Masayoshi; Obata, Atsushi; Adachi, Yukimasa (2019). MRI MRI-ESM2.0 model output prepared for CMIP6 ScenarioMIP ssp460. Version 20191101 Earth System Grid Federation. https://doi.org/10.22033/ESGF/CMIP6.6926

Yukimoto, Seiji; Koshiro, Tsuyoshi; Kawai, Hideaki; Oshima, Naga; Yoshida, Kohei; Urakawa, Shogo; Tsujino, Hiroyuki; Deushi, Makoto; Tanaka, Taichu; Hosaka, Masahiro; Yoshimura, Hiromasa; Shindo, Eiki; Mizuta, Ryo; Ishii, Masayoshi; 1210 Obata, Atsushi; Adachi, Yukimasa (2019). MRI MRI-ESM2.0 model output prepared for CMIP6 ScenarioMIP ssp585. Version 20191101 Earth System Grid Federation. https://doi.org/10.22033/ESGF/CMIP6.6929

Zhang, Jie; Wu, Tongwen; Shi, Xueli; Zhang, Fang; Li, Jianglong; Chu, Min; Liu, Qianxia; Yan, Jinghui; Ma, Qiang; Wei, Min (2018). BCC BCC-ESM1 model output prepared for CMIP6 CMIP historical. Version 20191101 Earth System Grid Federation. https://doi.org/10.22033/ESGF/CMIP6.2949

1215

| Model | Stratospheric Chemistry | Ozone | Water Vapor | References |
|---|---|---|---|---|
| BCC-CSM2-MR | CMIP6 dataset | Historical<br>SSP1-2.6<br>SSP2-4.5<br>SSP3-7.0<br>SSP5-8.5 | Historical<br>SSP1-2.6<br>SSP2-4.5<br>SSP3-7.0<br>SSP5-8.5 | Wu et al., 2019<br>Xin et al., 2019a<br>Xin et al., 2019b<br>Xin et al., 2019c<br>Xin et al., 2019d |
| BCC-ESM1 | CMIP6 dataset | Historical | Historical | Zhang et al., 2018 |
| CESM2 | Prescribed ozone fields | Historical<br>SSP1-2.6<br>SSP2-4.5<br>SSP3-7.0<br>SSP5-8.5 | Historical<br>--<br>SSP2-4.5<br>--<br>-- | Danabasoglu, 2019a<br>Danabasoglu, 2019b<br>Danabasoglu, 2019c<br>Danabasoglu, 2019d<br>Danabasoglu, 2019e |
| CESM2-WACCM | Interactive | Historical<br>SSP1-2.6<br>SSP2-4.5<br>SSP3-7.0<br>SSP5-8.5 | Historical<br>--<br>SSP2-4.5<br>--<br>-- | Danabasoglu, 2019e<br>Danabasoglu, 2019f<br>Danabasoglu, 2019g<br>Danabasoglu, 2019h<br>Danabasoglu, 2019i |
| CNRM-CM6 | Simplified online scheme | Historical<br>SSP1-2.6<br>SSP2-4.5<br>SSP3-7.0<br>SSP5-8.5 | Historical<br>SSP1-2.6<br>SSP2-4.5<br>SSP3-7.0<br>SSP5-8.5 | Voldoire, 2018a<br>Voldoire, 2019a<br>Voldoire, 2019b<br>Voldoire, 2019c<br>Voldoire, 2019d |
| CNRM-ESM2 | Interactive | Historical, SSP1-<br>SSP1-1.9<br>SSP1-2.6<br>SSP2-4.5<br>SSP3-7.0<br>SSP4-3.4<br>SSP4-6.0<br>SSP5-8.5 | Historical<br>SSP1-1.9<br>SSP1-2.6<br>SSP2-4.5<br>SSP3-7.0<br>SSP4-3.4<br>SSP4-6.0<br>SSP5-8.5 | Seferian, 2018<br>Voldoire, 2019e<br>Voldoire, 2019f<br>Voldoire, 2019g<br>Voldoire, 2019h;<br>Voldoire, 2019i<br>Voldoire, 2019j<br>Voldoire, 2019k |
| E3SM-1-0 | Simplified online scheme | Historical | -- | Bader et al., 2019 |
| FGOALS-g3 | CMIP6 dataset | Historical | -- | Li, 2019 |
| GFDL-CM4 | CMIP6 dataset | Historical<br>SSP2-4.5<br>SSP5-8.5 | Historical<br>SSP2-4.5<br>SSP5-8.5 | Guo et al., 2018a<br>Guo et al., 2018b<br>Guo et al., 2018c |
| GFDL-ESM4 | Interactive | Historical<br>SSP1-1.9<br>SSP1-2.6<br>SSP2-4.5<br>SSP3-7.0<br>SSP5-8.5 | Historical<br>SSP1-1.9<br>SSP1-2.6<br>SSP2-4.5<br>SSP3-7.0<br>SSP5-8.5 | Krasting et al., 2018<br>John et al., 2018a<br>John et al., 2018b<br>John et al., 2018c<br>John et al., 2018d<br>John et al., 2018e |
| IPSL-CM6A-LR | CMIP6 dataset | Historical<br>SSP1-1.9<br>SSP1-2.6<br>SSP2-4.5 | Historical<br>SSP1-1.9<br>SSP1-2.6<br>SSP2-4.5 | Boucher et al., 2018<br>Boucher et al., 2019a<br>Boucher et al., 2019b<br>Boucher et al., 2019c |

| | | SSP3-7.0 | SSP3-7.0 | Boucher et al., 2019d |
| | | SSP4-3.4 | SSP4-3.4 | Boucher et al.,2019e |
| | | SSP4-6.0 | SSP4-6.0 | Boucher et al., 2019f |
| | | SSP5-8.5 | SSP5-8.5 | -- |
| MRI-ESM2-0 | Interactive | Historical | Historical | Yukimoto et al., 2019a |
| | | SSP1-1.9 | SSP1-1.9 | Yukimoto et al., 2019b |
| | | SSP1-2.6 | SSP1-2.6 | Yukimoto et al., 2019c |
| | | SSP2-4.5 | SSP2-4.5 | Yukimoto et al., 2019d |
| | | SSP3-7.0 | SSP3-7.0 | Yukimoto et al., 2019e |
| | | SSP4-3.4 | SSP4-3.4 | Yukimoto et al., 2019f |
| | | SSP4-6.0 | SSP4-6.0 | Yukimoto et al., 2019g |
| | | SSP5-8.5 | SSP5-8.5 | Yukimoto et al., 2019h |
| SAM0-UNICON | CMIP6 dataset | Historical | -- | Park and Shin, 2019 |
| UKESM1-0-LL | Interactive | Historical | Historical | Tang et al., 2019 |
| | | SSP1-1.9 | SSP1-1.9 | Good et al., 2019a |
| | | SSP1-2.6 | SSP1-2.6 | Good et al., 2019b |
| | | SSP2-4.5 | SSP2-4.5 | Good et al., 2019c |
| | | SSP3-7.0 | SSP3-7.0 | Good et al., 2019d |
| | | SSP4-3.4 | SSP4-3.4 | Good et al., 2019e |
| | | SSP5-8.5 | SSP5-8.5 | Good et al., 2019f |

**Table 1. Overview of models and data available during the preparation of this manuscript.**
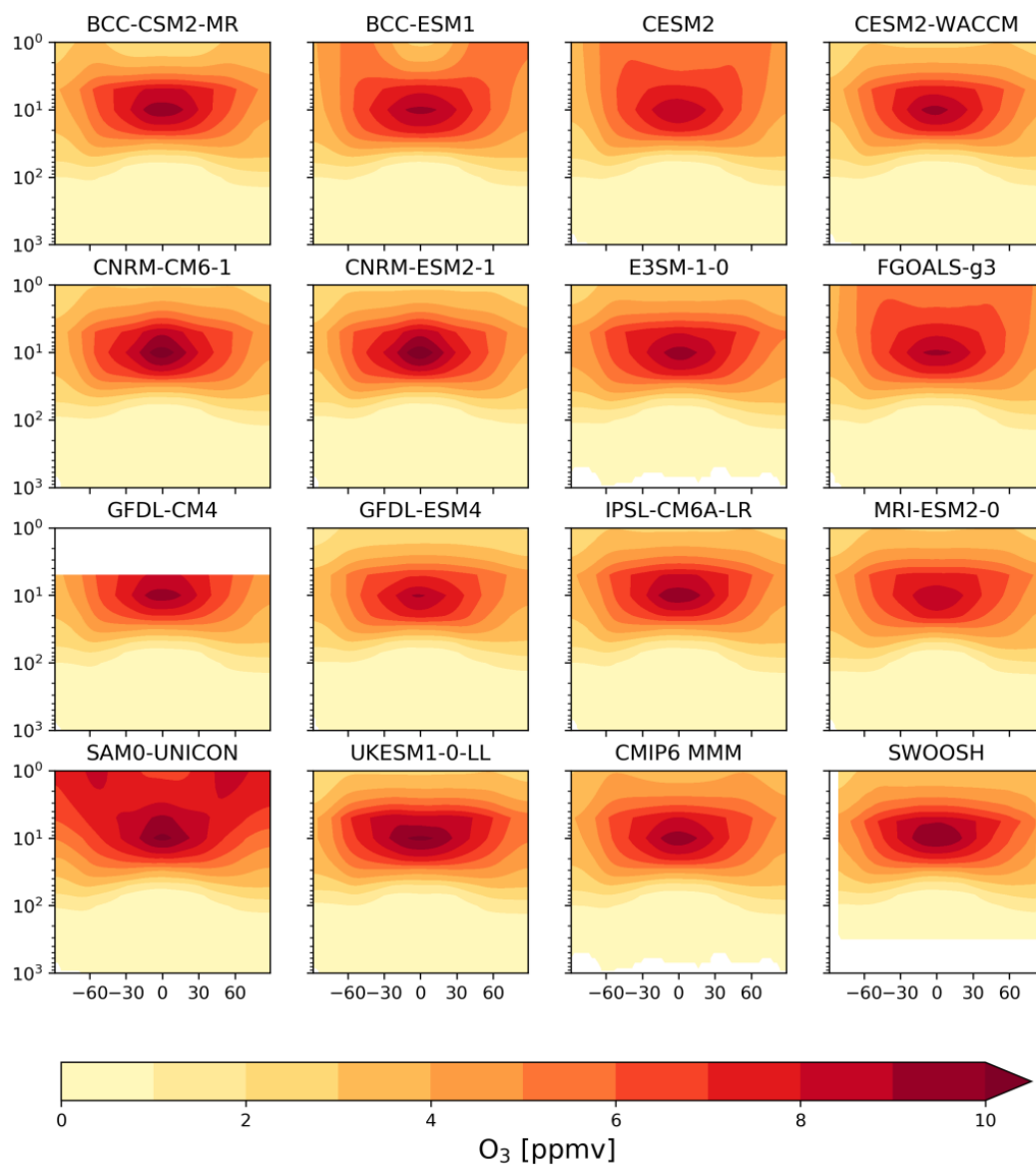
220

**Figure 1: Latitude vs altitude zonal mean ozone for CMIP6 models and observations. Climatological ozone volume mixing ratios (ppm) for 2000-2014 for each CMIP6 model, the CMIP6 multi-model mean (MMM) and SWOOSH combined dataset. GFDL-CM4 did not provide ozone output in the upper stratosphere, while the SWOOSH combined dataset only extends from ~300 hPa to 1 hPa.**
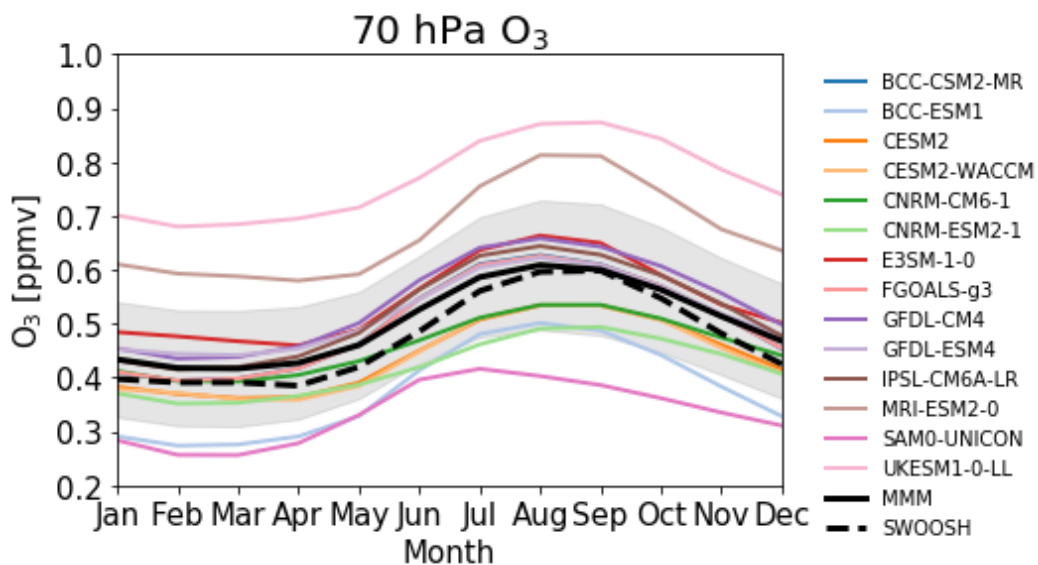
1225

**Figure 2: Climatological (2000-2014) seasonal cycle of ozone (in ppm) at 70 hPa (15°S-15°N average) for CMIP6 models, CMIP6 multi-model mean (MMM; solid black line) and SWOOSH combined ozone dataset (dashed black line).**
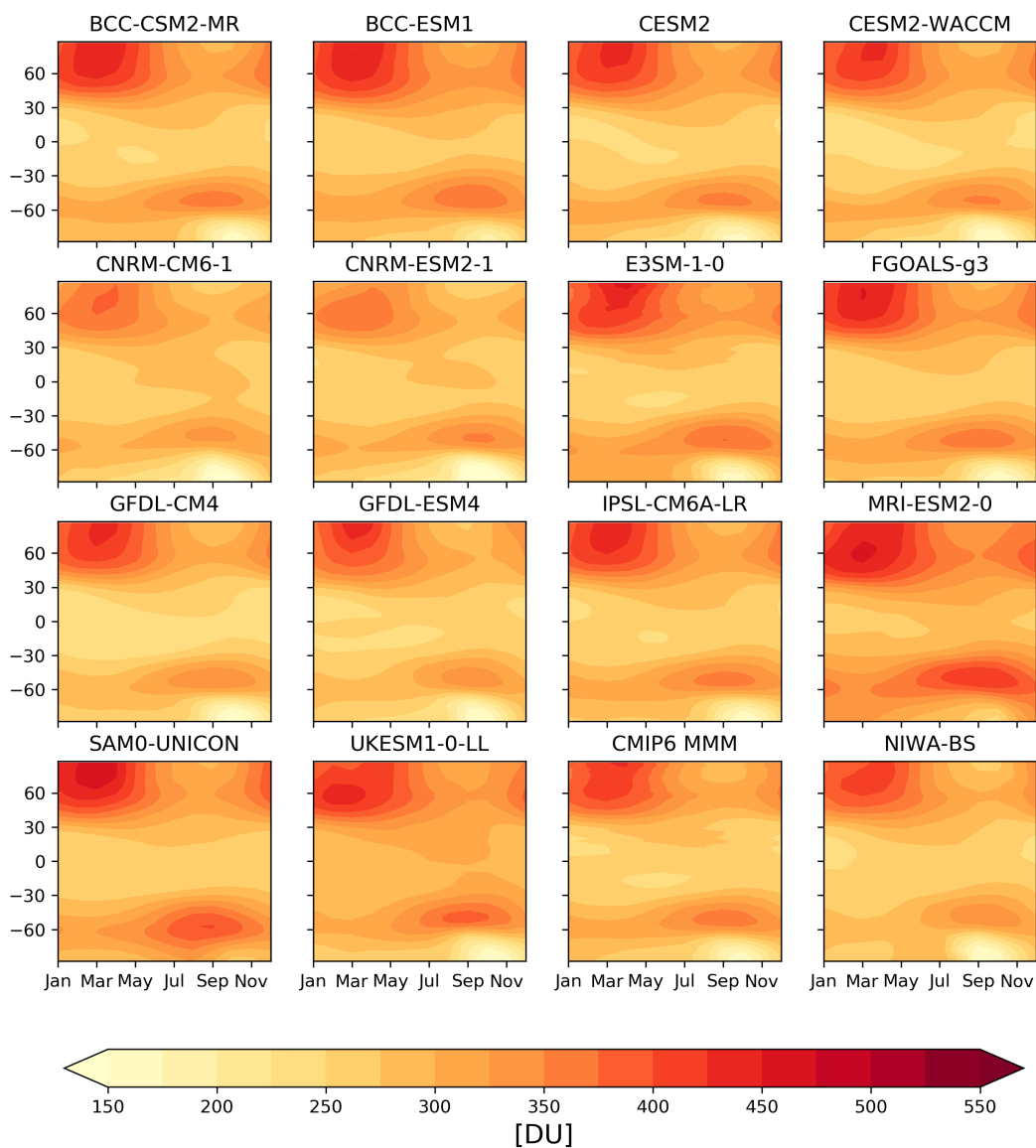
**Figure 3: Month vs latitude total column ozone for CMIP6 models and observations.** Climatological total column ozone (DU) for 2000-2014 for each CMIP6 model, the CMIP6 multi-model mean (MMM) and NIWA-BS dataset. (units to be corrected, MMM to be calculated and patched NIWA-BS dataset to be used
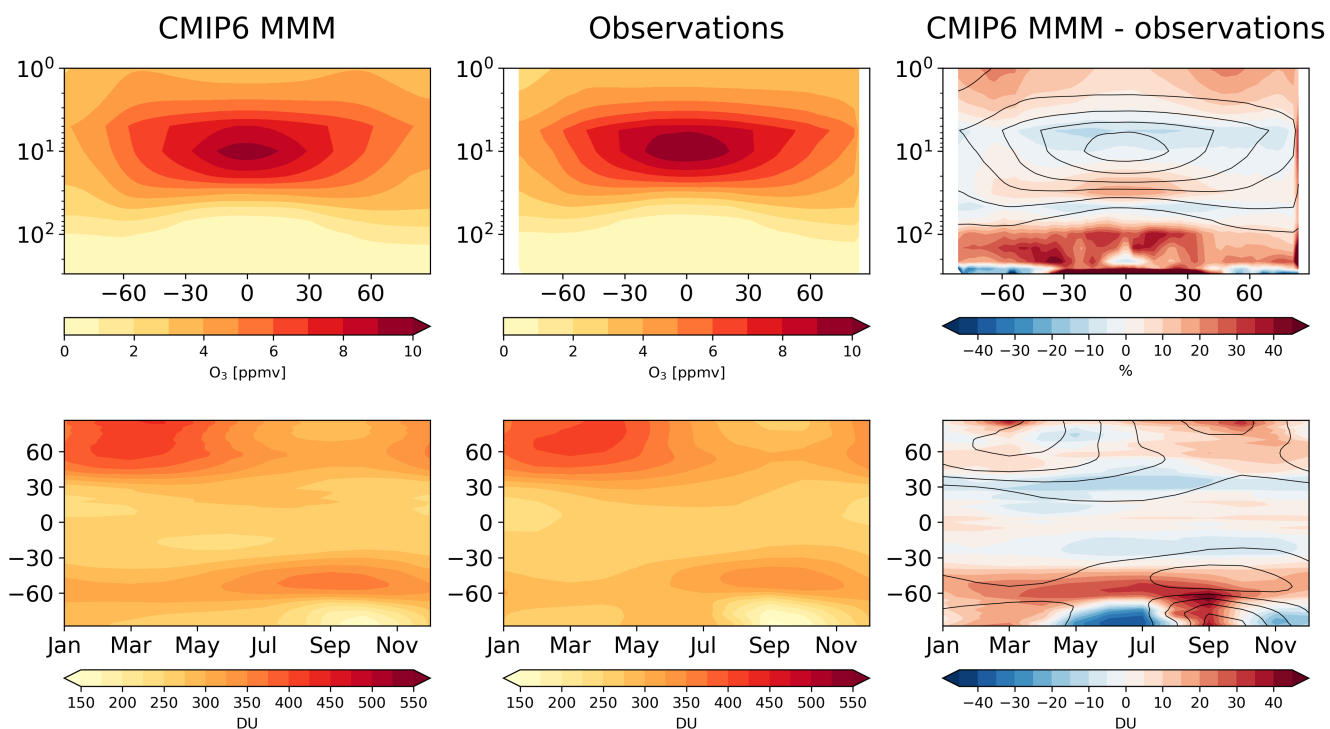
**Figure 4: Top row: 2000-2014 climatological zonal mean ozone for the CMIP6 multi-model mean (left), SWOOSH combined ozone dataset (centre) in ppm, and corresponding differences (right) in %. Bottom row: 2000-2014 climatological total column ozone for the CMIP6 multi-model mean (left), NIWA-BS dataset (centre) and corresponding differences (right) in DU.**

1240
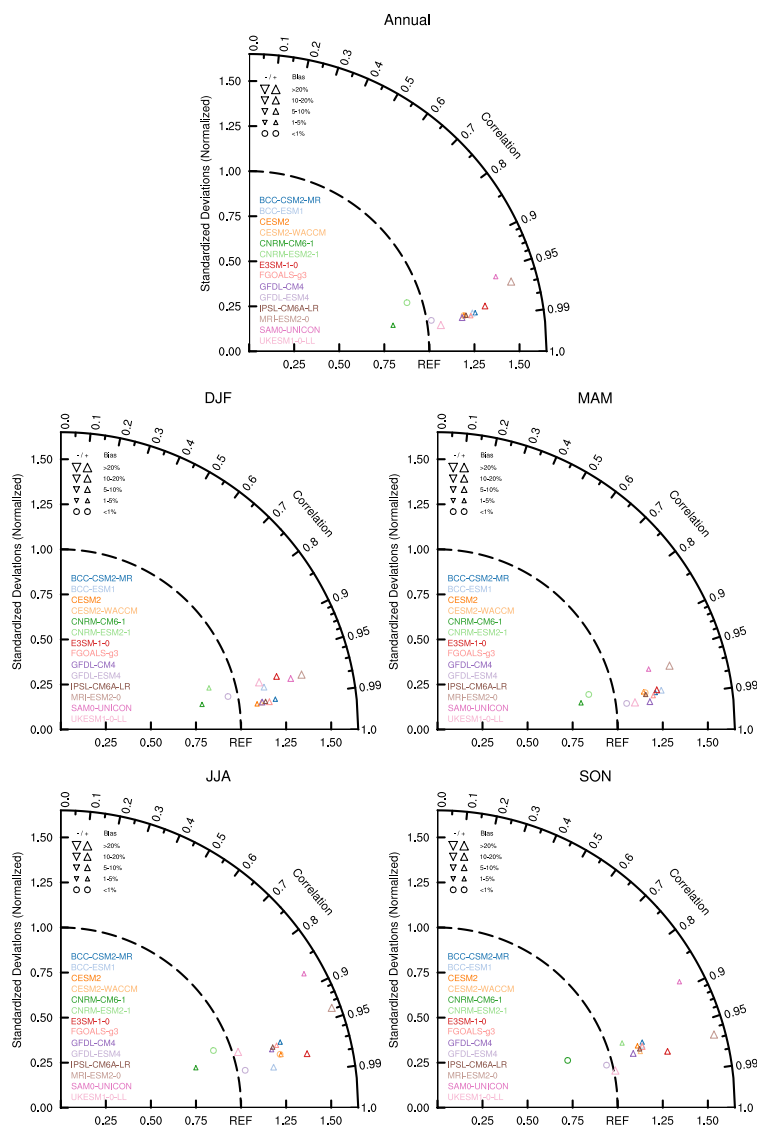
**Figure 5: Taylor diagrams for annual and seasonal (DJF, MAM, JJA and SON) mean TCO between the NIWA-BS dataset and 14 CMIP6 models over 60°S–60°N for the period 2000–2014. On the Taylor diagrams, angular axes show spatial correlations between modelled and observed TCO; radial axes show spatial standard deviation (root-mean-square deviation), normalized against that of the observation; 'REF' represents the reference line; different symbols denote the percentage bias between observation and model. Each dot represents a model.**

1245
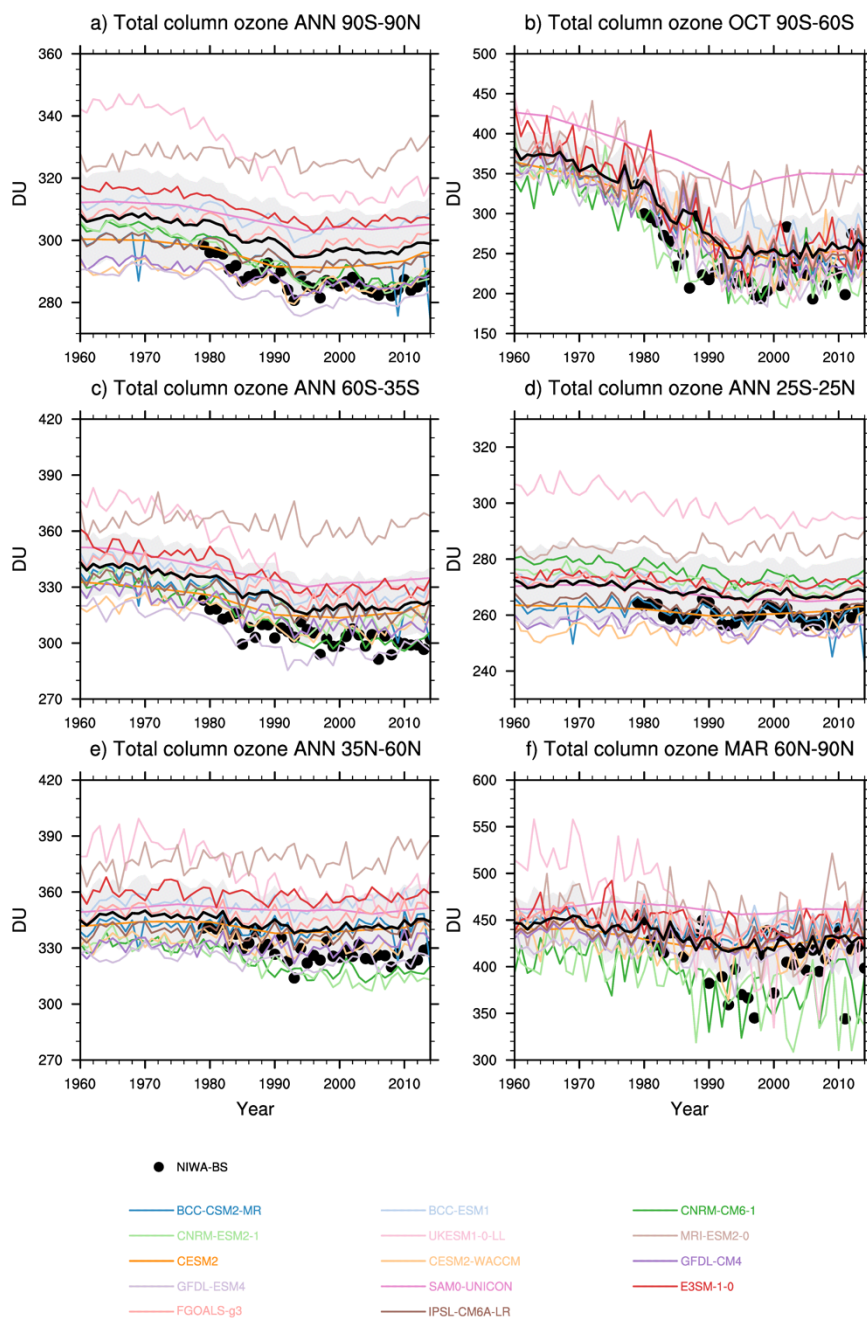
1250

**Figure 6: Total column ozone for CMIP6 models, from 1960-2014, for a) annual mean values averaged from 90°S-90°N, b) October monthly mean values averaged from 90°S-60°S, c) annual mean values averaged from 60°S-35°S, d) annual mean values averaged from 25°S-25°N, e) annual mean values averaged from 35°N-60°N and f) March monthly mean values averaged from 60°N-90°N.**

| | 90°S-90°N Annual mean | 25°N-25°S Annual mean | 35°N-60°N Annual mean | 35°S-60°S Annual mean | 60°N-90°N March mean | 60°S-90°S October mean |
|---|---|---|---|---|---|---|
| Models | Modelled trends in total column ozone (TCO) between 1980 and 2000 (DU/year) | | | | | |
| Ground-based | -0.56 ± 0.11 | -0.08 ± 0.10 | -0.84 ± 0.25 | -0.90 ± 0.17 | -3.18 ± 0.95 | -5.25 ± 0.77 |
| NOAA-SBUV | -0.74 ± 0.12 | -0.16 ± 0.13 | -1.12 ± 0.21 | -1.21 ± 0.18 | -3.30 ± 0.96 | -3.99 ± 0.80 |
| NASA TOMS-SBUV-OMI | -0.67 ± 0.13 | -0.19 ± 0.12 | -0.89 ± 0.23 | -1.06 ± 0.17 | -2.95 ± 0.91 | -3.70 ± 0.82 |
| NIWA-BS | -0.61 ± 0.12 | -0.10 ± 0.11 | -0.88 ± 0.23 | -0.87 ± 0.16 | -3.18 ± 0.92 | -3.80 ± 0.78 |
| BCC-CSM2-MR (3) | -0.44 ± 0.10 | -0.13 ± 0.10 | -0.28 ± 0.15 | -0.87 ± 0.18 | -0.80 ± 0.51 | -4.87 ± 0.98 |
| BCC-ESM1 (3) | -0.40 ± 0.09 | -0.13 ± 0.08 | -0.21 ± 0.14 | -0.92 ± 0.18 | -0.59 ± 0.46 | -4.22 ± 0.80 |
| CESM2 (11) | -0.32 ± 0.04 | -0.08 ±0.02 | -0.24 ± 0.04 | -0.59 ± 0.05 | -0.43 ± 0.08 | -3.98 ± 0.22 |
| **CESM2-WACCM (3)** | -0.37 ± 0.11 | -0.04 ± 0.09 | -0.25 ± 0.11 | -0.78 ± 0.15 | -0.55 ± 0.56 | -5.36 ± 0.76 |
| CNRM-CM6-1 (19) | -0.77 ± 0.06 | -0.37 ± 0.05 | -0.78 ± 0.08 | -1.32 ± 0.11 | -1.74 ± 0.34 | -4.52 ± 0.58 |
| **CNRM-ESM2-1 (5)** | -0.77 ± 0.06 | -0.33 ± 0.05 | -0.95 ± 0.08 | -1.09 ± 0.10 | -2.81 ± 0.48 | -4.70 ± 0.50 |
| E3SM-1-0 (5) | -0.44 ± 0.03 | -0.13 ± 0.04 | -0.17 ± 0.05 | -0.90 ± 0.07 | -0.75 ± 0.23 | -5.16 ± 0.60 |
| FGOALS-g3 (3) | -0.42 ± 0.10 | -0.18 ± 0.10 | -0.32 ± 0.15 | -0.89 ± 0.18 | -0.82 ± 0.47 | -4.66 ± 0.92 |
| GFDL-CM4 (1) | -0.41 ± 0.10 | -0.11 ± 0.09 | -0.25 ± 0.15 | -0.82 ± 0.18 | -0.73 ± 0.48 | -4.75 ± 0.95 |
| **GFDL-ESM4 (1)** | -0.50 ± 0.10 | -0.19 ± 0.09 | -0.34 ± 0.13 | -0.99 ± 0.17 | -0.79 ± 0.54 | -4.88 ± 1.15 |
| IPSL-CM6A-LR (20) | -0.43 ± 0.09 | -0.14 ± 0.09 | -0.29 ± 0.15 | -0.81 ± 0.17 | -0.78 ± 0.47 | -4.73 ± 0.94 |
| **MRI-ESM2-0 (5)** | -0.19 ± 0.08 | 0.01 ± 0.10 | -0.16 ± 0.15 | -0.47 ± 0.12 | -1.10 ± 0.58 | -2.88 ± 0.35 |
| SAM0-UNICON (1) | -0.29 ± 0.03 | -0.19 ± 0.01 | -0.06 ± 0.01 | -0.49 ± 0.04 | -0.64 ± 0.04 | -2.56 ± 0.25 |
| **UKESM1-0-LL (9)** | -1.04 ± 0.07 | -0.33 ± 0.08 | -1.20 ± 0.10 | -1.66 ± 0.11 | -4.74 ± 0.46 | -6.96 ± 0.50 |
| Mean (interactive) | -0.57 ± 0.08 | -0.18 ± 0.08 | -0.58 ± 0.11 | -1.00 ± 0.13 | -2.00 ± 0.52 | -4.95 ± 0.65 |
| Mean (all models) | -0.49 ± 0.08 | -0.17 ± 0.07 | -0.39 ± 0.11 | -0.90 ± 0.13 | -1.23 ± 0.41 | -4.59 ± 0.68 |

| Models | Modelled trends in total column ozone (TCO) between 2000 and 2014 (DU/year) | | | | | |
|---|---|---|---|---|---|---|
| BCC-CSM2-MR (3) | 0.12 ± 0.10 | 0.02 ± 0.15 | 0.40 ± 0.23 | -0.04 ± 0.26 | -0.03 ± 0.86 | 0.45 ± 1.15 |
| BCC-ESM1 (3) | 0.19 ± 0.09 | 0.13 ± 0.10 | 0.45 ± 0.19 | 0.08 ± 0.25 | -0.28 ±0.64 | 0.52 ± 0.89 |
| CESM2 (11) | 0.34 ± 0.03 | 0.18 ± 0.02 | 0.41 ± 0.05 | 0.53± 0.06 | 1.01 ± 0.04 | 0.92 ± 0.06 |
| **CESM2-WACCM (3)** | 0.31 ± 0.10 | 0.17 ± 0.14 | 0.37 ± 0.19 | 0.34 ± 0.19 | 1.54 ± 0.75 | 1.47 ± 0.83 |
| CNRM-CM6-1 (19) | -0.13 ± 0.13 | -0.14 ± 0.09 | -0.04 ± 0.14 | -0.13 ± 0.23 | -0.04 ± 0.51 | -0.24 ± 1.34 |
| **CNRM-ESM2-1 (5)** | 0.15 ± 0.10 | -0.05 ± 0.11 | 0.28 ± 0.16 | 0.27 ± 0.14 | 2.18 ± 1.39 | 1.13 ± 0.74 |
| E3SM-1-0 (5) | 0.16 ± 0.02 | 0.01 ± 0.03 | 0.29 ± 0.07 | 0.35 ± 0.06 | 0.34 ± 0.27 | 0.04 ± 0.87 |
| FGOALS-g3 (3) | 0.12 ± 0.10 | 0.04 ± 0.15 | 0.40 ± 0.23 | -0.02 ± 0.27 | 0.03 ± 0.79 | 0.42 ± 1.10 |
| GFDL-CM4 (1) | 0.10 ± 0.10 | 0.00 ± 0.14 | 0.38 ± 0.23 | -0.07 ± 0.26 | 0.00 ± 0.81 | 0.45 ± 1.11 |
| **GFDL-ESM4 (1)** | 0.10 ± 0.08 | 0.12 ± 0.13 | -0.02 ± 0.24 | 0.20 ± 0.20 | -0.18 ± 0.87 | 1.09 ± 1.66 |
| IPSL-CM6A-LR (20) | 0.10 ± 0.10 | 0.01 ± 0.14 | 0.36 ± 0.22 | -0.05 ± 0.25 | 0.03 ± 0.78 | 0.46 ± 1.12 |
| **MRI-ESM2-0 (5)** | 0.45 ± 0.13 | 0.10 ± 0.14 | 0.84 ± 0.32 | 0.60 ± 0.19 | 2.06 ± 1.36 | 2.35 ± 0.56 |
| SAM0-UNICON (1) | 0.08 ± 0.02 | 0.01 ± 0.02 | 0.12 ± 0.06 | 0.18 ± 0.01 | 0.24 ± 0.07 | 0.24 ± 0.11 |
| **UKESM1-0-LL (9)** | 0.26 ± 0.06 | 0.13 ± 0.04 | 0.34 ± 0.11 | 0.34 ± 0.09 | 1.49 ± 0.81 | 1.13 ± 0.32 |
| Mean (interactive) | 0.25 ± 0.09 | 0.09 ± 0.11 | 0.36 ± 0.20 | 0.35 ± 0.16 | 1.41 ± 1.04 | 1.43 ± 0.82 |
| Mean (all models) | 0.17 ± 0.08 | 0.05 ± 0.10 | 0.33 ± 0.17 | 0.18 ± 0.18 | 0.60 ± 0.71 | 0.75 ± 0.85 |

1255 **Table 2. Linear trends and errors in area-weighted total column ozone (TCO) (DU/year) over the periods of 1980-2000 and 2000-2014. Observed trends over 1980-2000 are taken from those in Table 2 in Eyring et al. (2013). Models highlighted in bold have interactive stratospheric ozone chemistry and their means are shown in bold. Numbers in parentheses next to the models are the number of ensembles used for that model.**

1260
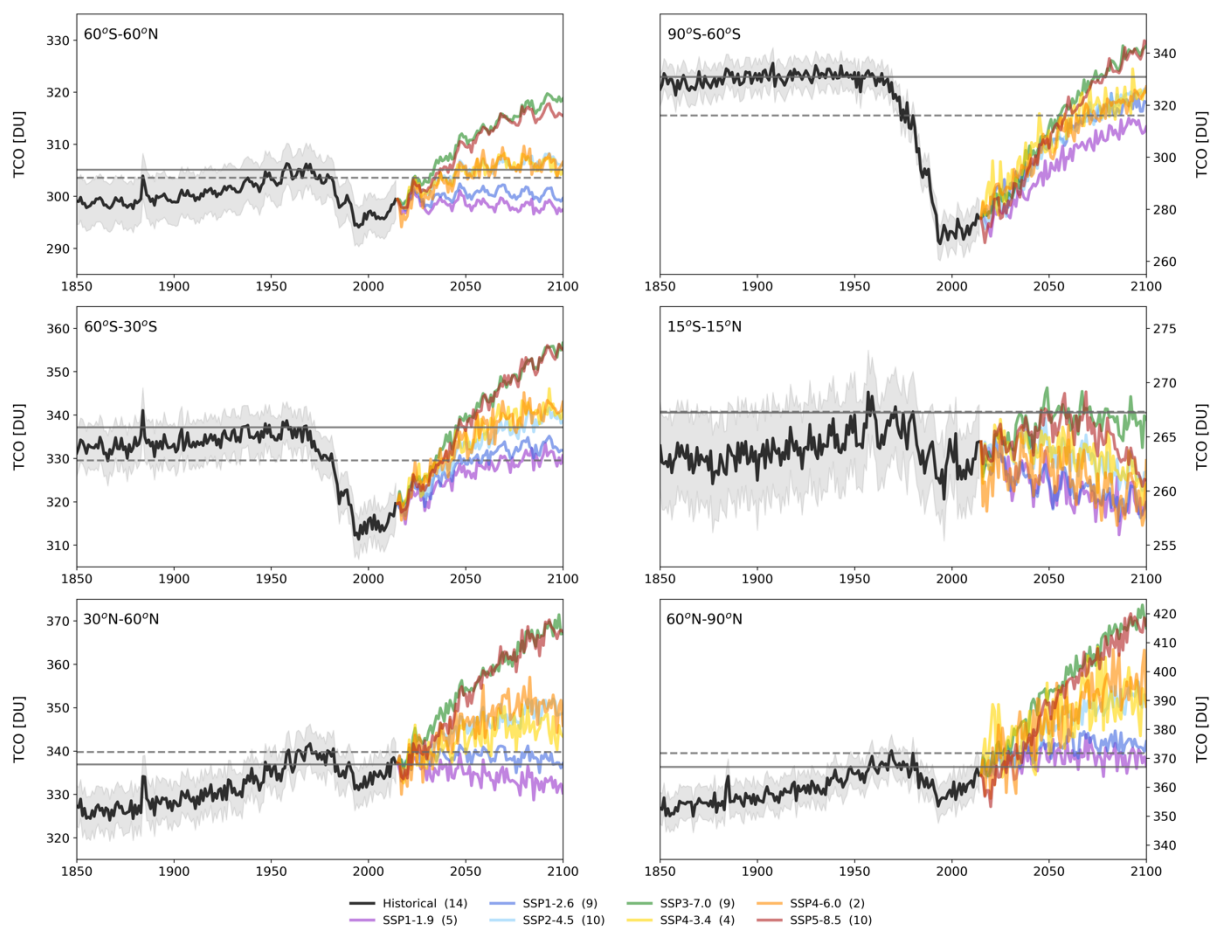
**Figure 7: Regional average CMIP6 multi-model mean total column ozone for the historical simulation (black line), and SSP scenarios (coloured lines). The number of models performing each simulation is provide in parentheses in the legend. The light grey envelope indicates the model spread for the historical simulations (calculated as the standard error). Total column ozone values for the 1960 annual mean and 1980 annual mean are given by the solid and dashed horizontal grey lines respectively.**

1265
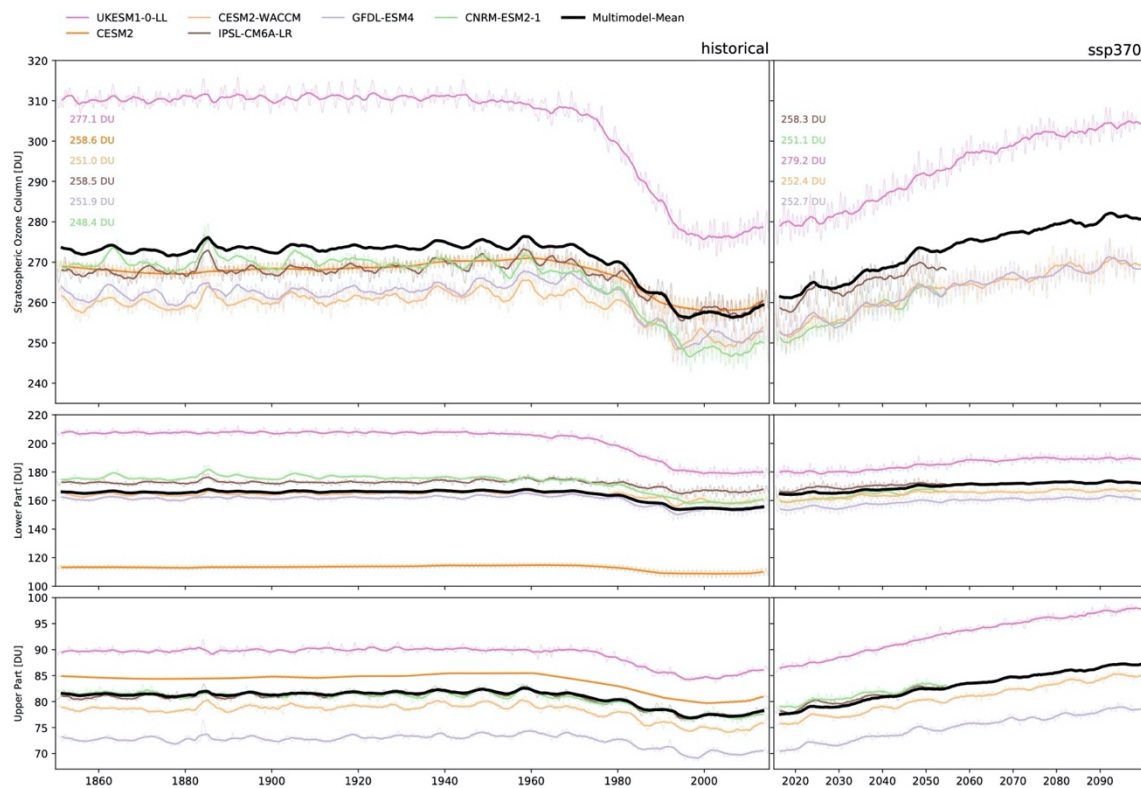
**Figure 8: Partial ozone columns from 1850-2014 following the historical simulation, and from 2014-2100 following the SSP3.7-0 scenario for a subset of the CMIP6 models evaluated in this study. Partial columns are calculated for the full stratosphere (tropopause to 1 hPa; upper panel), lower stratosphere (tropopause to 10 hPa; middle panel) and upper stratosphere (10 hPa to 1 hPa; lower panel).**

1270

1275
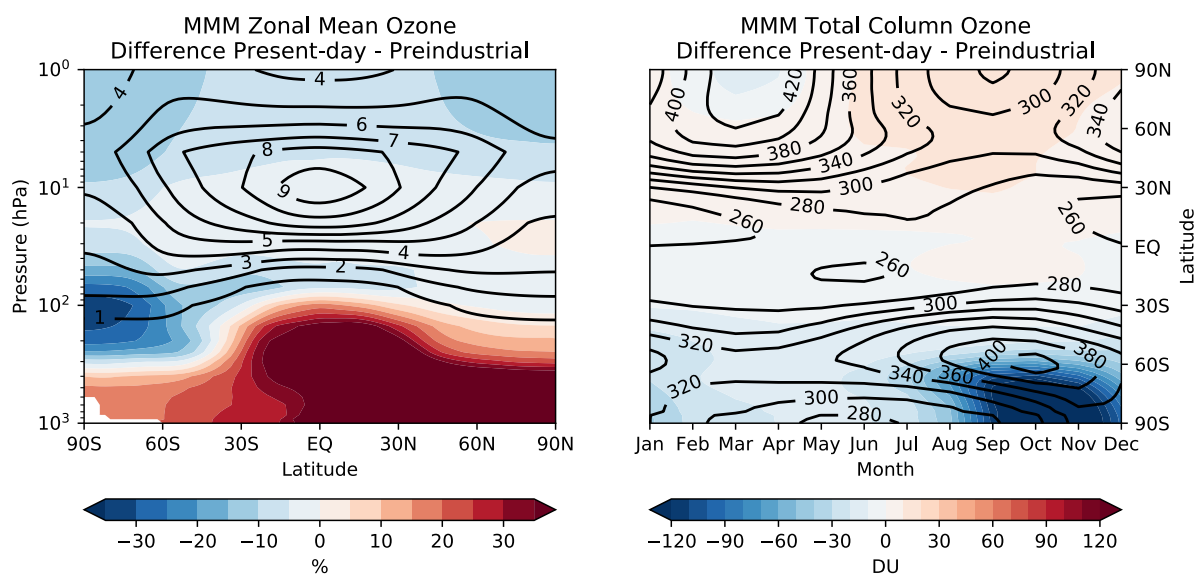
**Figure 9: CMIP6 MMM historical changes between the pre-industrial (1850-1864 averaged) and present day (2000-2014 averaged) modelled annual mean, zonal mean ozone mixing ratios in % (left), and seasonal TCO in DU (right), calculated for 13 of the 14 CMIP6 models evaluated in this study (GFDL-CM4 was excluded due to its low model top). The 2000-2014 averaged climatologies for both zonal mean ozone mixing ratios and TCO are shown in black contours.**

1280

1285
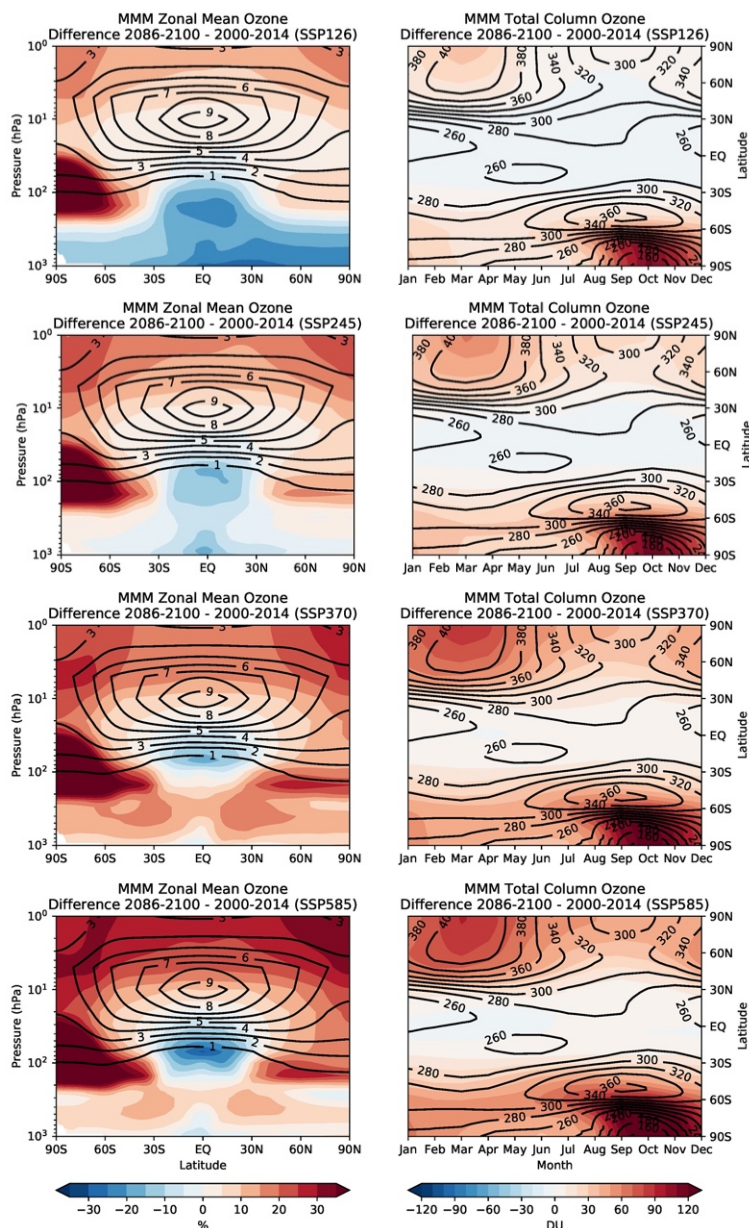
**Figure 10:** CMIP6 MMM projected changes under the SSP1-2.6, SSP2-4.5, SSP3-7.0 and SSP5-8.5 scenarios between the present
1290  day (2000-2014 averaged) and end of century (2086-2100 averaged) modelled annual mean, zonal mean ozone mixing ratios in %
(left), and seasonal TCO in DU (right), calculated using 9 of the 14 CMIP6 models evaluated in this study (BCC-CSM2-MR, CESM2,
CESM2-WACCM, CNRM-CM6-1, CNRM-ESM2-1, GFDL-ESM4, IPSL-CM6A-LR, MRI-ESM2-0 and UKESM1-0-LL). The
2000-2014 averaged climatologies for both zonal mean ozone mixing ratios and TCO are shown in black contours.
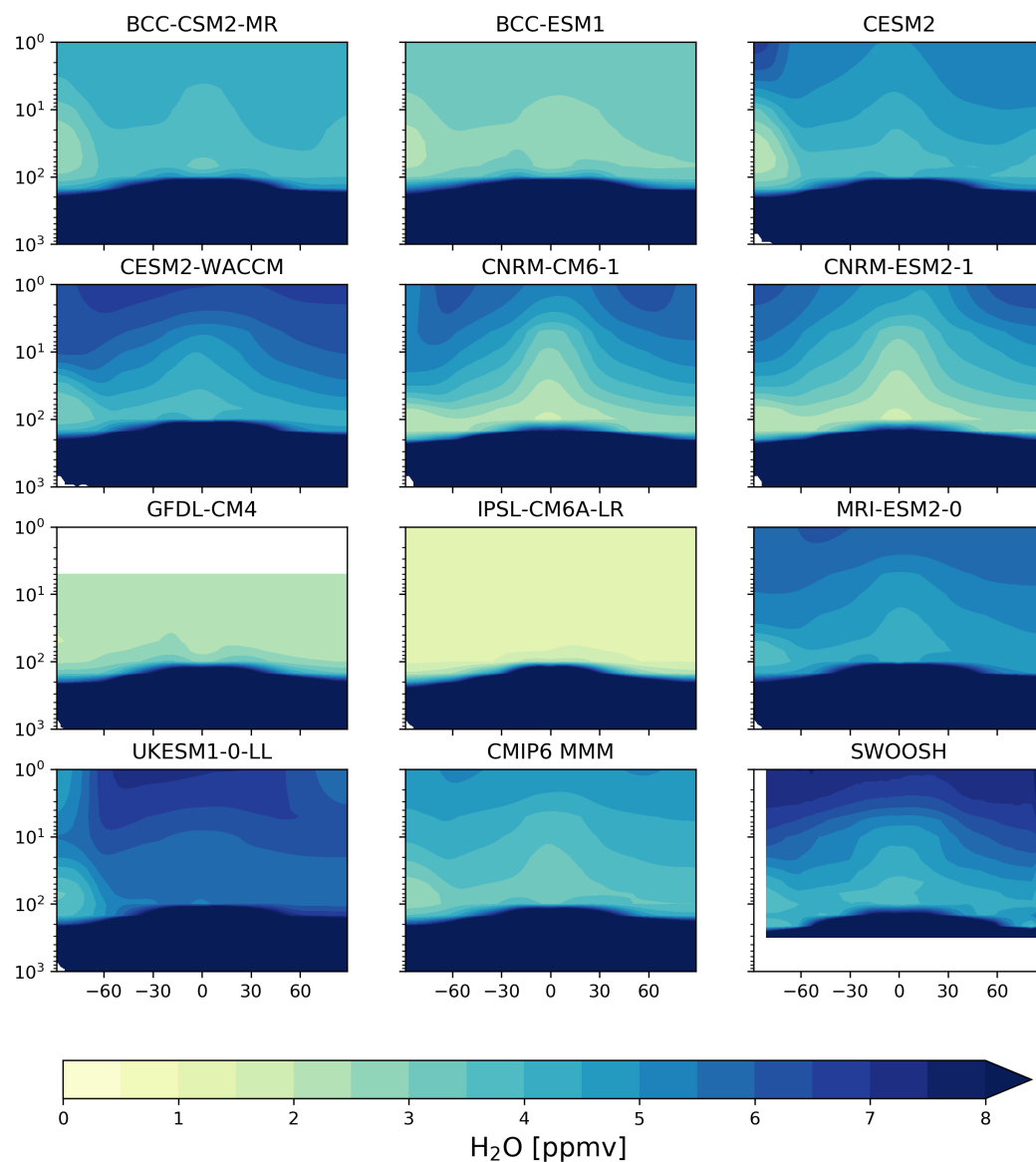
Figure 11: **Latitude vs altitude zonal mean H2O for CMIP6 models and observations. Climatological H2O volume mixing ratios (ppm) for the years 2000-2014 for each CMIP6 model, the CMIP6 multi-model mean (MMM) and SWOOSH combined dataset. GFDL-CM4 did not provide H2O data in the upper stratosphere, while the SWOOSH combined dataset only extends from ~300 hPa to 1 hPa.**
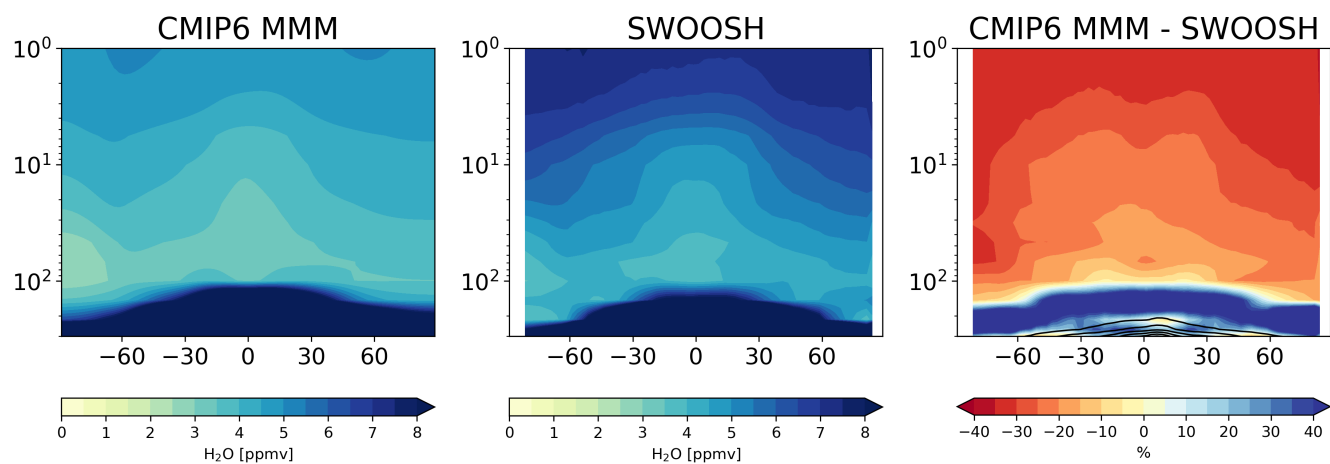
**Figure 12:** 2000-2014 climatological zonal mean H2O for the CMIP6 multi-model mean (left), SWOOSH combined H2O dataset (centre) in ppm, and corresponding differences (right) in %. Note that for the differences, red colours indicate the model is drier (i.e. less H2O in the CMIP6 MMM compared with the observations).

1305
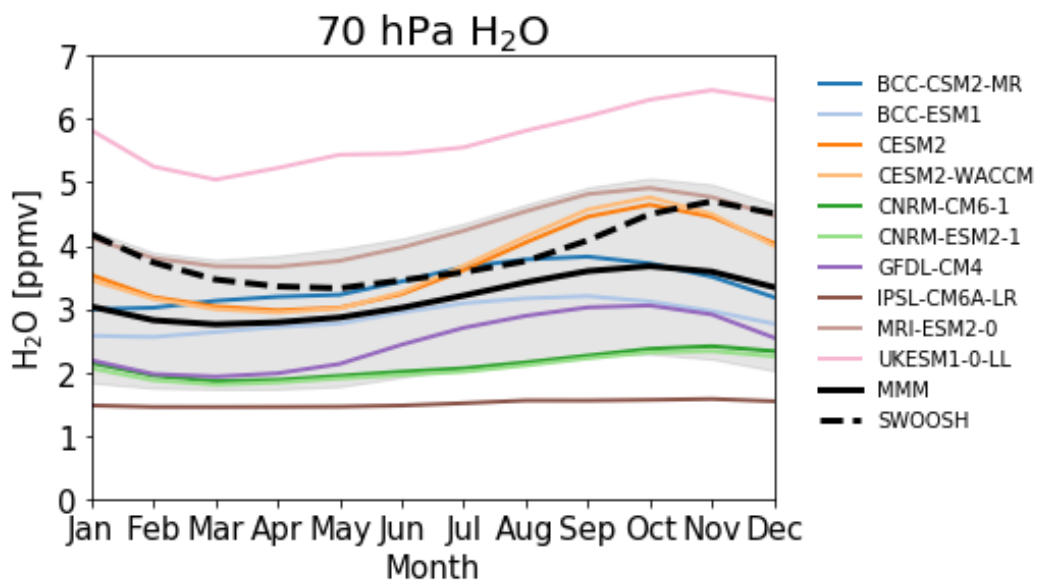
**Figure 13: Climatological (2000-2014) seasonal cycle of H2O (in ppm) at 70 hPa for CMIP6 models, CMIP6 multi-model mean (MMM; solid black line) and SWOOSH combined ozone dataset (dashed black line).**

1310
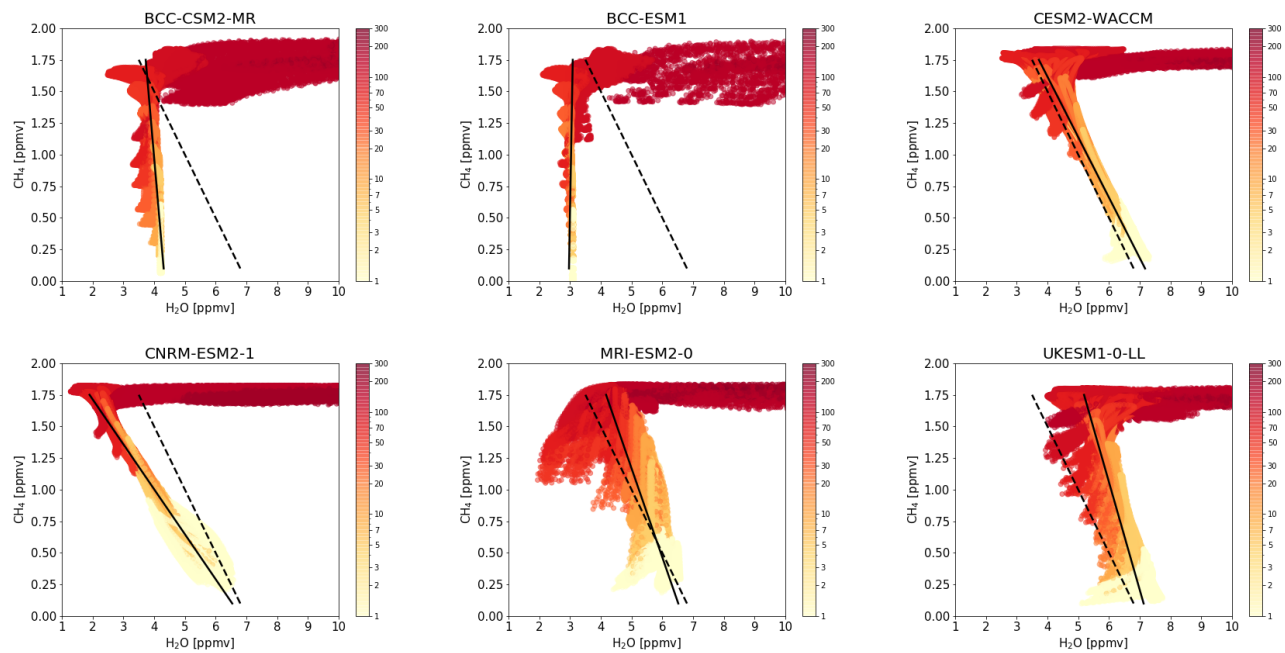
**Figure 14: H₂O vs CH₄ scatter plots. Black line gives model gradient, dashed black line gives SPARC estimate (H2O = 7-2*CH4)**

1315
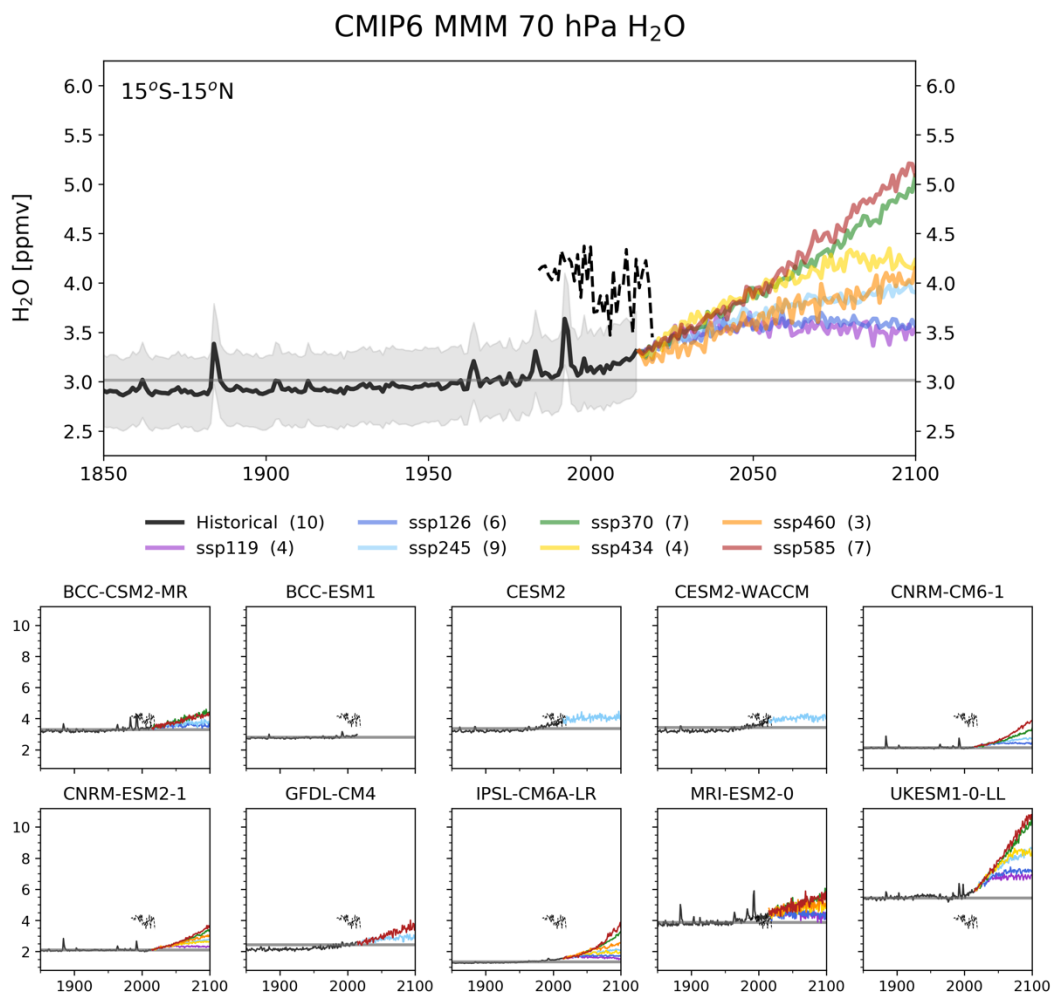
**Figure 15: Upper panel: CMIP6 multi-model mean H₂O mixing ratio (ppm), averaged from 15°S-15°N at 70 hPa for the historical simulation (black line), and SSP scenarios (coloured lines). The number of models performing each simulation is provide in parentheses in the legend. The light grey envelope indicates the model spread for the historical simulations (calculated as the standard error). H₂O mixing ratios for the 1960 annual mean is given by the horizontal grey line. Observations from the SWOOSH combined dataset are shown in the dashed black line. Lower panels: As upper panel, but for each individual CMIP6 model.**

1320
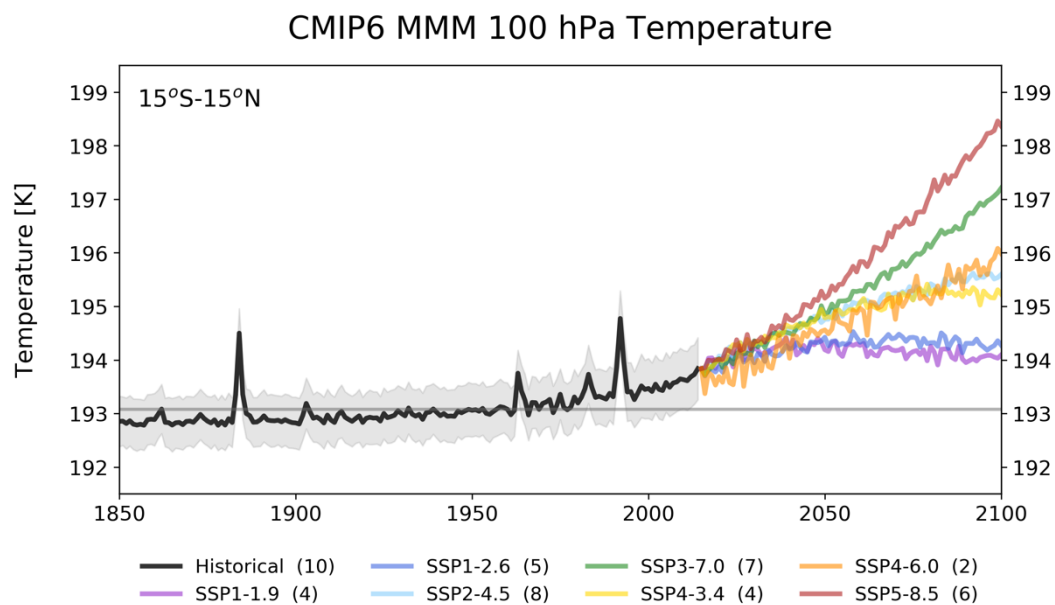
**Figure 16: MIP6 multi-model mean Temperature (K), averaged from 15°S-15°N at 100 hPa for the historical simulation (black line), and SSP scenarios (coloured lines). The number of models performing each simulation is provide in parentheses in the legend. The light grey envelope indicates the model spread for the historical simulations (calculated as the standard error). Temperature for the 1960 annual mean is given by the horizontal grey line.**
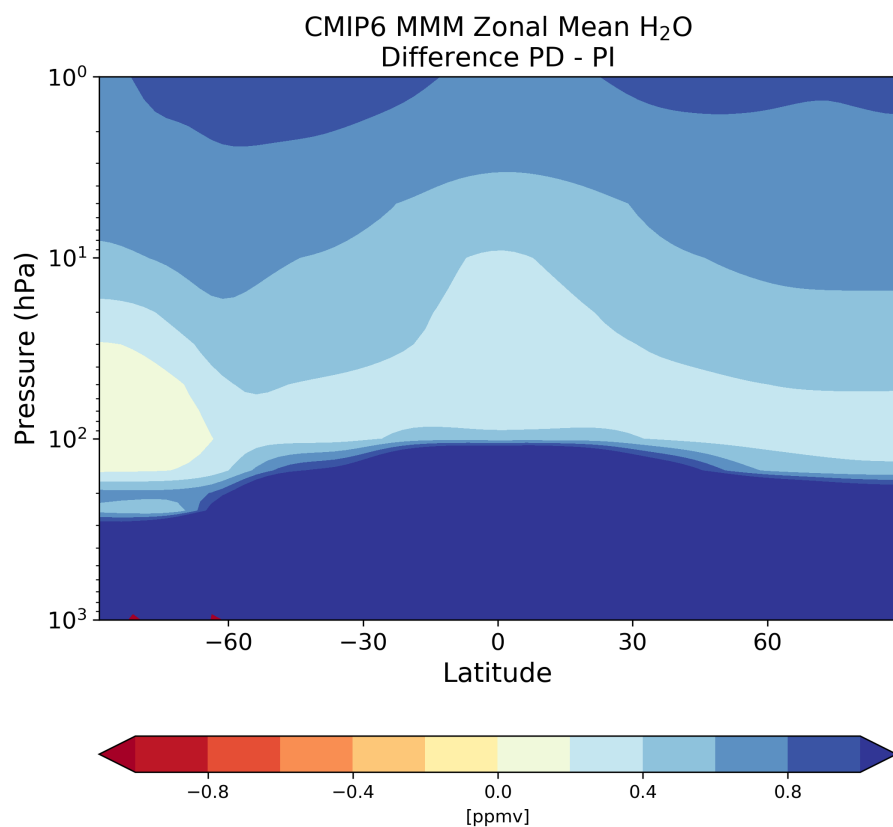
**Figure 17: Historical changes between the pre-industrial (1850-1864 averaged) and present day (2000-2014 averaged) modelled annual mean, zonal mean CMIP6 MMM H$_2$O mixing ratios (ppm), calculated using 9 of the 10 CMIP6 models evaluated in this study (GFDL-CM4 was excluded due to its low model top).**

1335
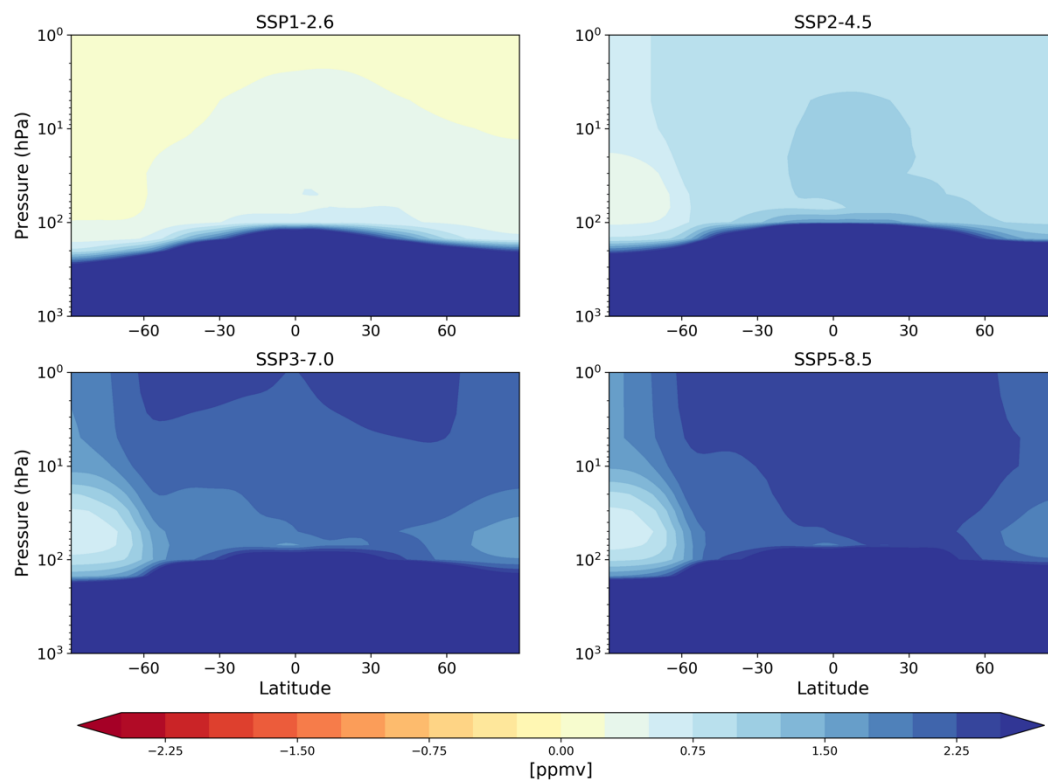
**Figure 18: Projected changes between the present day (2000-2014 averaged) and end of century (2086-2100 averaged) modelled annual mean, zonal mean CMIP6 MMM $H_2O$ volume mixing ratios (ppm), calculated using 5 of the 10 CMIP6 models evaluated in this study (BCC-CSM2-MR, CNRM-CM6-1, IPSL-CM6A-LR, MRI-ESM2-0 and UKESM1-0-LL).**

## Appendix
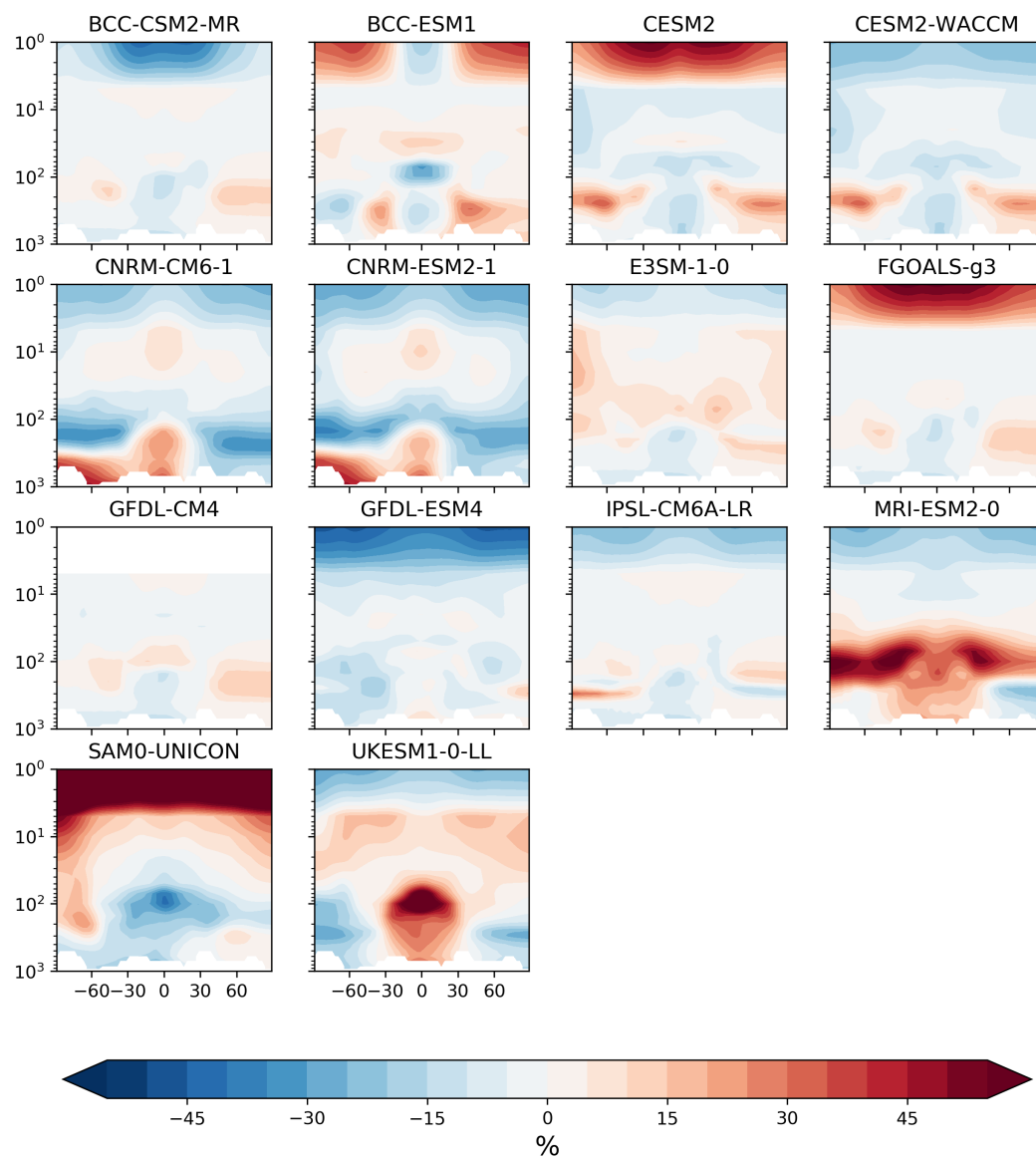
**Figure A1: Latitude vs altitude ozone anomalies (in %) for individual CMIP6 models compared to the CMIP6 multi-model mean (MMM) averaged for the years 2000-2014. Differences calculated as model – CMIP6 MMM.**

1345

**Figure A2: Regional average total column ozone from each CMIP6 model (coloured lines) for the historical simulation, the CMIP6 multi-model mean (black line), and the multi-model spread (calculated as the standard error; grey shading).**

l350

CMIP6 MMM Total Column Ozone
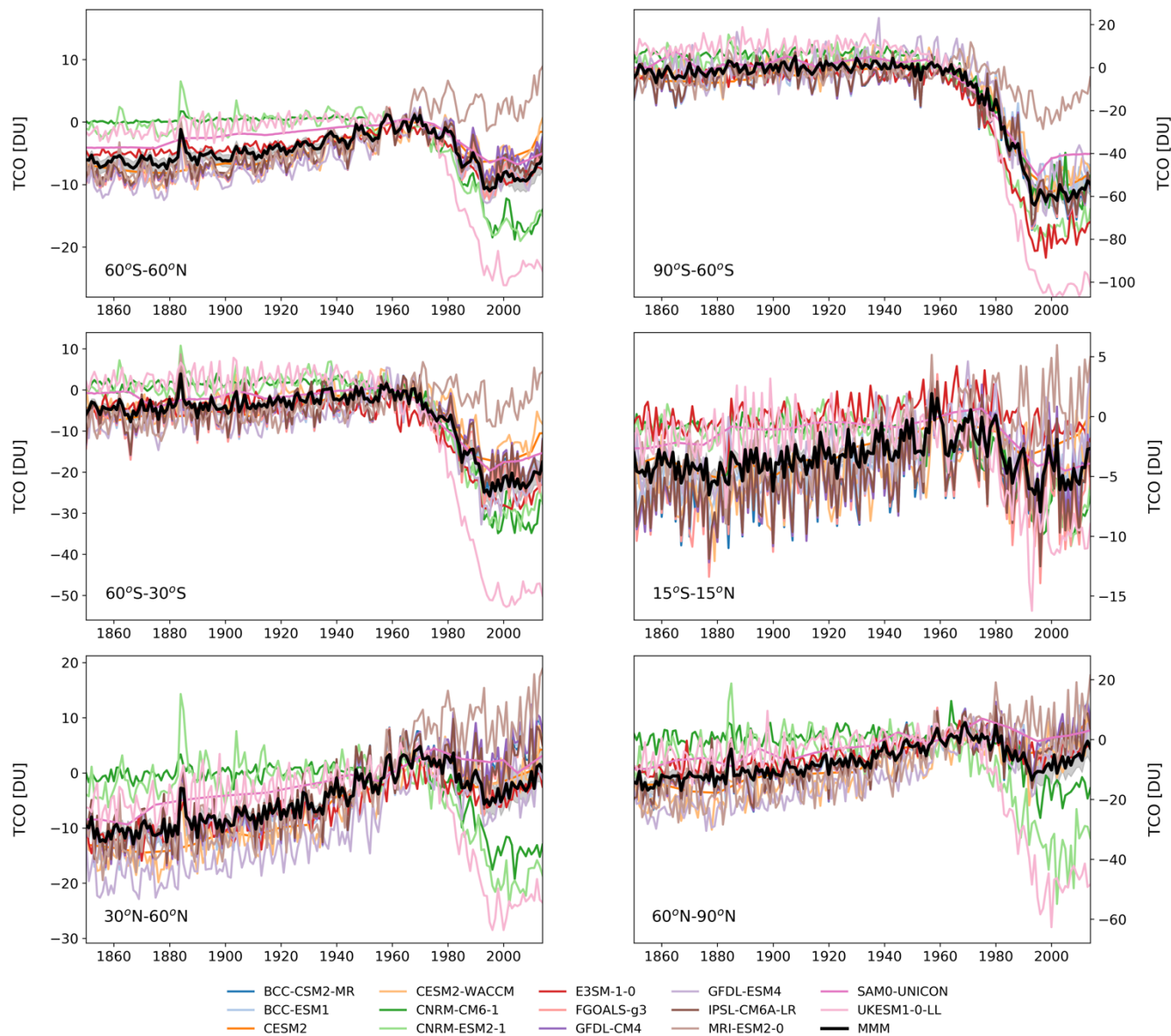
**Figure A3: As for A2, but each model is normalised to its 1960 value.**
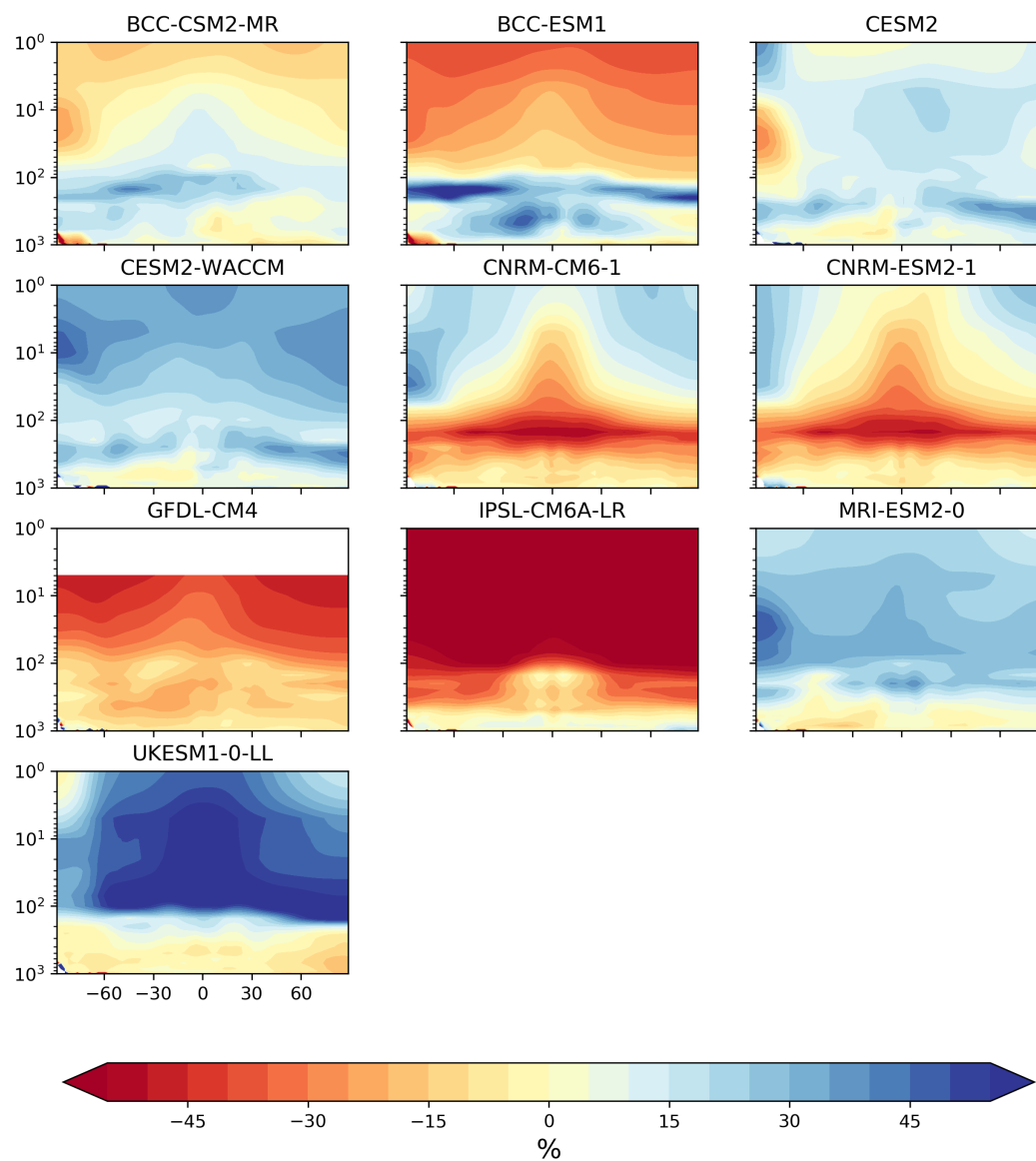
ǀ355

**A4: Latitude vs altitude H2O anomalies (in %) for individual CMIP6 models compared to the CMIP6 multi-model mean (MMM) averaged for the years 2000-2014. Differences calculated as model – CMIP6 MMM. Note that for the differences, red colours indicate the model is drier (i.e. less H2O in the CMIP6 MMM compared with the observations).**

ǀ360
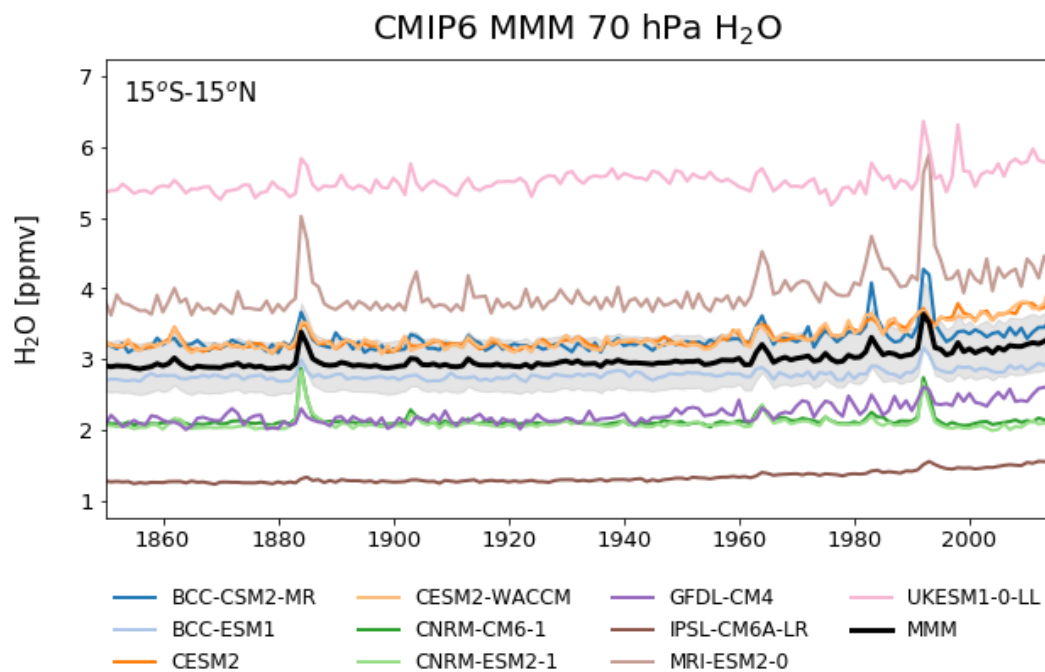
**Figure A5: 70 hPa H2O mixing ratio (ppm) from each CMIP6 model (coloured lines) for the historical simulation, the CMIP6 multi-model mean (black line), and the multi-model spread (calculated as the standard error; grey shading).**